UNIVERSITY OF OKLAHOMA

GRADUATE COLLEGE

INVESTIGATION OF FLOW REVERSAL IN A VERTICAL CHANNEL WITH A CYCLIC HEATER

A THESIS

SUBMITTED TO THE GRADUATE FACULTY

In partial fulfillment of the requirements for the

degree of

MASTER OF SCIENCE

By

PAUL L. DINIUS

Norman, Oklahoma

1999

INVESTIGATION OF FLOW REVERSAL IN A VERTICAL CHANNEL WITH A CYCLIC HEATER

A THESIS APPROVED FOR THE
SCHOOL OF AEROSPACE AND MECHANICAL ENGINEERING

BY

[redacted]

[redacted]

[redacted]

Dr. William Sutton

ACKNOWLEDGEMENTS

I must first thank Dr. Feng-Chyuan Lai for his tireless support as my thesis advisor. Having worked with a variety of college professors and military engineers within the submarine community, I have had the opportunity to associate with a dedicated and capable group of engineering professionals. Dr. Lai clearly ranks among the most dedicated of that group. His patience, humor, and pleasant demeanor are refreshing in the engineering community. I must also thank Dr. Lai's wife, Hongshing Lai, for her work at installing and troubleshooting the FIDAP Computational Fluid Dynamics program used in this study. I also must thank Dr. Bruce Roe, George Lynn Cross Research Professor, with the Biochemistry Department at the University of Oklahoma for loaning the Sun workstation required for use with the FIDAP program.

I must acknowledge Colonel Phil Hughes, Commanding Officer of the Naval ROTC Unit at the University of Oklahoma, who allowed my day-time participation in graduation studies, and Senior Chief Doug Myers, Janet Willauer, and Drenda Fisher, who carried the administrative burden while I was occupied with my studies.

I would like to thank Dr. George Emanuel and Dr. William Sutton for their guidance and support as my thesis committee members.

Finally, I must offer my greatest appreciation to my wife Stephanie. My tour of duty at the University of Oklahoma was an opportunity to spend time with my wife after three years of sea duty. My graduate studies often occupied a majority of my time, where it seemed that I might as well have been deployed at sea. Her patience and understanding were instrumental in my completion of this degree.

TABLE OF CONTENTS

LIST OF TABLES

LIST OF FIGURES

NOMENCLATURE

b	half channel width
c_p	specific heat
D	channel width
g	gravity
G	gap width
Gr	Grashof number, $g\beta(T_{in} - T_o)b^3/\nu^2$
k	thermal conductivity
L	channel length
L_h	heated channel length
Nu	Nusselt number, hb/k
p, P^*	pressure and dimensionless pressure
Pr	Prandtl number, $\mu c_p/k$
q, q^*	heat flux and dimensionless heat flux
Q, Q_e	dimensionless half channel flow rate and flow rate at exit
R	radius
Ra	Rayleigh number, GrPr
Ra^*	channel Rayleigh number, $Ra^* = PrGr(b/L_h)$
t	time
T, T^*	temperature and dimensionless temperature
u,U^*	x velocity component and dimensionless x velocity component
U_{ref}	reference velocity scale, $U_{ref} = \alpha PrGr^{1/2}/b$
v, V^*	v velocity component and dimensionless v velocity component

v_r	radial velocity component
v_θ	tangential velocity component
W	channel width
x, y	cartesian coordinates
X^*, Y^*	dimensionless cartesian coordinates

Greek Symbols

α	thermal diffusivity
β	volumetric expansion coefficient
ε	penalty parameter
θ	dimensionless temperature
θ'	dimensionless side wall temperature rate of change
μ	dynamic viscosity
ν	kinematic viscosity
ρ	density
σ	stress
τ	dimensionless time
ω	ratio of cyclic heater operating time
ψ	dimensionless stream function

Subscripts

b, d, D	value based on channel width or diameter
c, cs	values based on transient and steady state convection
e	value at channel exit

i, inlet	value at semi-circular inlet boundary
L	value based on channel length
o	ambient or initial value
r, radial	value referenced to the radial direction
ref	reference value
w	value for the channel wall

ABSTRACT

A numerical study of airflow in a vertical channel between parallel plates with a channel heater has been conducted. The numerical model parallels a typical home fireplace. The primary objective of the study is to verify the existence of flow reversal due to a cyclic heater in the channel. Both steady state (isothermal heater) and transient (cyclic heater) analyses were performed for dimensionless heater temperatures of T_{heater} = 1.0, 1.5, and 2.0 and with heated inlet air at T_{inlet} = 1.0. The steady state runs were completed for Grashof numbers between 0 and 10^5 and the transient runs were for Grashof numbers of 10^4 and 10^5. Three cyclic heater operating times were also analyzed. The results conclude that reversed flow occurs for each heater temperature and cyclic heater operating time studied for Gr = 10^4. The reversed flow was independent of cyclic heater operating time for a fixed heater temperature at Gr = 10^4. The rate of flow reversal is successively faster as the cyclic heater temperature approaches the inlet temperature. Reversed flow did not exist for a fixed heater temperature over the range of cyclic heater operating times considered at Gr = 10^5. However, the flow did exhibit perturbations with slowly decreasing flow rates followed by slowly increasing flow rates as the heater cycled. The present study concludes that, for the given geometry and thermal boundary conditions, the cyclic nature of a channel heater will cause reversed flow for Gr = 10^4.

CHAPTER 1

INTRODUCTION

1.1 Introduction

Forced convection, where fluid motion is induced by external forces such as fans and pumps, is a common method of supplying heat or removing waste heat. Most conventional heating, ventilating, and air conditioning (HVAC) systems are prominent examples of forced convection systems that supply or remove heat and provide fresh supplies of conditioned breathing air.

Over the last two decades there has been a renewed interest in the most common form of convection: natural or free convection. This form of convection arises from density differences in a fluid that result from changes in temperature from a particular fluid system. Due to the large cost of operating and maintaining forced convection systems, engineers have been focusing on the feasibility of designing systems which use free convection to remove waste heat. Systems that employ natural convection can eliminate or reduce mechanical components that are costly, noisy, and subject to failure that leads to equipment downtime and further expenditures.

The most common example of recent waste heat removal studies by natural convection involves printed circuit boards (PCBs). PCBs are found in virtually all electronic applications and specifically in computers. Fans located in computer mini-towers or housing units currently remove the heat generated by PCBs. Much research

has focused on the proper spacing and geometry of PCBs to maximize natural convection to the point of removing sufficient potentially damaging waste heat without using fans.

Another area that has received significant focus concerns the propagation of fire in buildings and rooms. Numerous research efforts have modeled the natural flow of fires in compartments with the goal of predicting the spread of fire and improving room and building designs to minimize the damaging effects of a fire.

However, relatively little research has been done on the effects of deliberate and controlled fires, specifically fires in home chimneys or fireplaces. A wealth of research exists on the effects of heat transfer in a vertical channel with an applied constant heat flux or constant wall temperatures. The primary goal of such research is to focus on the heat transfer rates that can be obtained using only natural convection.

The focus of this study is to examine the flow of air in a home fireplace. The goal is not to study heat transfer, but rather the flow of the products of combustion and heated air in the fireplace chimney. Recent Environmental Protection Agency (EPA) policies indicate that the emissions of harmful combustion by-products from home fireplaces may be of enough significance to require regulation. Some corporate efforts are underway to anticipate possible forthcoming regulations from EPA and provide an engineering solution to the emission of by-products from home fireplaces.

The design envisions an electric heater element in the upper portion of the common fireplace chimney. This cyclic heater element is intended to provide sufficient heat to the incomplete products of combustion in the fireplace to ensure complete combustion. This will minimize the more harmful by-products of combustion from entering the atmosphere.

One concern of placing a heater element in the upper portion of a chimney is the effect it may have on the normal natural circulation outflow of the combustion by-products. A negative temperature gradient could cause the flow of gases to, at least in part, reverse and enter the home. This flow reversal would have two possible negative consequences. First, harmful by-products of combustion, such as carbon monoxide and carbon dioxide, pose a significant health hazard to the occupants of a household. The effects of both short term and long term exposure demand that all of the combustion by-products exit to the atmosphere and not enter the house. Secondly, if sufficient disruption of the natural convection outflow of gases exists, then insufficient combustion air will be drawn into the chimney. This may cause the flame to "search" for combustion air and could cause the flame to leave the firebox of the fireplace and effectively shoot or propagate into the room being heated. Each of these conditions is, for obvious reasons, undesirable and demands rigorous engineering analysis.

1.1.1 Common Fireplace Operation and Design

To better understand the project at hand, a basic understanding of modern home fireplace operation and design is essential. According to the Chimney Safety Institute of

America (CSIA) [1], there are two general categories of fireplaces: Masonry (bricks and mortar) and factory built (metal firebox and chimney). Each of these types of fireplace has the same desired goals of safely combusting wood in the firebox for heat generation and expelling the exhaust gases to the atmosphere. Figures 1.1a and 1.1b show the basic schematic of the masonry and factory built fireplaces. Either of the chimneys above, according to the CSIA, must have some common requisites for proper and safe operation. One of the critical factors is the overall chimney height. The Institute recommends an overall chimney height of 10 or 12 feet in order to provide sufficient channel length for the development of the necessary draft. This draft will be referred to later as the "chimney effect" and will be examined more rigorously.

Furthermore, the "fireplace opening to flue size opening" ratio should generally not exceed 10 to 12. This reported rule of thumb directs that the opening of the fireplace into the firebox can become excessive, relative to the flue size, such that the volume of air entering, and consequently smoke produced, will become too great for the flue size. This can result in exhaust gases entering the house, effectively taking the path of least resistance. Some manufactured fireplaces have been reported to work sufficiently with a 15 to 1 ratio. The accumulation of soot in a chimney can also reduce this ratio and cause the back flow of gases into the house.

Another issue of concern, addressed by Hayden [2], is the typical airflow requirements of a conventional fireplace. Hayden reports that the nominal excess air requirement of a conventional fireplace is about 1500%. This high mass flow rate of air

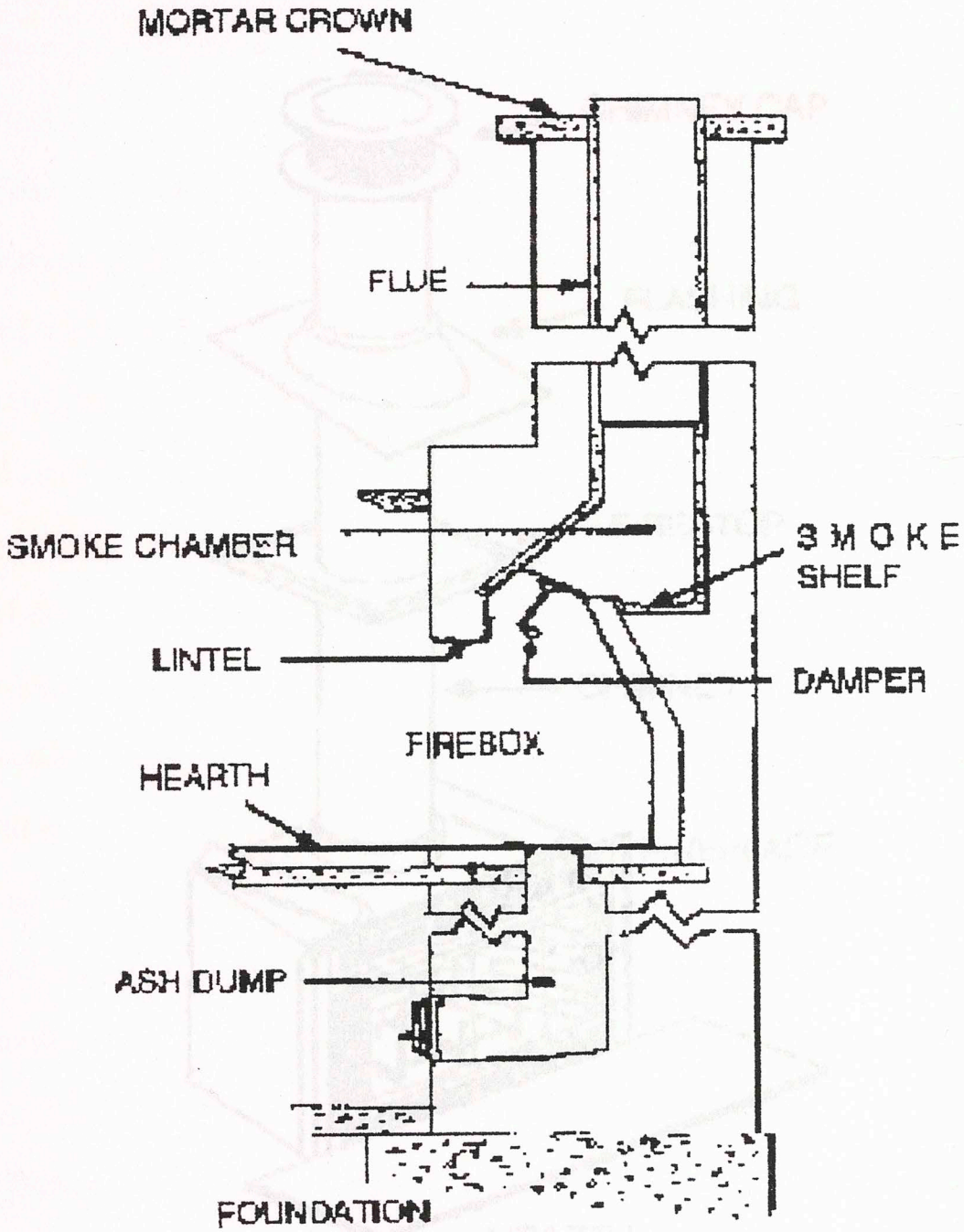

Figure 1.1.a Masonry fireplace

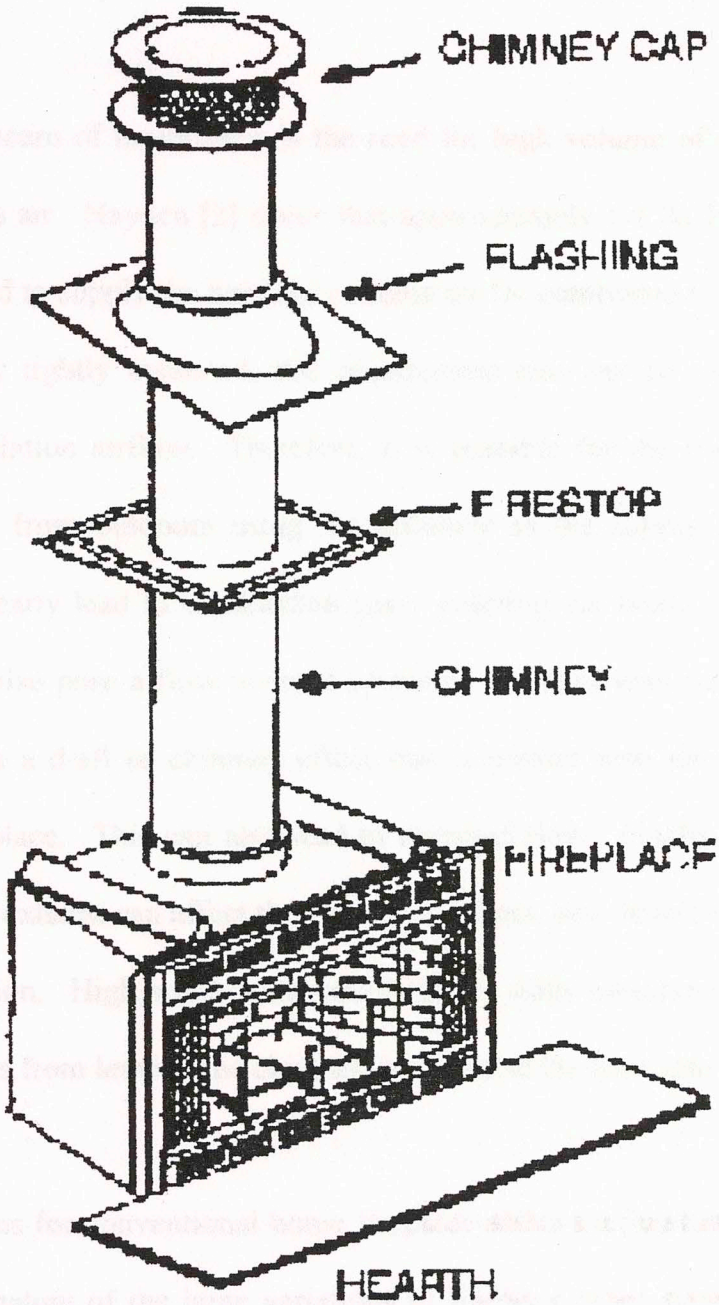

Figure 1.1.b Prefabricated fireplace

poses further difficulties. A high mass flow rate of air reduces overall heat transfer to the house and increases heat transfer to the convective flow, out the chimney, and into the atmosphere.

The other concern of importance is the need for high volume of combustion air and the source of this air. Hayden [2] states that approximately 1.4 ACH (Air Changes per Hour) are required to supply the necessary excess air for combustion. In an era when most homes are very tightly insulated, this requirement may not be satisfied without external forced circulation airflow. Therefore, it is possible for the fire to "find" the necessary excess air from outdoors using the chimney as the supply channel. This reversed flow can clearly lead to combustion gases entering the house. An older, less insulated house can also pose a flow reversal problem. A home with sufficient leakage can potentially create a draft or chimney effect that is greater than the buoyant forces produced in the fireplace. This can also lead to reversed flow. Finally, ambient wind conditions at the flue exhaust can affect the pressure gradient, and therefore the resistance to exhaust fluid motion. High winds with circulating or eddy currents can prevent the buoyant exhaust gases from leaving the chimney and reverse the flow into the house.

These concerns for conventional home fireplace safety are legitimate. However, due to the complex nature of the large variations of fireplace sizes, types, and location within the home, the varying degrees of home insulation, the level of soot buildup in a chimney, and the possible wind variations, these issues will not be addressed in this

study. The primary motivation of this analysis concerns the particulates of combustion discussed in the next section.

1.1.2 Particulates of Combustion

Regardless of the inefficiency of the vast majority of conventional home fireplaces as a source of home heating [2], most people enjoy the ambiance provided by a fireplace. As this is the case, most individuals desire to continue to be allowed to use home fireplaces. However, concerns over particulate emissions caused the Environmental Protection Agency, and the Canadian equivalent of the EPA, to pass performance guidelines for such emissions from home fireplaces. These guidelines are known as EPA 1990 and the Canadian CSA B415.

As wood burns in the firebox of a fireplace, incomplete combustion occurs to a large degree. Insufficient combustion air, low burning temperatures, and moist wood are the common causes. The by-products of incomplete combustion are CO_2 and the more deadly CO, as well as particulates, collectively known as soot. Furthermore, as the wood is burned, some of the volatile substances will boil out of the wood before they can be burned. These products contribute particulates to soot formation. The onset of noticeable effects (headaches) from carbon monoxide occurs at exposures of 300 ppm for one hour [3]. This corresponds to a mere 0.03% of CO, by volume, for only a single hour. Exposure at twice this rate, 600 ppm or 0.06% CO, can lead to throbbing headaches in one hour and coma or death in 10 hours.

The rate of particulate emissions from wood fireplaces is reported at 50 g/h [2], which is a significant amount of pollutants. These emissions are the primary focus of any commercial fireplace manufacturing company. Anticipated EPA regulations [4] would reduce emissions even further than the EPA 1990 regulations. Therefore, one such proposal to reduce pollutants is to place an afterburner heating element in the upper portion of the chimney to provide sufficient heating to completely combust the particulates emitted and to limit CO production by providing complete combustion to CO_2. This design consideration will be numerically modeled in the present study.

1.1.3 Prototype Fireplace Design

As mentioned previously, a prototype fireplace, as reported by Lai [4], has been designed and built in an effort to control particulate emissions. The prototype design is illustrated in Figure 1.2.

The cyclic heater, depicted as the "burner section" in Figure 1.2, is turned on when the temperature difference between the exhaust flue gas and the ambient air reaches 40°F. The burner section remains energized until the surface of the heater bundle reaches 1200°F. When this upper temperature limit is reached, the heater is turned off in order to minimize the electricity used. The surface temperature of the heater bundle will then fall, and will cycle back on at a lower temperature limit of 1050°F. The heater bundle will continue to cycle between 1050°F and 1200 °F. The operation of the heater is monitored and controlled through a microprocessor.

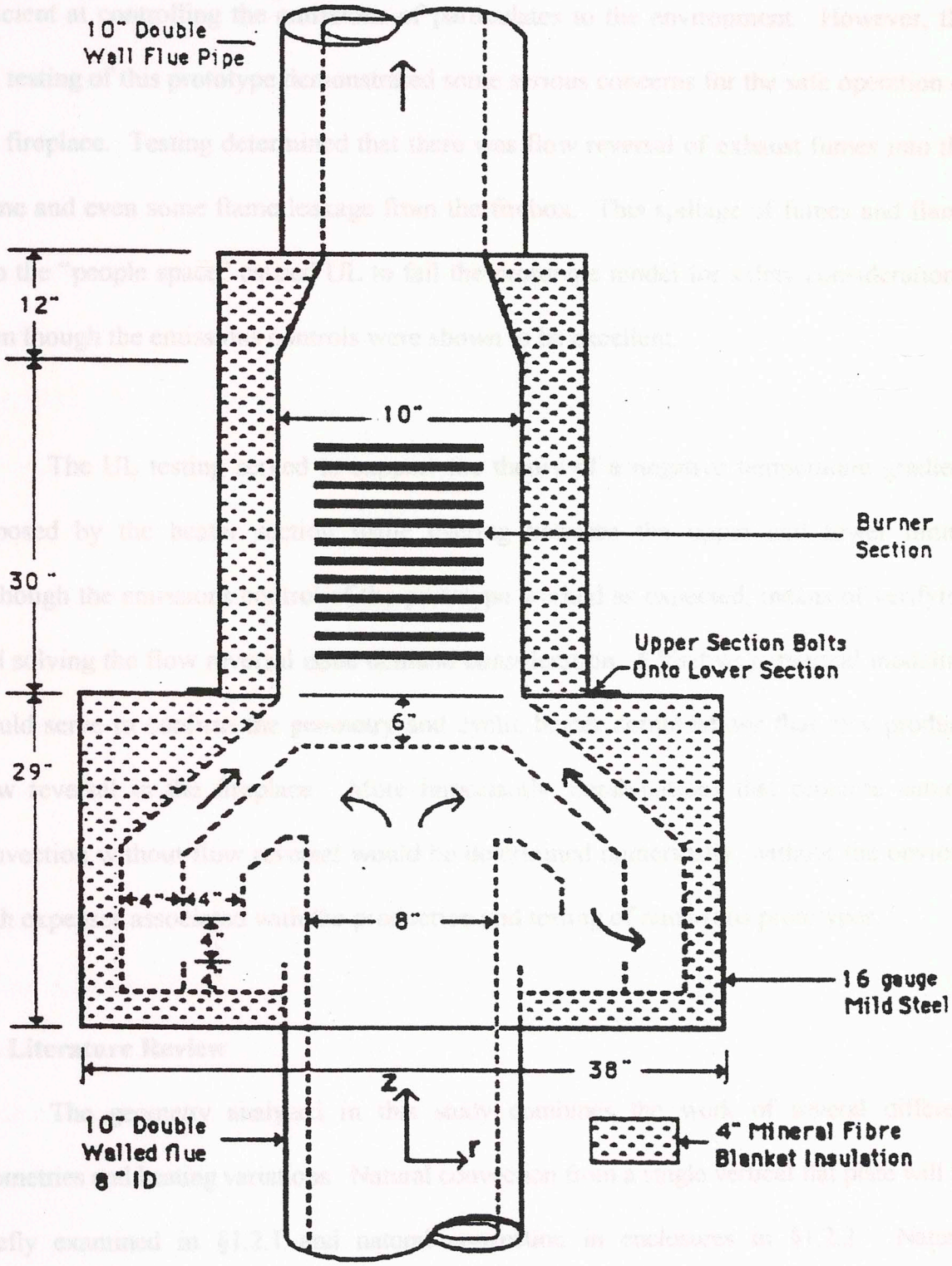

Figure 1.2 Prototype fireplace

Underwriter Laboratories Inc. (UL) conducted preliminary testing of this prototype on June 17, 1995. The UL testing generally concluded that heater elements are efficient at controlling the emissions of particulates to the environment. However, the UL testing of this prototype demonstrated some serious concerns for the safe operation of the fireplace. Testing determined that there was flow reversal of exhaust fumes into the home and even some flame leakage from the firebox. This spillage of fumes and flame into the "people space" caused UL to fail the prototype model for safety considerations, even though the emissions controls were shown to be excellent.

The UL testing served to support the theory of a negative temperature gradient imposed by the heater section while cycling between the upper and lower limits. Although the emissions control of the prototype worked as expected, means of verifying and solving the flow reversal issue demand consideration. Effective numerical modeling would serve to confirm the geometry and cyclic heater combinations that may produce flow reversal in the fireplace. More importantly, combinations that promote natural convection without flow reversal would be determined numerically, without the obvious high expenses associated with the production and testing of numerous prototypes.

1.2 Literature Review

The geometry analyzed in this study combines the work of several different geometries and heating variations. Natural convection from a single vertical flat plate will be briefly examined in §1.2.1 and natural convection in enclosures in §1.2.2. Natural convection between vertical parallel plates will be evaluated in §1.2.3. Vertically vented

enclosures and partial enclosure fires will be reviewed in §1.2.4. The final section, §1.2.5., discusses natural convection in vertical divided channels.

1.2.1 Natural Convection from a Single Vertical Plate

Free convection from a single vertical surface is the most elemental and perhaps most widely studied geometry. The single plate case should be briefly examined as a foundation for understanding other research with more complex geometries and heating conditions. One specific single vertical plate analysis of interest to this study was performed by Cheesewright [5] in 1967. Cheesewright studied laminar natural convection from a plane vertical surface in non-isothermal surroundings. Similarity solutions are derived and numerical solutions of the ordinary differential equations resulting from the similarity transformation are reported. Cheesewright numerically found a specific case that would lead to flow reversal. When the rate of heat transfer from the vertical plate to fluid in the outer part of the boundary layer is less than the heat lost from the boundary to the surroundings, a temperature differential is created. This differential prevents the boundary layer temperature from remaining in line with ambient conditions, which causes the buoyancy of the boundary layer to be overpowered by the buoyancy of the ambient surroundings. This condition of an isothermal surface in non-isothermal surroundings is a special case. However, this case is consistent with the present study, where temperature gradients from cycling heaters are suspected to create non-isothermal surroundings at the heater bundle thereby resulting in flow oscillations and reversal.

1.2.2 Natural Convection in Enclosures

Studies of natural convection in full enclosures also provide important insight and information concerning the model of this study. There has been considerable research into free convection of air in enclosures. In 1961, Eckert and Carlson [6] performed an experimental analysis with a Zehnder-Mach interferometer on the temperature and flow conditions for air enclosed between hot and cold plates with an adiabatic top and bottom. Their tests were for $8.0\text{x}10^4 \leq Gr \leq 2.0\text{x}10^5$ and aspect ratios from 2.5 to 10. They concluded that various flow and temperature regimes exist; specifically conduction, transition, and boundary layer. Below a specific Grashof number and above a certain aspect ratio, heat transfer from the hot to the cold boundary is by conduction through the center part of the cavity. For larger Grashof numbers and smaller aspect ratios, boundary layers exist on the hot and cold walls and the constant temperature lines through the central part of the cavity are nearly horizontal. This indicates heat transfer by the convection of the formed boundary layers. The transition regime occurs at a point between the conduction and boundary layer regimes where the boundary layers have grown together causing an isothermal line in the center of the enclosure. Eckert and Carlson [6] determined the following correlation for the Nusselt number in the boundary layer regime:

$$\text{Nu}_\text{L} = 0.119(Gr)^{0.3}\left(\frac{L}{D}\right)^{-0.1} \tag{1.1}$$

Chu et al. [7] performed a numerical analysis for rectangular cavities with upper and lower walls insulated and a right wall maintained at a uniform cold temperature. The left wall was insulated except for a heater strip positioned at various heights on the wall. The

analysis was for air of Pr = 0.7, aspect ratios ranging from 0.4 to 5, and Rayleigh numbers from 0 to 10^5. For the limiting case of the heater strip occupying the entire left wall, their results were in good agreement with previous investigators.

In 1977, Yin et al. [8] performed another experimental analysis for air contained in an enclosure with differentially heated vertical walls. Their experiment was for a wider range of aspect ratios and Grashof numbers, covering aspect ratios from 4.9 to 78.7 and $1.5\text{x}10^3 \leq \text{Gr} \leq 7.0\text{x}10^6$. Yin et.al. [8] produced results consistent with Eckert and Carlson [6] concerning the conduction, transition, and boundary layer regimes. They produced a Nusselt number correlation that was in good agreement with Eckert and Carlson [6], and with reports by Batchelor [9] and Schmidt et al. [10]

$$\text{Nu}_D = 0.21(Gr_D)^{0.269}\left(\frac{L}{D}\right)^{-0.131} \tag{1.2}$$

The paper by de Vahl Davis and Jones [11, 12] provided a comparison, as well as independent analysis, of natural convection studies for air in a square cavity. Their use of a square cavity with air of Pr = 0.7 for Ra = 10^3, 10^4, 10^5, 10^6, and differentially heated vertical walls allowed for comparison with the multitude of other reports with the same geometry and fluid. The report compared the results of Nusselt number with various grid and mesh sizes, as well as with different numerical techniques, and serves as an excellent summation of the work completed to that date on natural convection in a square cavity.

Another study of natural convection in a square cavity was studied by Cless and Prescott [13] using a liquid metal fluid of Pr = 0.005. Grashof numbers of 3×10^6 and 10^7 were considered with steady and time varying sidewall temperatures. Although the fluid and geometry are not identical to the present study, the formulation of the cooling rates for the time varying sidewall temperatures is of particular interest. In their model, after reaching steady state conditions the time varying thermal boundary conditions are imposed as noted in equations 1.3 and 1.4 below:

$$\theta_{hot} = 0.5 + \theta' (\tau - \tau_o) \tag{1.3}$$

$$\theta_{cold} = -0.5 + \theta' (\tau - \tau_o) \tag{1.4}$$

Equations 1.3 and 1.4 describe the left (hot) and right (cold) wall dimensionless temperatures, respectively. θ' is the dimensionless rate of change of the sidewall temperatures and τ_o is the time at which cooling begins. Each wall is cooled at the same rate to maintain a constant differential temperature between the hot and cold walls. Three cooling rates of θ' = -0.1, -1.0, -2.0 were considered. They found that for θ' = -0.1 there was little noticeable difference in streamline, isotherm, and vorticity plots compared to the steady state boundary conditions. θ' = -1.0 corresponds to a case when the overall rate of energy removal from the system is equal to the rate at which heat conduction occurs across the cavity in the steady state condition. The case of θ' = -2.0 approximates the rate of convection heat transfer in the steady state case. These larger cooling rates resulted in chaotic flow and temperature patterns, with the formation of several secondary cells within the cavity. Secondary cell formation and chaotic flows are of paramount concern to the present study, as the heating and cooling rates of the burner section could result in the disruption of the outward natural convection flow akin to those predicted by Cless and Prescott [13] for their enclosure.

Ju and Chen [14] performed a numerical simulation of natural convection in an enclosure with discrete protruding heaters. The model used five discrete protruding heaters mounted on one vertical wall, with cooling from above, and the other surfaces adiabatic. The working fluid is ethylene glycol with Pr = 100 and $5.0 \times 10^5 \leq Ra \leq 1.0 \times 10^7$. At lower heater powers, a secondary flow cell developed above the uppermost heater and the cooled wall. This secondary flow cell is of interest. Heating elements of the prototype model could develop secondary flow cells, similar to the cells produced in the Ju and Chen [14] study, which could increase channel flow resistance and possibly lead to reversed flow.

1.2.3 Natural Convection between Vertical Parallel Plates

Natural convection between vertical parallel plates provides some of the most important fundamental information for the present study. The flue of the common fireplace can be accurately modeled in two-dimensions as vertical parallel plates. Numerous studies of this geometry have been published and supply critical insight into the natural convection problem associated with fireplaces.

Aung et al. [15] reported a study on developing laminar free convection between parallel plates with asymmetric heating. They studied cases numerically and experimentally for uniform wall temperature (UWT) and uniform heat flux (UHF). Their numerical results generally agreed well with experimental results, with the most dramatic differences having no more than a 10% underpredication or overpredication of Nusselt number. They used the assumption of a uniform entrance velocity profile, which was experimentally confirmed to be

a less-than-accurate approximation and most likely attributed to the errors seen between experimental and numerical results.

Ofi and Hetherington [16] studied natural convection in an open vertical channel using the finite element method. Their analysis was for steady laminar flow with uniform wall temperatures. They employed the variational principle techniques to generate natural boundary conditions at the channel entrance and exit. The formulation of natural boundary conditions for the channel entrance and exit was found to be satisfactory and produced Nusselt number correlations that were in agreement with other authors (such as Bodoia and Osterle [17]).

Further correlation for natural convection between heated vertical plates was reported by Ramanathan and Kumar [18]. This study added a large enclosure to the model in an effort to provide more accurate boundary conditions for the entering and exiting flow conditions. The enclosure boundaries were placed at some distance from the vertical plates to ensure that the enclosure does not affect the flow between the plates yet requires that no entrance or exit conditions at the vertical plates be specified, as flow is allowed to develop naturally. To this end, sensitivity tests determined that the vertical plates should be kept closer to the bottom of the defined enclosure boundary, as the flow out of the channel was more sensitive to the defined enclosure boundaries than the entrance flow.

Ramanthan and Kumar [18] obtained results in agreement with other similar studies, with the exception of the case of small aspect ratios (i.e. less than 10) and small Rayleigh

numbers, where they concluded that vertical conduction is significant and cannot be disregarded as in previous works.

Hung and Chang [19] also used the enclosure type boundary conditions, similar to Ramanthan and Kumar [18], for their vertical finite-length vertical channel. The Grashof number was 10^5 with channel aspect ratios ranging from 1 to 8 and Prandtl numbers of 0.7, 7, and 25. A notable difference is the heating condition used. A transient symmetric isoflux heating condition was employed. This isoflux heating is of a form proposed by Hung and Perng [20]:

$$\frac{q_c}{q_{cs}} = 1 - e^{(-0.0025t)} \tag{1.5}$$

The ratio of q_c to q_{cs} represents the transient convective heat fluxes at time t and at steady state. At time t = 0, the plates and fluid are at the initial temperature T_o. When t > 0, the channel plates are heated according to equation 1.5 until a steady state isoflux value is achieved. Hung and Chang also performed numerical calculations using the same geometry and flux condition for a wider range of Grashof numbers [21]. They used an aspect ratio of 5, Pr = 0.7, and Grashof numbers of $10 \leq Gr \leq 10^8$. This type of modeling is significant for the present study by providing insight into the application of time varying heat flux conditions within a vertical channel.

Aung and Worku [22] studied a mixed convection problem for developing flow and flow reversal in a vertical channel with asymmetric wall temperatures. A forced flow enters the bottom of the vertical parallel plates and is heated as the flow moves up the channel.

They found that for specific Gr/Re ratios, flow separation occurred closer to the entrance of the channel, leading to conditions favorable to flow reversal. Lin et al. [23] studied natural convection in vertical channels with opposing mixed flow. They also determined criteria for the onset of reversed flow due to the opposing buoyancy of the rising heated flow and the downward moving forced flow. Such formulation is parallel to the present study. Air heated in the firebox rises while air cooling at the cyclic heaters falls while the heaters are secured, essentially forming an opposing flow condition as the upward velocity decreases and the relative velocity between the rising air and the slowing heater air increases. As shown by the study of Lin et al. [23], opposing buoyancy force conditions can lead to a reversal of flow.

1.2.4 Vertically Vented Enclosures and Partial Enclosure Fires

The study of vertically vented enclosures and partial enclosure fires represents work that is closely related to the present study. Vertically vented enclosures represent geometries that are most directly associated with the basic shape of a common fireplace. In addition to dealing with a related geometry, the vertically vented enclosures cited here also allow for the entrance effects of a developing flow based on heat generated buoyancy conditions within the enclosure channel. The study of partial enclosure fires also uses related geometric configurations of interest. However, these studies primarily differ from the vertically vented enclosures in that they incorporate chemical reaction rates, such as the Shvab-Zeldovich formulation, to analyze the generated flow patterns consistent with the diffusion flame theory.

One early paper governing laminar convection between vertically heated plates, with entrance effects, was published by Kettleborough [24]. The geometry used by Kettleborough is nearly identical to the vertical parallel plates discussed earlier. However, he included horizontal side boundaries at the channel entrance, effectively creating a stepped channel. He also added, as illustrated in Figure 1.3, an artificial boundary similar to Ramanthan et al. [18] and Hung et al. [19, 21].

Kettleborough [24] used air with $Pr = 0.73$ and $100 \leq Gr \leq 10^4$. Initially the fluid is at rest and the channel walls are at ambient conditions. At time $t \geq 0$, the walls are heated to T_w. The outer boundaries are specified far enough from the entrance to negate their effects on the developing flow into the channel. The critical result from this analysis is the indication of reversed flow in the channel at advanced times for $Gr = 10^4$. The larger Grashof number produces an accelerated flow up the channel. There is also a fairly large horizontal velocity indicated at the channel entrance. Therefore, Kettleborough deduced that the reversed flow resulted from the need to satisfy the continuity equation. Specifically, more flow is exiting the channel than is entering at the actual channel entrance. This requires a reverse flow into the channel from the channel exit in order to maintain continuity. The only condition in which reverse flow did not develop was when the channel walls were far enough apart that they were essentially two independent vertical plates with single boundary layers formed on each wall that do not interfere with each other. This result, that high Grashof numbers induce buoyancy forces of such magnitude that fluid is drawn in at the side of the channel exit, cannot be the result of an assumption of uniform entrance velocity distribution, as the inflow was allowed to form naturally.

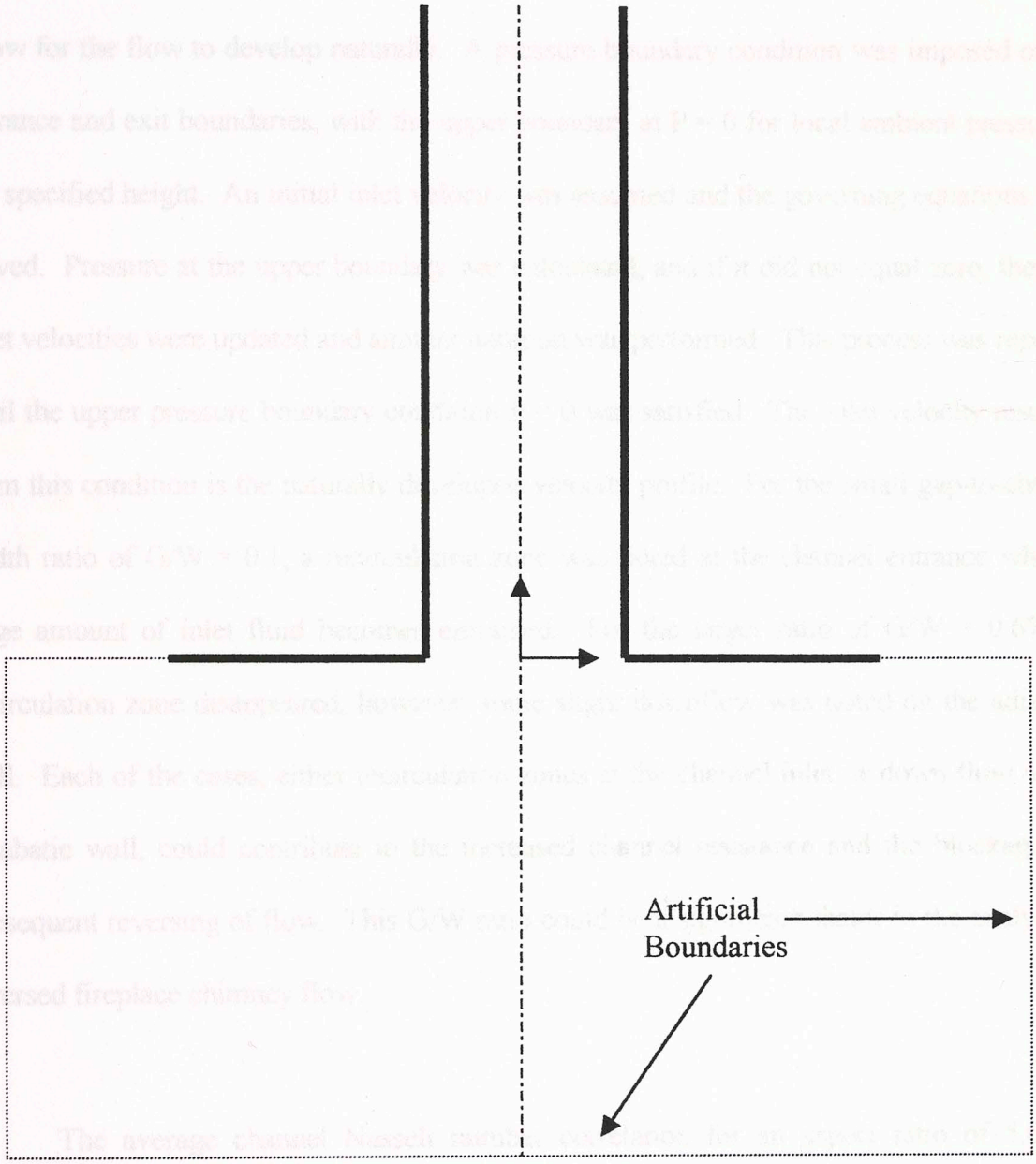

Figure 1.3 Natural convection between vertical parallel plates with artificial inlet boundaries (Kettleborough [24])

Sefcik et al. [25] studied a vertically vented enclosure with top and bottom vents. The left wall is isothermal at T_w and the right wall is adiabatic. The model is illustrated in Figure 1.4. This model did not include artificial boundaries, as in previous examples, to allow for the flow to develop naturally. A pressure boundary condition was imposed on the entrance and exit boundaries, with the upper boundary at P = 0 for local ambient pressure at the specified height. An initial inlet velocity was assumed and the governing equations were solved. Pressure at the upper boundary was calculated, and if it did not equal zero, then the inlet velocities were updated and another iteration was performed. This process was repeated until the upper pressure boundary condition P = 0 was satisfied. The inlet velocity resulting from this condition is the naturally developed velocity profile. For the small gap-to-channel width ratio of G/W = 0.1, a recirculation zone was noted at the channel entrance where a large amount of inlet fluid becomes entrained. For the larger ratio of G/W = 0.67, the recirculation zone disappeared, however, some slight downflow was noted on the adiabatic wall. Each of the cases, either recirculation zones at the channel inlet or down flow on the adiabatic wall, could contribute to the increased channel resistance and the blockage and subsequent reversing of flow. This G/W ratio could be a significant factor in the analysis of reversed fireplace chimney flow.

The average channel Nusselt number correlation for an aspect ratio of 5.0 and channel exit length to channel width of 1.33 was found to be:

$$\mathrm{Nu} = 0.33\mathrm{Gr}^{0.261}\left(\frac{G}{W}\right)^{0.175}\mathrm{Pr}^{0.345} \tag{1.6}$$

for the ranges $0.33 \le G/W \le 1.0$, $10^4 \le Gr \le 10^7$, and $0.7 \le Pr \le 20$.

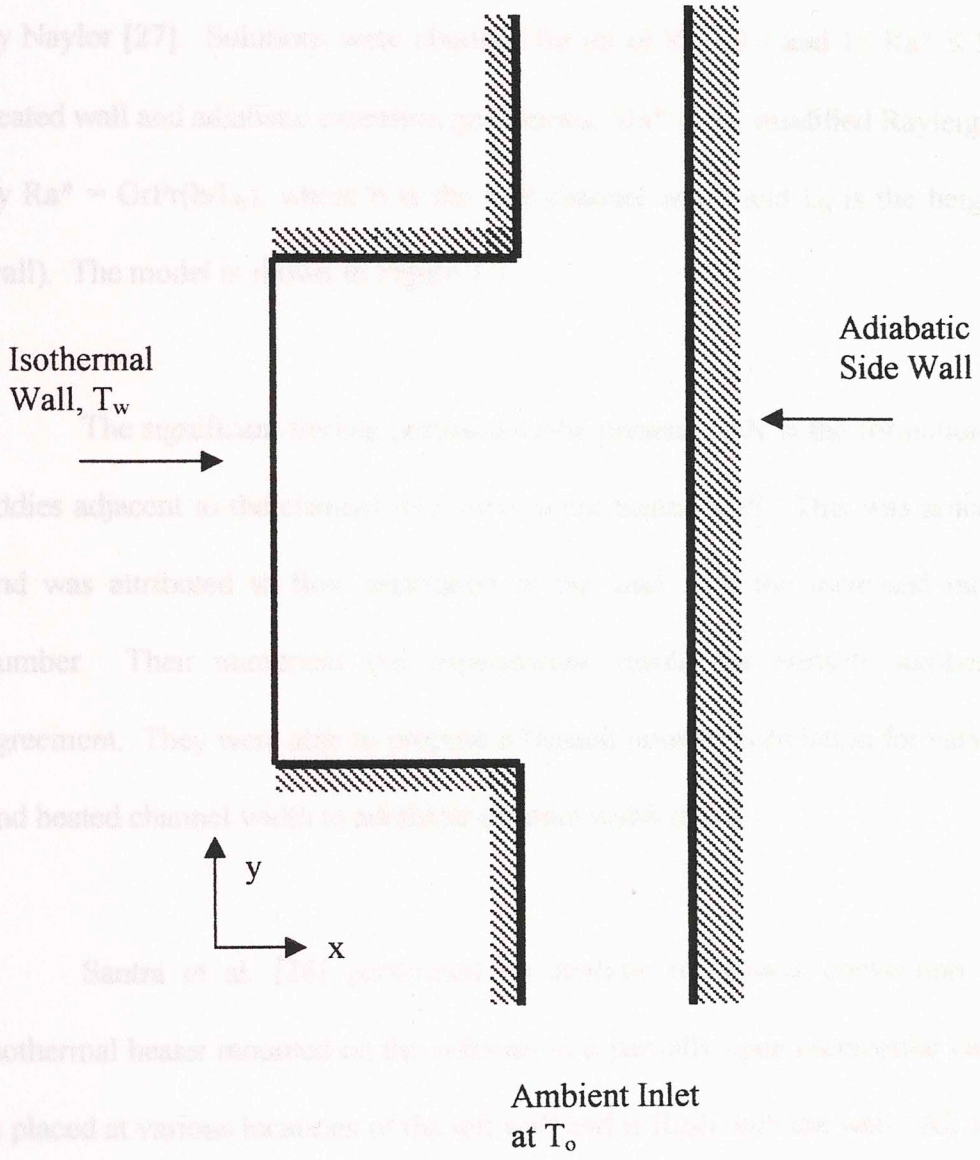

Figure 1.4 Vertically vented enclosure with single isothermal wall (Sefcik et al. [25])

Straatman et al. [26] performed a numerical and experimental analysis of a stepped channel, similar to Kettleborough [24], with the addition of an adiabatic extension at the channel exit with spacing larger than the channel inlet. The lower channel is heated to an isothermal temperature T_w. The inlet boundary is semi-circular and is modeled to allow the natural development of flow into the channel based on Jeffrey-Hamel type flow as described by Naylor [27]. Solutions were obtained for air of $Pr = 0.7$ and $1 \leq Ra^* \leq 500$ with various heated wall and adiabatic extension geometries. Ra^* is the modified Rayleigh number (given by $Ra^* = GrPr(b/L_h)$, where b is the half-channel width and L_h is the height of the heated wall). The model is shown in Figure 1.5.

The significant finding pertinent to the present study is the formation of recirculation eddies adjacent to the channel inlet next to the heated wall. This was noted for $Ra^* = 411$ and was attributed to flow separation at the wall with the increased modified Rayleigh number. Their numerical and experimental results for Nusselt number were in good agreement. They were able to propose a Nusselt number correlation for varying aspect ratios and heated channel width to adiabatic channel width ratios.

Santra et al. [28] performed an analysis of natural convection from a discrete isothermal heater mounted on the sidewall of a partially open rectangular cavity. The heater is placed at various locations of the left wall and is flush with the wall. All surfaces, with the exception of the heater, of course, are adiabatic. Figure 1.6 illustrates the geometry.

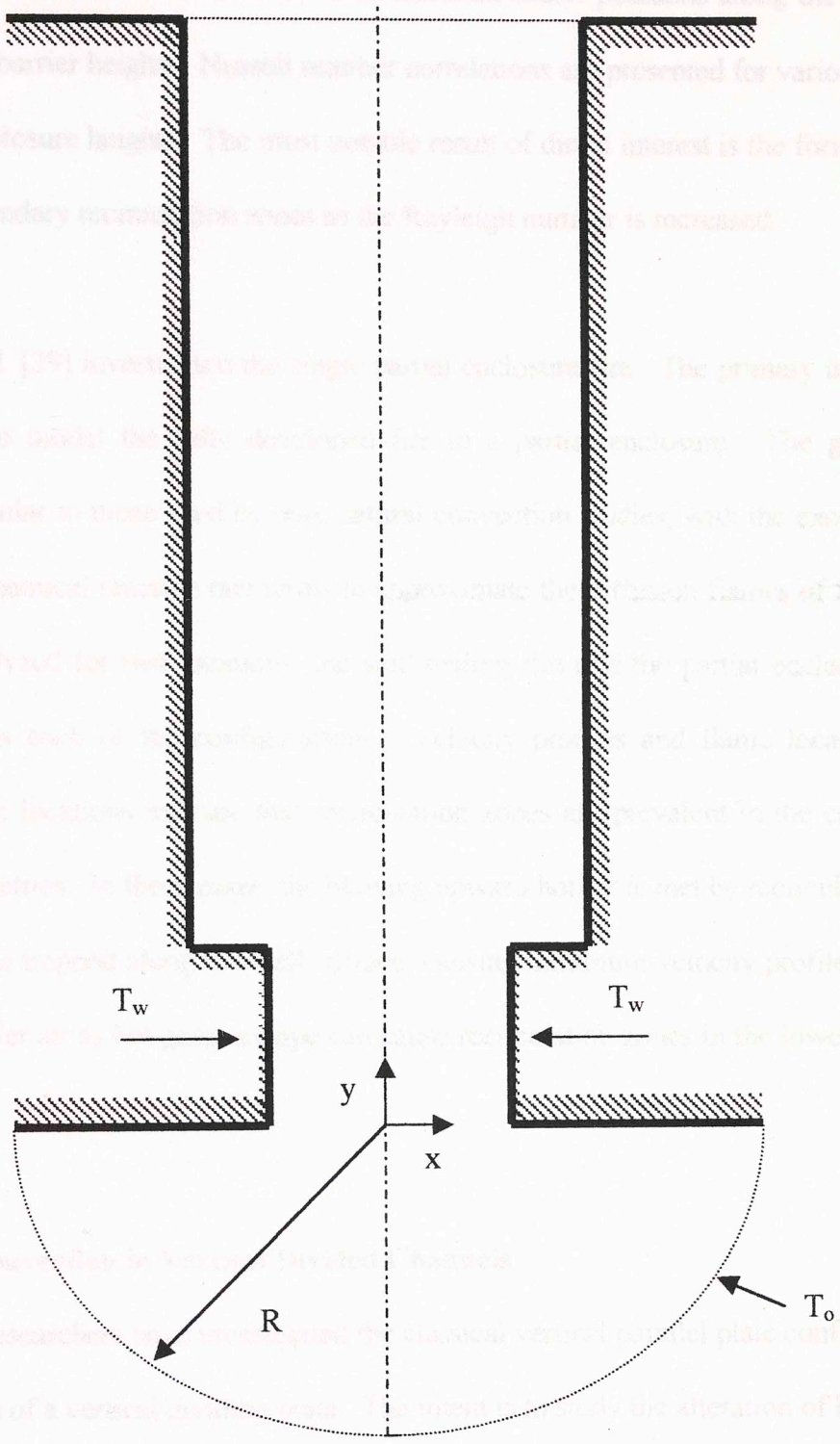

Figure 1.5 Natural convection in a stepped channel with vertical isothermal segments and semi-circular inlet boundary (Straatman et al. [26])

Studies are performed for $10^3 \leq Ra \leq 10^6$ with different heater positions along the left wall and for different barrier heights. Nusselt number correlations are presented for various heater positions and enclosure heights. The most notable result of direct interest is the formation of primary and secondary recirculation zones as the Rayleigh number is increased.

Mao et al. [29] investigated the single partial enclosure fire. The primary interest of this study was to model the fully developed fire in a partial enclosure. The governing equations are similar to those used by pure natural convection studies, with the exception of the addition of chemical reaction rate terms to approximate the diffusion flames of fire. The flames were analyzed for two locations: the wall-ceiling fire and the partial enclosure fire. Figure 1.7 shows each of the configurations. Velocity profiles and flame locations are presented. These locations indicate that recirculation zones are prevalent in the corners of each of the geometries. In these cases, the blowing upward hot air is met by recirculating hot gases that become trapped along the wall surface, causing minimum velocity profiles. Also, the inrush of cooler air as hot gases escape can cause recirculation zones in the lower corners of the enclosure.

1.2.5 Natural Convection in Vertical Divided Channels

Several researchers have investigated the classical vertical parallel plate configuration with the insertion of a vertical dividing plate. The intent is to study the alteration of boundary layer formation by the dividing plate and the effects on the channel Nusselt number. Such research is of interest to the present study in that the heater elements at the upper flue section of the chimney could cause disruption of flow as if they were dividing plates in the channel.

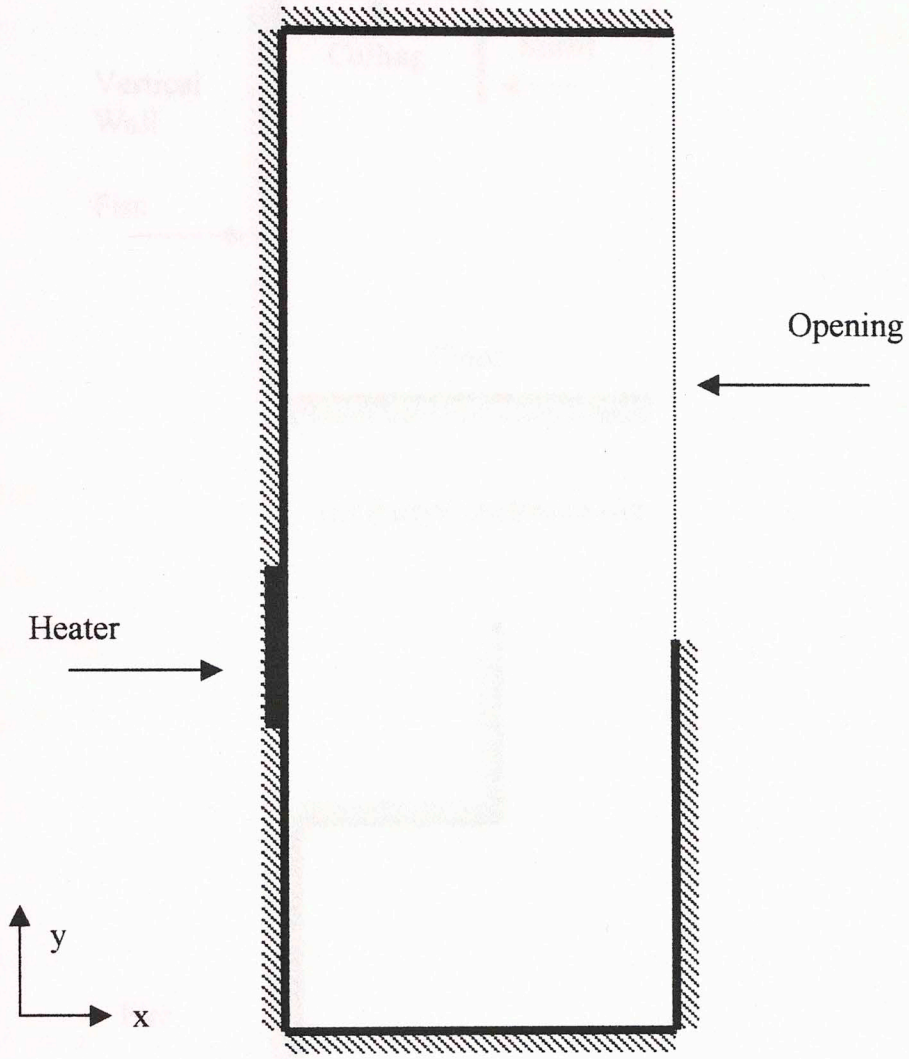

Figure 1.6 Natural convection from a discrete isothermal heater mounted on sidewall of a partially open rectangular cavity (Santra et al. [28])

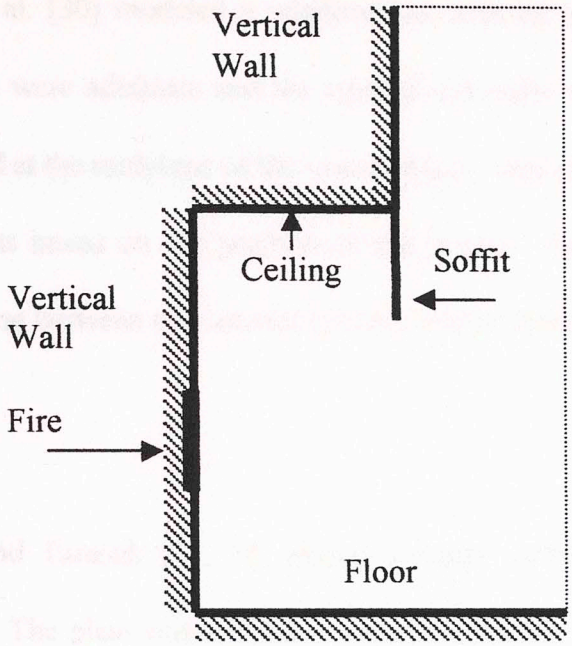

(a) Partial enclosure fire

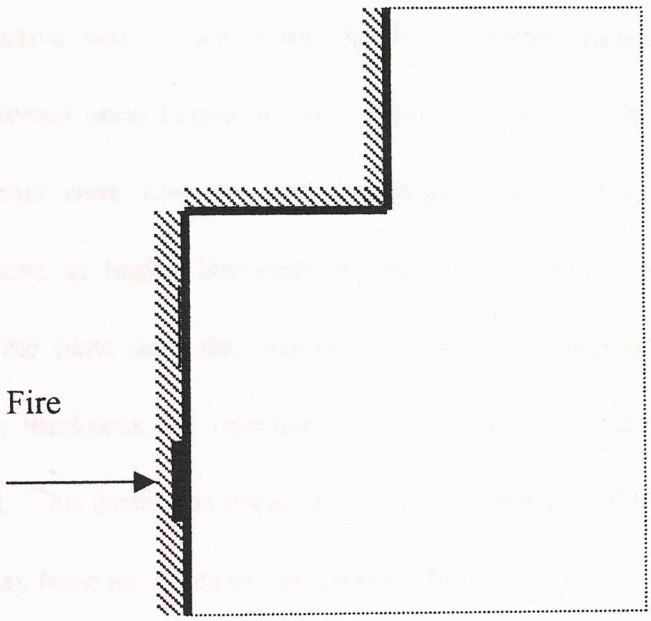

(b) Wall ceiling fire

Figure 1.7 Enclosure Fires: (a) Partial enclosure fire
(b) Wall-ceiling fire (Mao et al. [29])

Zhang et al. [30] modeled a windowpane with an internal screen. The upper and lower boundaries were adiabatic and the vertical sidewalls were differentially heated. The screen was placed at the midplane of the windowpane, with tilting blades to allow for various gap configurations based on the position of the screen. Zhang et al. [30] determined the critical gap spacing between the internal screens where their position would disrupt the flow as desired.

Naylor and Tarasuk [31, 32] placed a single vertical dividing plate in a vertical parallel channel. The plate was studied at various locations within the channel. The model also included the entrance effects by extending the boundaries and allowing the flow to develop using a Jeffrey-Hamel flow model. Figure 1.8 illustrates the geometry analyzed. Their primary objective was to determine the heat transfer enhancements that might be gained with the inserted plate based on the "chimney effect." They determined that heat transfer enhancements were possible with the plate positioned near the entrance of the channel. Furthermore, at higher Rayleigh numbers (10^4) flow separation occurred at the channel inlet with the plate near the channel entrance. Additionally, when the plate was modeled as having thickness, as opposed to a negligible thickness, some channel flow blockage was noted. This finding is important, as the thickness of the heater elements used in the present study may have an effect on the channel flow.

Ohara et al. [33] also reported on the same basic case as Naylor et al [27, 31, 32]. Their general conclusions were consistent with Naylor et al., specifically noting an increase in channel flow resistance with the dividing plate at the top of the channel.

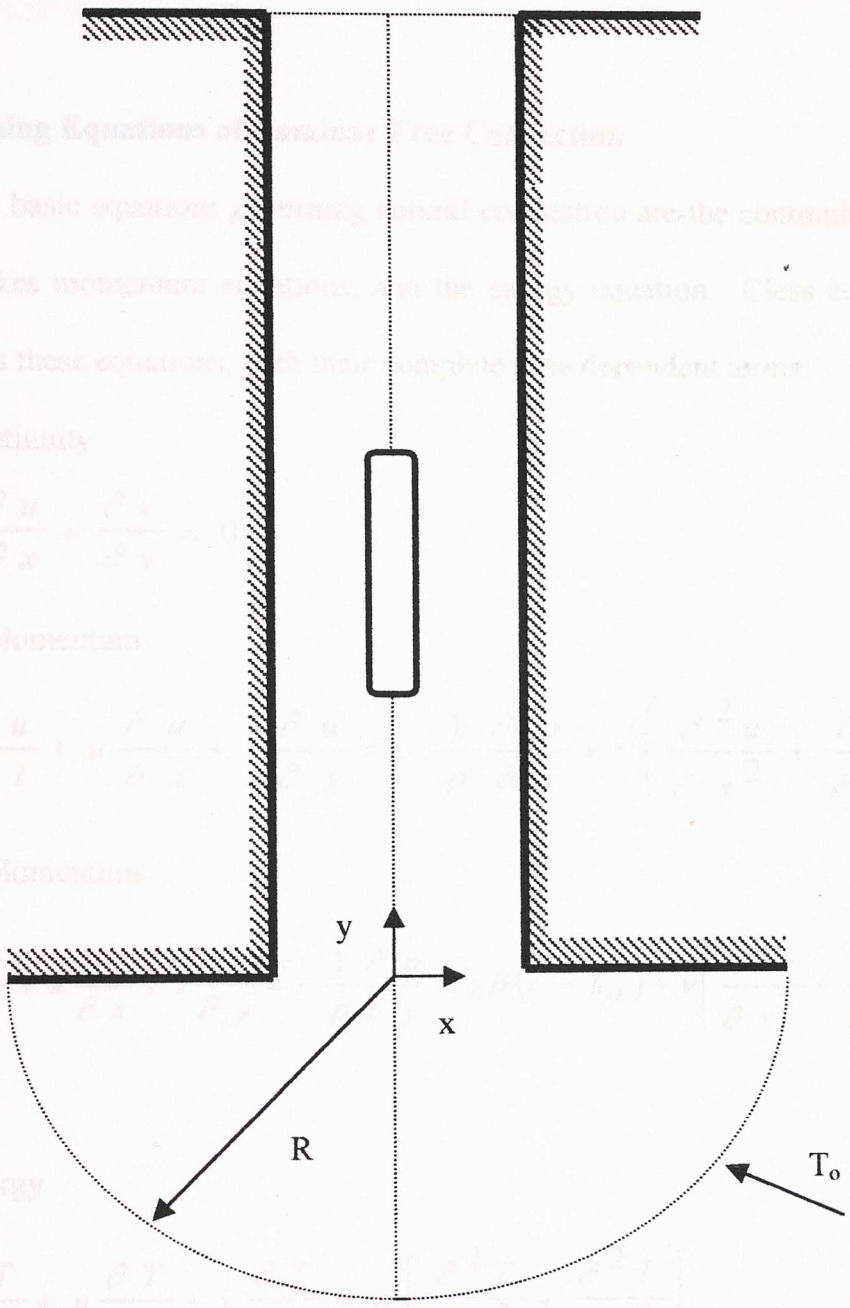

Figure 1.8 Natural convection between vertical parallel plates with isothermal dividing plate and semi-circular inlet boundary (Naylor et al. [27, 31, 32])

CHAPTER 2

NUMERICAL METHOD

2.1 Governing Equations of Laminar Free Convection

The basic equations governing natural convection are the continuity equation, the Navier-Stokes momentum equations, and the energy equation. Cless et al. [13] nicely summarizes these equations, with their complete time dependent terms:

Continuity

$$\frac{\partial u}{\partial x} + \frac{\partial v}{\partial y} = 0 \tag{2.1}$$

X-Momentum

$$\frac{\partial u}{\partial t} + u\frac{\partial u}{\partial x} + v\frac{\partial u}{\partial y} = -\frac{1}{\rho}\frac{\partial p}{\partial x} + \nu\left(\frac{\partial^2 u}{\partial x^2} + \frac{\partial^2 u}{\partial y^2}\right) \tag{2.2}$$

Y-Momentum

$$\frac{\partial v}{\partial t} + u\frac{\partial v}{\partial x} + v\frac{\partial v}{\partial y} = -\frac{1}{\rho}\frac{\partial p}{\partial y} + g\beta(T - T_o) + \nu\left(\frac{\partial^2 v}{\partial x^2} + \frac{\partial^2 v}{\partial y^2}\right) \tag{2.3}$$

Energy

$$\frac{\partial T}{\partial t} + u\frac{\partial T}{\partial x} + v\frac{\partial T}{\partial y} = \alpha\left(\frac{\partial^2 T}{\partial x^2} + \frac{\partial^2 T}{\partial y^2}\right) \tag{2.4}$$

The common Boussinesq approximation is employed. This approximation assumes that the density variation in the continuity and x-momentum equations is

negligible except in the buoyancy term of the y-momentum equation. It is further assumed that the fluid is incompressible. Therefore, density is not a function of pressure and is considered only a function of temperature, i.e. $\rho = \rho(T)$. The following relation more specifically defines the density term

$$\rho = \rho_O\left[1 - \beta_T\left(T - T_O\right)\right] \tag{2.5}$$

where ρ_o and T_o are reference values and β_T is the coefficient of volumetric expansion associated with the temperature variations for a specified fluid. Thermodynamic properties such as specific heat, thermal conductivity, and viscosity are assumed constant and viscous dissipation is neglected.

Solving equations 2.1-2.4 involves introducing reference parameters such that the basic equations can be non-dimensionlized. The advantages of dimensionless equations are discussed by White [34]. By dividing the dependent and independent variables with constant reference values, the basic equations, which are originally dimensional, can be transformed into equations that depend upon fewer parameters for analysis. For example, solving the equations may only require the specification of a Prandtl and Grashof number, as opposed to the multitude of velocities and physical parameters that would otherwise be necessary. This simplification reduces the complexity of the programming required to analyze various flow conditions and geometries. The specific non-dimensional values used in this study and a comparison with values used by other researchers will be presented later when the numerical formulation for this project is discussed.

The concept of stream function and vorticity is also employed to simplify the analysis. White [34] discusses the substitution of a stream function parameter, Ψ. Using the continuity equation, the following identities are given:

$$u = \frac{\partial \Psi}{\partial y}; v = -\frac{\partial \Psi}{\partial x} \tag{2.6}$$

Substitution for the velocities u and v introduces the single variable Ψ. The continuity equation is identically satisfied with this substitution. The vorticity value is given by

$$\Omega = -\nabla^2\Psi \tag{2.7}$$

Plots of stream function and vorticity, along with the isotherm plots, are important in analyzing the results of the free convection flow in the channel (fireplace chimney) and the recirculation or flow reversal which may develop.

2.2 FIDAP

The computational fluid dynamics program FIDAP (Fluid Dynamics Analysis Package) developed by Fluid Dynamics International, Inc., was used to perform the numerical analysis of this study. FIDAP is a finite element program that is widely used in commercial and research applications and will be discussed in more detail in the following sections. The FIDAP program is capable of handling single fluid or multi-component fluid mixtures, single or two-phase flow, under either laminar or turbulent flow conditions. As previously stated, the flow for the present model is a single fluid,

single phase, and laminar flow. The program solves the full elliptical set of continuity, momentum, and energy equations simultaneously. In the following sections details on the design and application of the FIDAP package will be discussed. This is critical to fully comprehending the modeling process used in this study. Without an insight into the options and capabilities of FIDAP, the program is nothing more than a "black box" which simply receives user defined input and produces a result. Understanding the numerical methods used and the means in which the model is meshed, boundary conditions are applied, and parameters are established, allows the user to make more informed judgements as to the confidence in the results obtained.

FIDAP applies the conservation of mass (continuity equation (2.1)) equation in the form

$$\frac{\partial \rho}{\partial t} + \left(\rho u_j\right)_{,j} = 0 \tag{2.8}$$

The $(u_j)_{,j}$ term can be expressed in the more commonly known notation of $\nabla \bullet u$ or div u.

In tensor form, FIDAP views the energy equation (equation 2.4) as

$$\rho c_p \left(\frac{\partial T}{\partial t} + u_i T_i \right) = -q_{i,i} + H \tag{2.9}$$

where T is temperature, c_p is specific heat at constant pressure, q_i is the flux of thermal energy, and H is a general heat generation term potentially composed of several other forms of heat generation. FIDAP assumes Fourier's Law for the q_i heat flux term, which is given in tensor notation

$$q_i = -k_{ij} T_{,j} \tag{2.10}$$

where the thermal conductivity term, k_{ij}, is tensor in form. However, for isotropic fluids, k is a scalar and the equation reduces to

$$q_i = -k T_{,i} \tag{2.11}$$

The heat generation term H is a combination of several terms. FIDAP can account for generation due to applied sources or sinks, viscous dissipation, chemical reactions, and electrical (Joule) heating, and radiation from participating media. Compressible fluid analysis requires the addition of an equation of state relationship. It should be noted that the chemical species terms that would be used for mixed, multiple species fluids have been omitted here, as they are not used in this analysis.

2.3 Boundary Conditions

In general, FIDAP requires specific boundary and initial conditions for the computation domain being analyzed. The momentum equations require that velocity components or surface stresses be specified. The temperature boundary conditions require either a specific temperature or heat flux be prescribed. In the absence of any specification of initial condition, FIDAP assumes "zero" values for all initial condition parameters.

Velocity boundary conditions can be specified for u_x and u_y velocities, or for their tangential and radial equivalents, u_t and u_θ. The "no slip" boundary condition is easily specified by setting "velocity" equal to zero, which zeroes all velocities on the specified boundary. For the case of forced convection, inlet boundary conditions can be specified for either uniform entrance flow with constant velocity or develop flow (including fully-developed) by entering the appropriate polynomial equation.

Temperature and heat flux conditions can be constant or polynomial in form. For the present study, time-varying temperature conditions are necessary to simulate the prototype model being analyzed. FIDAP provides for a time function command which allows any boundary condition, specifically temperature and/or heat flux conditions, to vary based on a user specified input criterion. Therefore, the afterburner heating element can be cycled on and off as directed by the programmer.

Pressure and boundary stress conditions may also be specified. Pressure conditions are easily applied by entering the desired pressure. Surface stress conditions can be established through the expression of the relationship between velocity and pressure conditions. The inlet boundary, for example, can be expressed as having zero stress which forces the inlet velocity and inlet pressure to be directly coupled. The outlet boundary can be left free, set to a specified pressure (e.g. 1 bar or 14.7 psi for atmospheric pressure), or specified with the FIDAP boundary specification of OUTFLOW. This condition approximates the pressure-stress relationship at the outlet of a natural convection system without having to enter an actual boundary pressure value or

constructing a plume region to account for exit conditions. In most conditions, the natural stress-free boundary condition is acceptable. However, if significant temperature or species concentration gradients exist across the outlet boundary, then the natural boundary condition could generate spurious flow separation and recirculation at the outlet boundary. The natural boundary condition dictates that the normal surface stress at the outlet equals zero. Therefore, if the viscous effects are small, then the pressure term is forced to zero to maintain the normal surface stress equal to zero. The OUTFLOW specification eliminates pressure from the natural boundary condition and includes it in the right-hand side vector of the global system of equations. The FIDAP Theory Manual [35] does not specify the exact conditions to be met to satisfy the "significant temperature gradients across the outlet boundary" which would require the OUTFLOW boundary condition be employed. Therefore, since the OUTFLOW condition more accurately models the flow condition, this specification is used for all analyses in this study.

Velocities, temperature, and pressure are the primary variables that are solved during the solution process. FIDAP offers the use of the Penalty Method (Penalty Matrix Evaluation) for the solution of the pressure conditions. This approach is summarized in the FIDAP Theory Manual [35] and in advanced engineering math texts [36]. The Penalty Method discretizes pressure, yet removes it from the global system of equations prior to solving for the unknowns. The elimination of this variable in the solution phase greatly reduces the computer time required for the solution of the unknowns. Pressure is recovered after the solution is reached. Pressure is replaced by the following expression

$$\mathbf{P} = -\left(\frac{1}{\varepsilon}\right)\nabla \mathbf{U} \qquad (2.12)$$

where

P = pressure

ε = penalty parameter (FIDAP default = 10^{-6}, recommended range: 10^{-3} to 10^{-12})

$\nabla \mathbf{U}$ = continuity equation

The Penalty formulation is a discontinuous pressure model and the conservation of mass flow rate is dependent upon the value of ε chosen. Therefore, the FLOWRATE command should be used in the post-processing analysis (FIPOST) to ensure conservation of the inlet and outlet flow rates.

2.4 Discretization

The FIDAP Finite Element Method (FEM) seeks to reduce the continuity, momentum, and energy equations defined previously from an infinite number of degrees of freedom to a finite number of degrees of freedom. The problem is then represented by a system of algebraic equations that describe the model to be solved. The elements are assumed to be fixed in space. Within each element, the dependent variables of velocity, temperature, and pressure are determined for each nodal point. The momentum, continuity, and energy equations are solved with the boundary conditions applied. The results of these equations are known as the residuals or errors. The Galerkin form of the Method of Weighted Residuals [37, 38] is applied to attempt to reduce the errors or residuals to zero.

A critical aspect of applying the FEM is the proper selection of the elements used in the analysis. For two-dimensional analysis, FIDAP offers 4, 8, and 9 node quadrilaterals and 3 and 6 node triangles. The present study uses nine-node quadrilateral elements, as illustrated in Figure 2.1, for the greater accuracy provided by the larger number of nodes-per-element.

Once the geometry is defined and the type of finite element specified, the FIDAP program can proceed with the meshing of the model to be analyzed. FIDAP provides for two means of mesh generation: Mapped and Paved. Mapped meshes form neatly shaped quadrilaterals, i.e. rectangles, at the interval specified by the analyst. The mesh can be

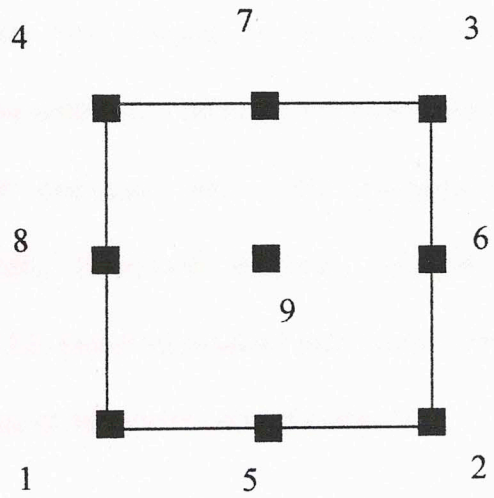

Figure 2.1 A Nine-node quadrilateral used for the present study

graded based on user defined parameters to allow for a larger number of smaller sized elements in areas where higher gradients are expected, such as in the boundary layer region. The limitation of the mapped mesh procedure is that the area to be meshed must be a simple shape. The paved mesh is an automatic mesh generation scheme completed by the FIDAP program. The user must specify the interval for node formation, as in the mapped method, however, FIDAP will generate quadrilaterals (or triangles if desired) for meshing that are not necessarily evenly sized and shaped. The smoothing algorithm attempts to keep each element as uniform as possible; however, for an oddly shaped region the paved mesh will alter the element shapes as necessary to completely map the region. This method is a quick and accurate means of meshing a complex geometry with little difficulty.

FIDAP employs four different solution options to solve the system of nonlinear equations during a steady-state analysis or at each time step of an implicit transient solution: Successive Substitution, Newton-Raphson, Modified-Newton, and Quasi-Newton. For transient analyses, three time integration techniques are available: Backward Euler (implicit), Trapezoid (implicit), and Forward Euler (explicit). The FIDAP Theory Manual [35] provides detailed information on the application, advantages, and disadvantages of each of the above named methods.

Non-dimensional analysis is also fully possible with FIDAP. The FIDAP tutorial manual [39] provides the necessary entries that need to be made to perform a non-

dimensional analysis. Such analyses provide for simple changes in flow conditions without having to make detailed changes in the problem description with variable parameters. Additionally, the FIDAP post-processing model is able to calculate the heat flux at a boundary surface, which for non-dimensional problems is identical to the Nusselt number, which will be discussed in more detail later.

2.5 Code Validation

In order to verify the accurate employment of the FIDAP program an accepted simulation needs to be accurately modeled with the consistent reproduction of the results. Naylor's model [27, 31, 32] of an undivided channel will be used for this verification. Naylor also used the FIDAP program; however, his employment was with an earlier version of FIDAP. The current version used (7.62) has several advantages over earlier versions but should produce identical results to those achieved by Naylor.

The Naylor study was primarily interested in natural convection in a divided vertical channel. However, his first model used for his verification was of free convection in a vertical undivided channel. It is this model of an undivided channel that will serve as the program verification for the present study. The model for the present study, which will be defined later, will follow the same general geometry and boundary conditions of the Naylor model, with some critical exceptions (i.e. cyclic heat flux conditions, adiabatic channel walls, inlet temperature conditions). Therefore, by reproducing the results of the Naylor undivided channel model, the program code for the

present study will only require some slight modifications to conform to the prototype fireplace model of interest.

The undivided channel model studied by Naylor [27] is illustrated in Figure 2.2. The channel has an aspect ratio of 12:1, or L/2b = 12. The channel walls are maintained at a constant temperature of T_w with a no-slip velocity boundary condition. The exit boundary at the top of the channel is simply left with the default stress-free boundary condition. Extending the boundary to encompass the plume region proved to interfere with the natural exiting of the exhaust gases, unless the boundary is placed sufficiently far of the channel exit. However, such an extension of the plume region would require significant finite element meshing which in turn increases the already limited computer memory and processing time. Furthermore, the experimental measurements by Naylor [27] were consistent with the numerical study with respect to the plume region. This experimental evidence supports the decision not to extend the plume region with the FIDAP program. Furthermore, the current version of FIDAP provides for an OUTFLOW boundary condition, as discussed previously, which is specifically designed to account for exit boundaries in natural convection models with significant temperature gradients.

The inlet boundary condition requires further discussion. Naylor's model employs a Jeffrey-Hamel flow approximation on the semi-circular inlet boundary as first proposed by Naylor [27] in 1991 and used by Straatman et. al [26] in 1993. Naylor proposed that for a sufficiently large inlet radius the flow at the inlet of the channel will

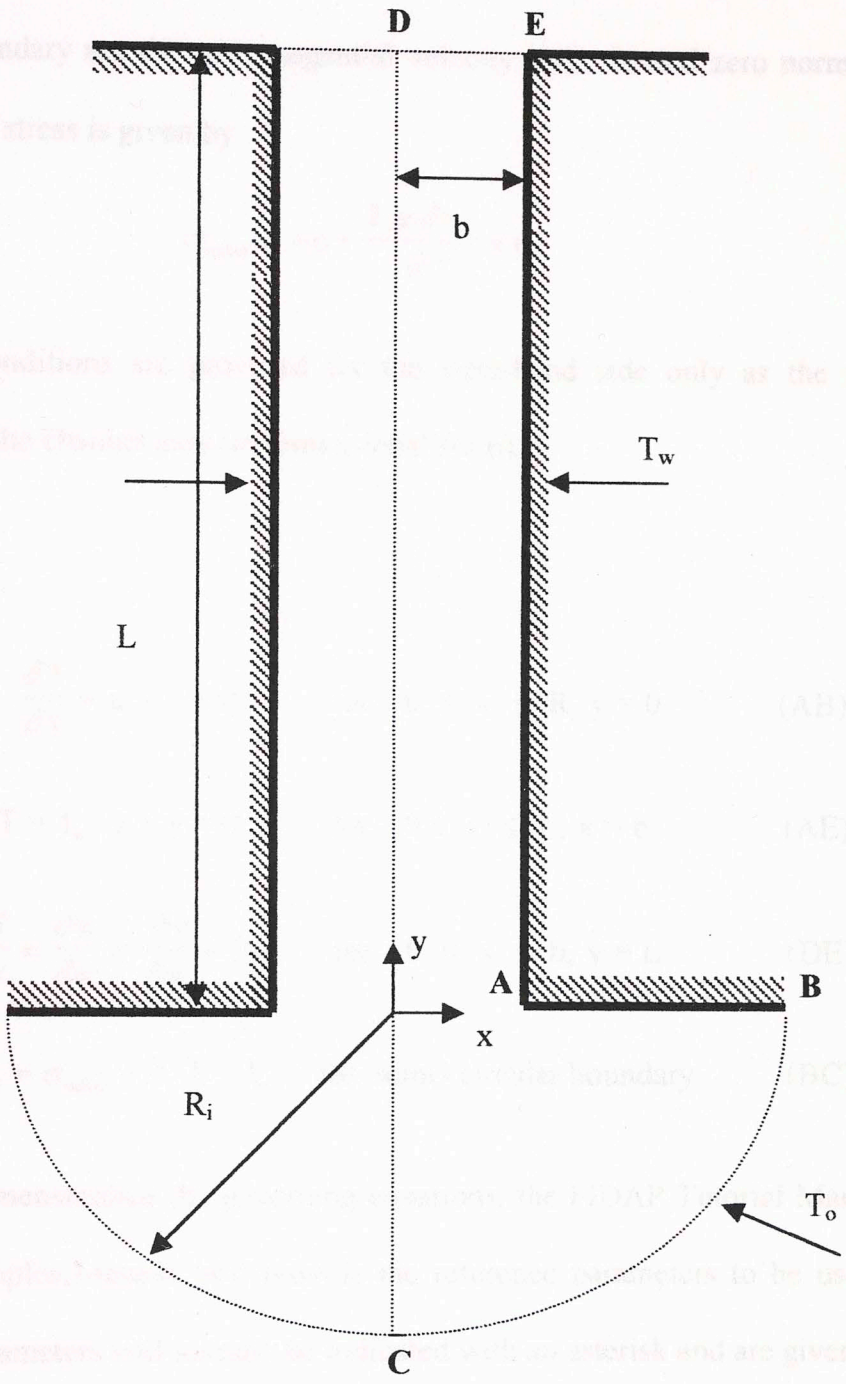

Figure 2.2 The undivided vertical channel studied by Naylor [27]

approximate the flow produced by a point sink. The conditions imposed on the semi-circular inlet boundary are the zero tangential velocity ($v_\theta = 0$) and zero normal stress, where the normal stress is given by

$$\sigma_{radial} = -p + \frac{2\mu \partial v_r}{\partial r} = 0 \qquad (2.13)$$

The boundary conditions are provided for the right-hand side only as the model is symmetric about the channel axis (in dimensional form):

$$\frac{\partial T}{\partial y} = u = v = 0 \qquad \text{for} \quad b \le x \le R,\ y = 0 \qquad (AB)$$

$$T = T_w,\ u = v = 0 \qquad \text{for} \quad 0 \le y \le L,\ x = b \qquad (AE)$$

$$\frac{\partial T}{\partial y} = \frac{\partial u}{\partial y} = \frac{\partial v}{\partial y} = 0 \qquad \text{for} \quad 0 \le x \le b,\ y = L \qquad (DE)$$

$$v_\theta = \sigma_{radial} = 0,\ T = T_o \qquad \text{for semi-circular boundary} \qquad (BC)$$

To non-dimensionlize the governing equations, the FIDAP Tutorial Manual [39] and FIDAP Examples Manual [40] provide the reference parameters to be used. The dimensionless parameters will initially be indicated with an asterisk and are given below:

$$U^* = \frac{u}{U_{ref}} \tag{2.14a}$$

$$V^* = \frac{v}{U_{ref}} \tag{2.14b}$$

$$T^* = \frac{(T - T_o)}{(T_w - T_o)} \tag{2.14c}$$

$$X^* = \frac{x}{b} \tag{2.14d}$$

$$Y^* = \frac{y}{b} \tag{2.14e}$$

$$P^* = \frac{p\,b}{\mu U_{ref}} \tag{2.14f}$$

$$\tau = \frac{t\,U_{ref}}{b} \tag{2.14g}$$

where

$$U_{ref} = \frac{\alpha \mathrm{PrGr}^{1/2}}{b} \quad \text{and} \quad \mathrm{Gr} = \frac{g\beta(T - T_o)b^3\rho^2}{\mu^2} \tag{2.14h}$$

Therefore, the dimensionless steady state governing equations are (with the asterisks dropped):

$$\frac{\partial U}{\partial X} + \frac{\partial V}{\partial Y} = 0 \tag{2.15}$$

$$Gr^{\frac{1}{2}}\left(U\frac{\partial U}{\partial X} + V\frac{\partial U}{\partial Y}\right) = -\frac{\partial P}{\partial X} + \left(\frac{\partial^2 U}{\partial X^2} + \frac{\partial^2 U}{\partial Y^2}\right) \tag{2.16}$$

$$Gr^{\frac{1}{2}}\left(U\frac{\partial V}{\partial X} + V\frac{\partial V}{\partial Y}\right) = -\frac{\partial P}{\partial Y} + Gr^{\frac{1}{2}}T + \left(\frac{\partial^2 V}{\partial X^2} + \frac{\partial^2 V}{\partial Y^2}\right) \tag{2.17}$$

$$Gr^{\frac{1}{2}}\,\mathrm{Pr}\left(U\frac{\partial T}{\partial X}+V\frac{\partial T}{\partial Y}\right)=\left(\frac{\partial^2 T}{\partial X^2}+\frac{\partial^2 T}{\partial Y^2}\right) \tag{2.18}$$

The dimensionless boundary conditions then become:

$$\frac{\partial \mathrm{T}}{\partial \mathrm{Y}}=\mathrm{U}=\mathrm{V}=0 \qquad \text{for} \quad \mathrm{b}\le \mathrm{x}\le \mathrm{R},\ \mathrm{Y}=0 \tag{AB}$$

$$\mathrm{T}=1.0,\ \mathrm{U}=\mathrm{V}=0 \qquad \text{for} \quad 0\le \mathrm{Y}\le \frac{\mathrm{L}}{\mathrm{b}},\ \mathrm{X}=1.0 \tag{AE}$$

$$\frac{\partial \mathrm{T}}{\partial \mathrm{Y}}=\frac{\partial \mathrm{U}}{\partial \mathrm{Y}}=\frac{\partial \mathrm{V}}{\partial \mathrm{Y}}=0 \qquad \text{for} \quad 0\le \mathrm{X}\le 1.0,\ \mathrm{Y}=\frac{\mathrm{L}}{\mathrm{b}} \tag{DE}$$

$$\sigma_{\text{radial}}=\mathrm{V}_\theta=-P+\frac{2\,\partial V_r}{\partial R}=0,\ \mathrm{T}=0 \qquad \text{for semi-circular boundary} \tag{BC}$$

As is evident from the boundary conditions and problem statement, this problem could be analyzed using the symmetrical property along the y-axis. By taking advantage of this property the computer time and memory required can be greatly reduced. The only additional boundary condition necessary is to set the velocity component normal to the line-of-symmetry equal to zero. In this case, setting U = 0 along the symmetrical boundary satisfies this condition. The illustration of the symmetrical case is shown in Figure 2.3. Temperature and the y direction velocity, V, are allowed to vary during the iterative process along the symmetrical boundary. The flow and temperature fields developed can then be "folded" to illustrate the velocity and temperature for the full channel.

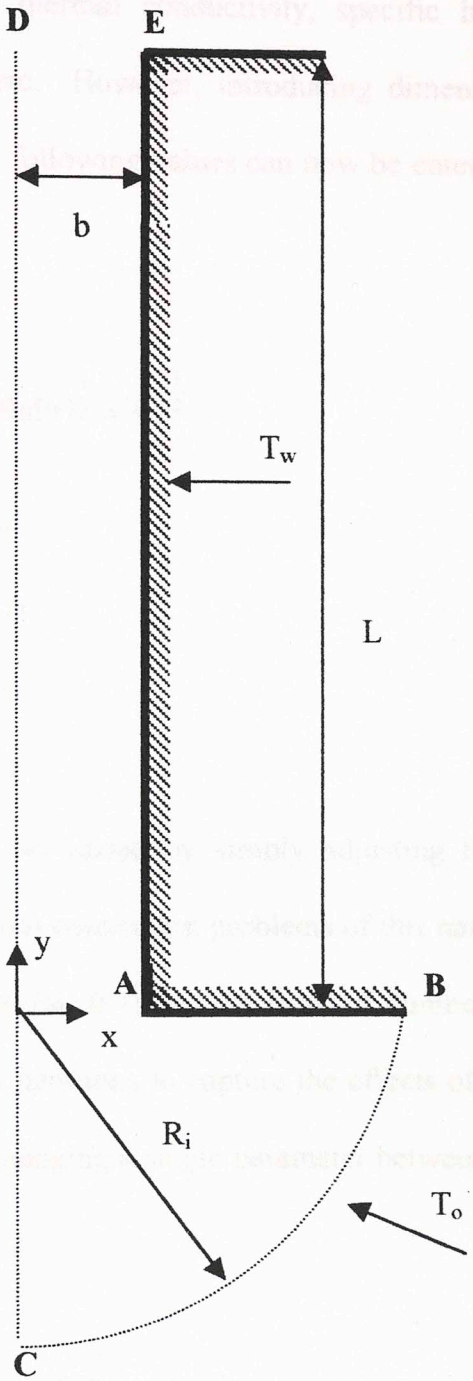

Figure 2.3 Naylor's undivided symmetrical channel model [27]

FIDAP is designed to allow specific properties to be entered for all necessary terms, such as density, viscosity, thermal conductivity, specific heat capacity, and coefficient of thermal expansion, etc. However, introducing dimensionless equations poses no difficulty for FIDAP. The following values can now be entered during the pre-processing stage of FIDAP:

$$\rho = (\mathrm{RaPr})^{\frac{1}{2}} = \mathrm{Gr}^{\frac{1}{2}} \tag{2.19a}$$

$$c_p = \mathrm{Pr} \tag{2.19b}$$

$$g = 1.0 \tag{2.19c}$$

$$\beta = 1.0 \tag{2.19d}$$

$$k = 1.0 \tag{2.19e}$$

Therefore, the problem can easily be varied by simply adjusting the Prandtl and/or Grashof numbers. In fact, most natural convection problems of this nature are performed for air with the Prandtl number fixed (at 0.7) and the Grashof number or, in effect, the Rayleigh number is altered between iterations to capture the effects of different buoyant conditions. The advantage of only changing a single parameter between iterations should be obvious.

Another advantage to the use of dimensionless equations concerns the analysis performed in the FIDAP post-processing stage. The Nusselt number is defined as

$$\mathrm{Nu} = \frac{hL}{k} \quad \text{where} \quad h = \frac{q}{\Delta T} \tag{2.20}$$

The dimensionless heat flux is given by

$$q^* = \frac{q}{Q} = -k\frac{\partial T^*}{\partial X}, \text{ where } Q = k\frac{\Delta T}{L} \tag{2.21}$$

Therefore, after substitution, the Nusselt number is given by

$$Nu = \frac{qL}{k\,\Delta T} = q^*, \qquad \text{where } q^* \text{ is the dimensionlss heat flux.} \tag{2.22}$$

Finally, it is seen that, for dimensionless problems, Nusselt number is equivalent to the heat flux given by the FIDAP post-processing heat flux analysis. This is another powerful argument for the use of dimensionless parameters, because the Nusselt number can be given directly by FIDAP without the need to generate user defined subroutines for the integration of temperature over the channel wall to determine the heat flux. Although the determination of Nu is not of prime importance in the present study, it is necessary for the program verification and it will be used here as the critical parameter for comparison of numerical results. However, the Nusselt number could be of importance to the present study from a heat transfer aspect. Specifically, the cyclic heater modeled here could easily represent a cyclic load in a PCB or other electronic application, in which case the potential disruption of the natural buoyancy flow would be of great significance.

Another useful option in FIDAP is the RESTART simulation command. This option allows the problem to be solved for varying parameters, such as the Grashof number, by using the previous solution as the initial starting condition for the next

problem. For example, the initial steady state problem may be solved for $Gr = 10^2$. The next iteration may then be performed for $Gr = 10^3$ using the previous solution with $Gr = 10^2$ as the initial condition for the current formulation. This method of restarting allows for solutions to be viewed for increasing values of Grashof number and speeds the solution of larger Grashof number problems by using the already available solutions as the starting points.

The results obtained in this study for the undivided channel are compared with those obtained by Naylor [27] for an undivided channel with $L/b = 24$ and $50 \leq Gr \leq 10^4$, for air with $Pr = 0.7$. The wall Nusselt number, buoyancy-induced flow rate, isotherm and streamline plots, are compared for verification of the FIDAP program for current applications. This model was chosen for program validation due to its similarity to the model used in the present study.

The undivided channel has a half-channel aspect ratio of 24 with a semi-circular inlet region of $R_{inlet} = 5$. The model used the now outdated FIDAP mesh generator FIMESH. This mesh generation program is a code-based program without the significant graphical user interface capabilities of the FIGEN mesh generator used in this analysis. FIMESH requires nodal points to be entered in both logical space and integer space in order to establish the appropriate points for mesh generation whereas FIGEN has graphical point-and-click mesh generation capabilities.

Each model uses nine-node quadrilaterals for the finite elements. However, the previous model used 2,456 elements with a total of 10,033 nodes. This required about 1.7 CPU-hours for convergence to four-digit accuracy. The present model was significantly less dense, with only 694 elements with 2,411 nodes. The solution converged in only minutes with 24% of the nodes used. Figure 2.4 shows a side-by-side comparison of the inlet region and channel meshes. The inlet region of the verification model uses an automatic paved mesh generator, which accounts for the non-uniform shape of the elements.

The data used for comparison is the Nusselt number and the buoyancy-induced flow rate. Naylor [27] calculated the Nusselt number by supplying a subroutine which calculated the heat balance in the channel by specifying integrals to calculate the heat convected out of the top of the channel, heat convected into the channel at the entrance, and the heat conducted out of the channel entrance. Similarly, the dimensionless buoyancy-induced flow rate was determined by integrating the velocity at the channel outlet. The present version of FIDAP allows for direct computation of the channel exit flow rate and Nusselt number in the postprocessor. Table 2.1 compares the Nusselt number and buoyancy-induced flow rates (Q_e) for the range of Grashof numbers.

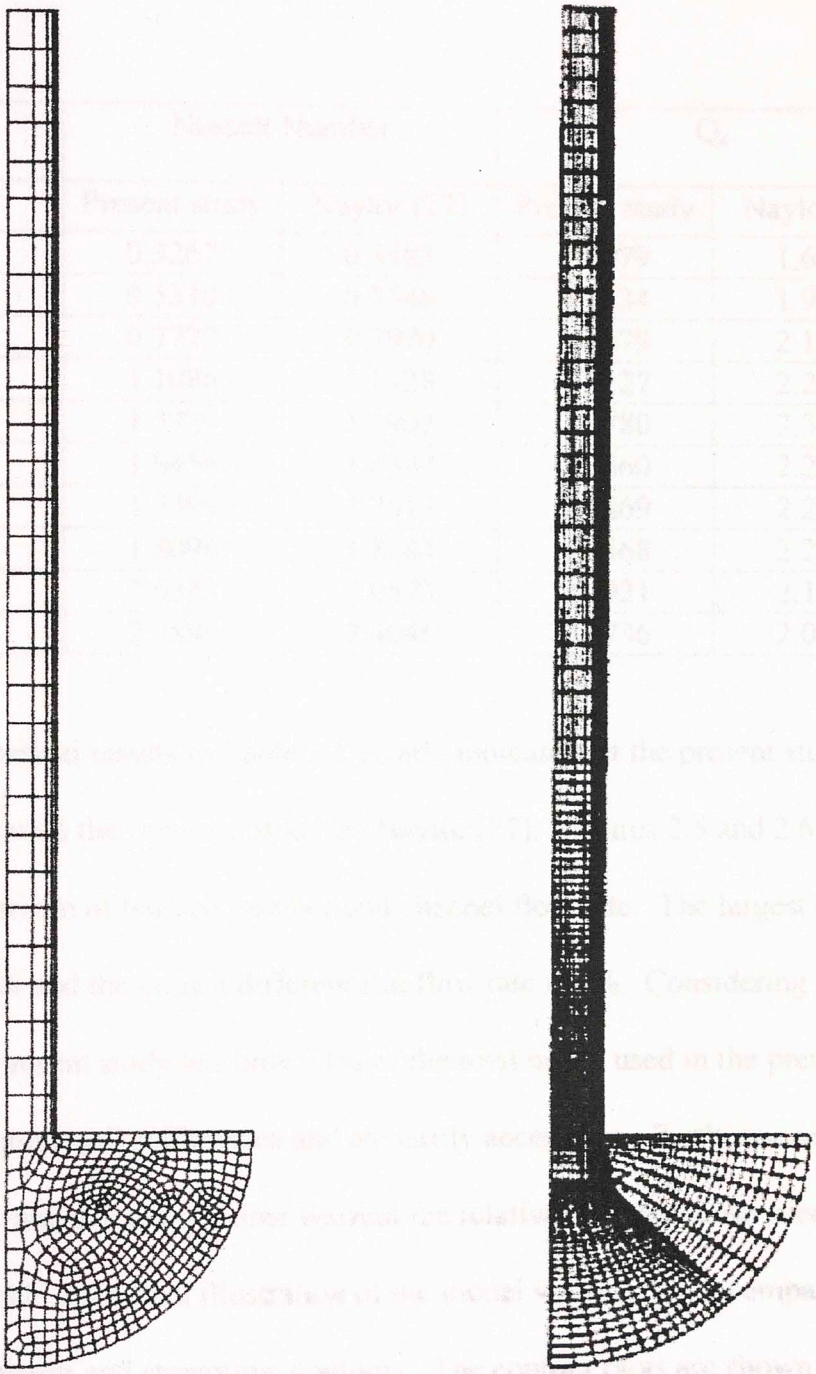

(a) (b)

Figure 2.4 Finite element mesh used for code verification:
(a) Verification model (b) Naylor's model [27]

Table 2.1 Comparison of numerical results for natural convection in an undivided vertical channel

	Nusselt Number		Q_e	
Gr	Present study	Naylor [27]	Present study	Naylor [27]
50	0.3267	0.3483	1.6979	1.6967
100	0.5310	0.5546	1.9734	1.9649
200	0.7722	0.7970	2.1679	2.1512
500	1.1086	1.1328	2.3127	2.2780
1,000	1.3729	1.3902	2.3780	2.3046
2,000	1.6456	1.6597	2.3860	2.2821
2,500	1.7399	1.7513	2.3869	2.2726
3,000	1.8096	1.8284	2.3468	2.2574
5,000	2.0383	2.0573	2.2921	2.1978
10,000	2.3899	2.4046	2.1736	2.0734

The numerical results in Table 2.1 clearly indicate that the present study is in good agreement with the previous study by Naylor [27]. Figures 2.5 and 2.6 show the graphical comparison of Nusselt number and channel flow rate. The largest difference in Nu number is 2% and the largest difference in flow rate is 5%. Considering that the mesh has used in the present study has only 24% of the total nodes used in the previous model, 2 and 5 percent are small differences and are easily acceptable. Furthermore, the savings in CPU memory and calculation time warrant the relatively coarse mesh used in the verification model. As a final illustration of the model verification, a comparison is made between the isotherm and streamline contours. The contour plots are shown in Figures 2.7 and 2.8 for Gr = 50 and Figures 2.9 and 2.10 for Gr = 10^4.

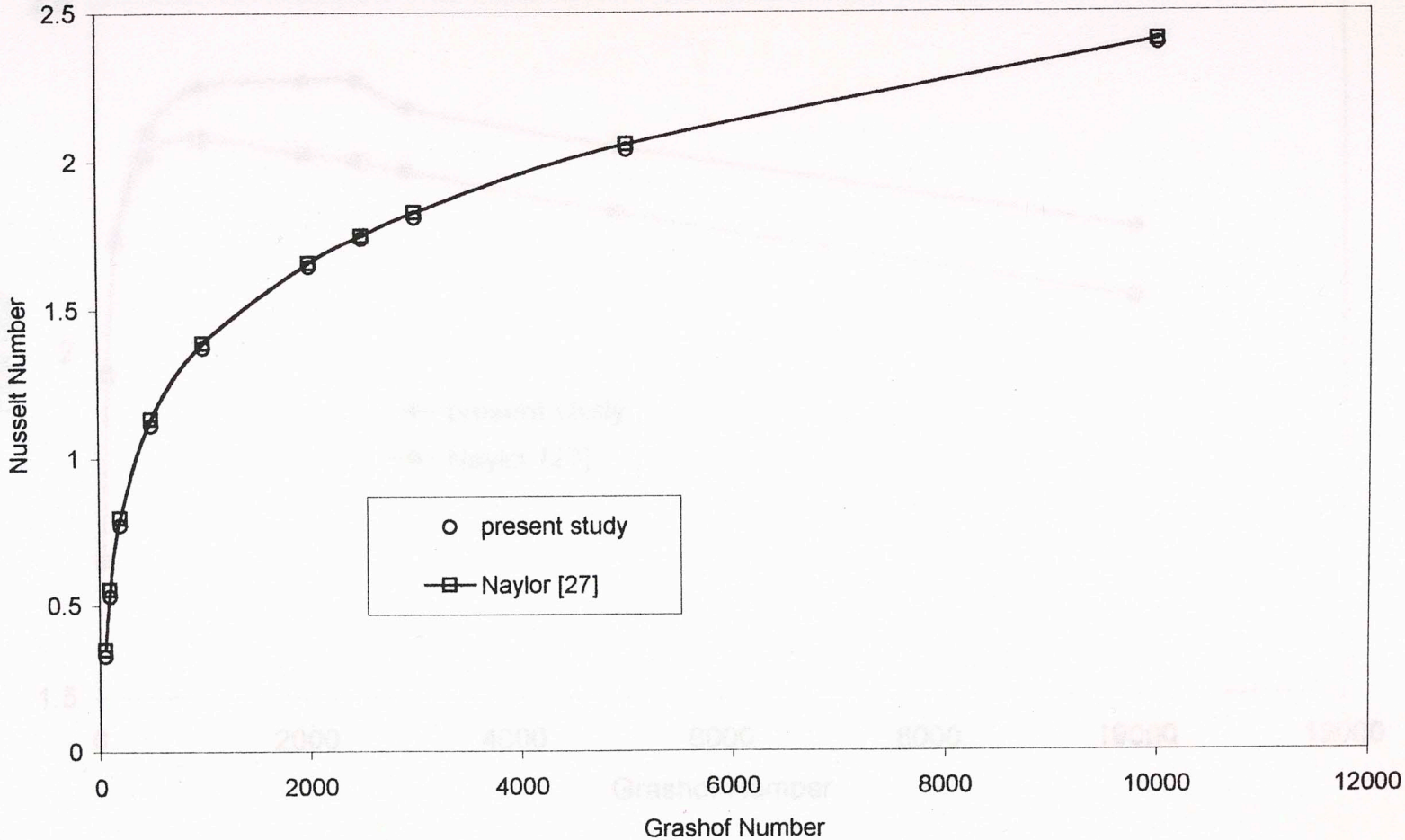

Figure 2.5 Nusselt number comparison between present study and Naylor [27]

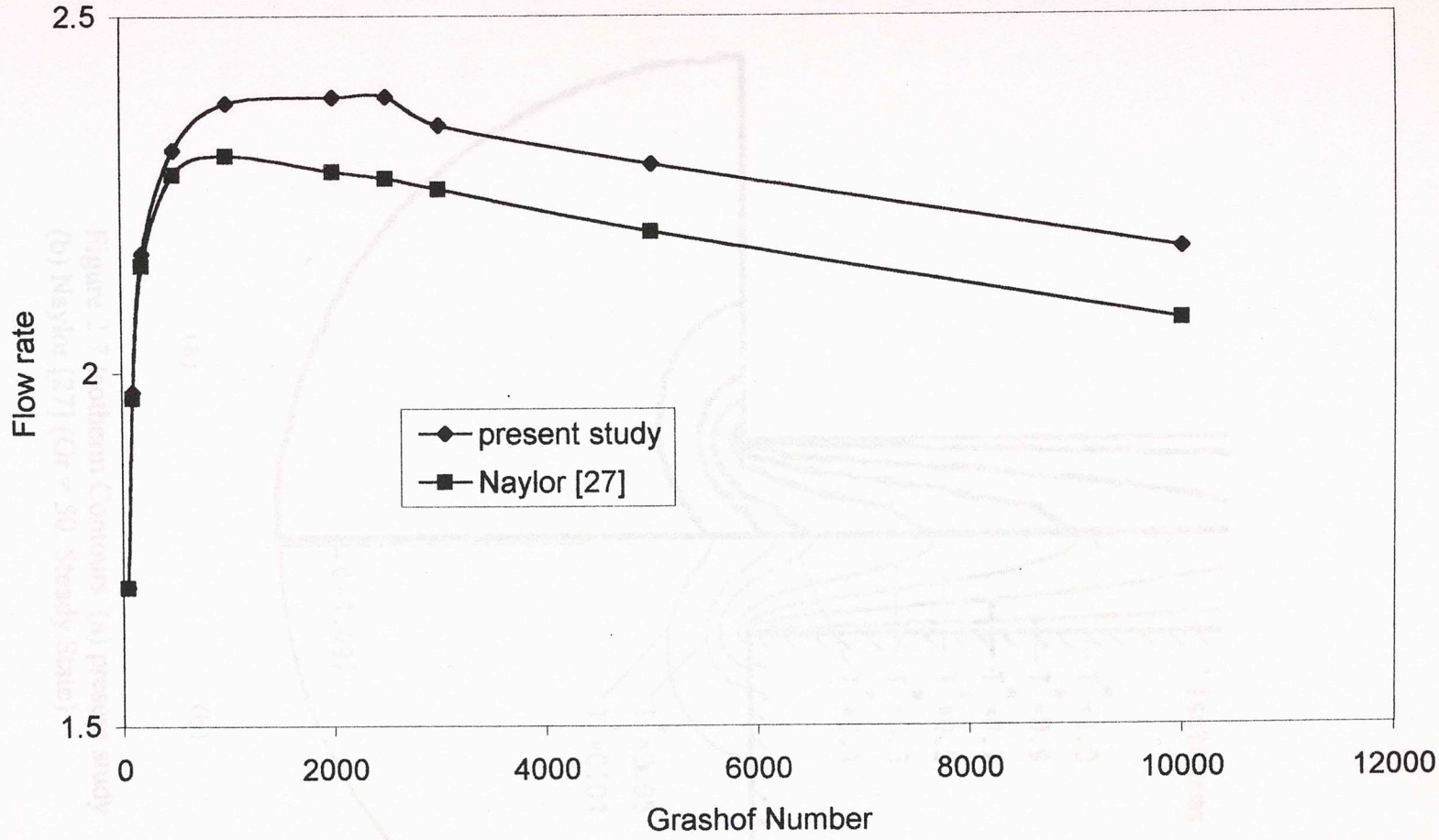

Figure 2.6 Flow rate comparison between present study and Naylor [27]

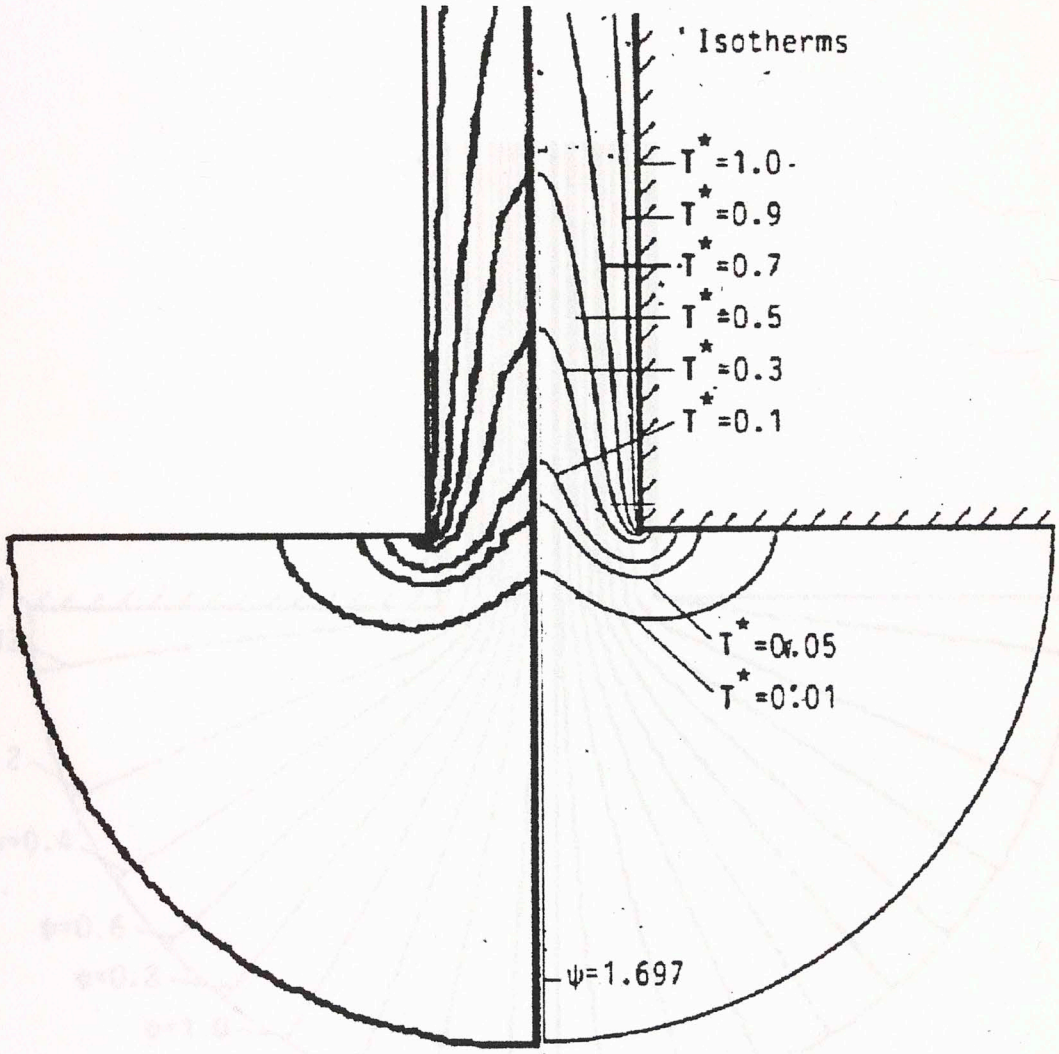

(a) (b)

Figure 2.7 Isotherm Contours: (a) present study
(b) Naylor [27] (Gr = 50, Steady State)

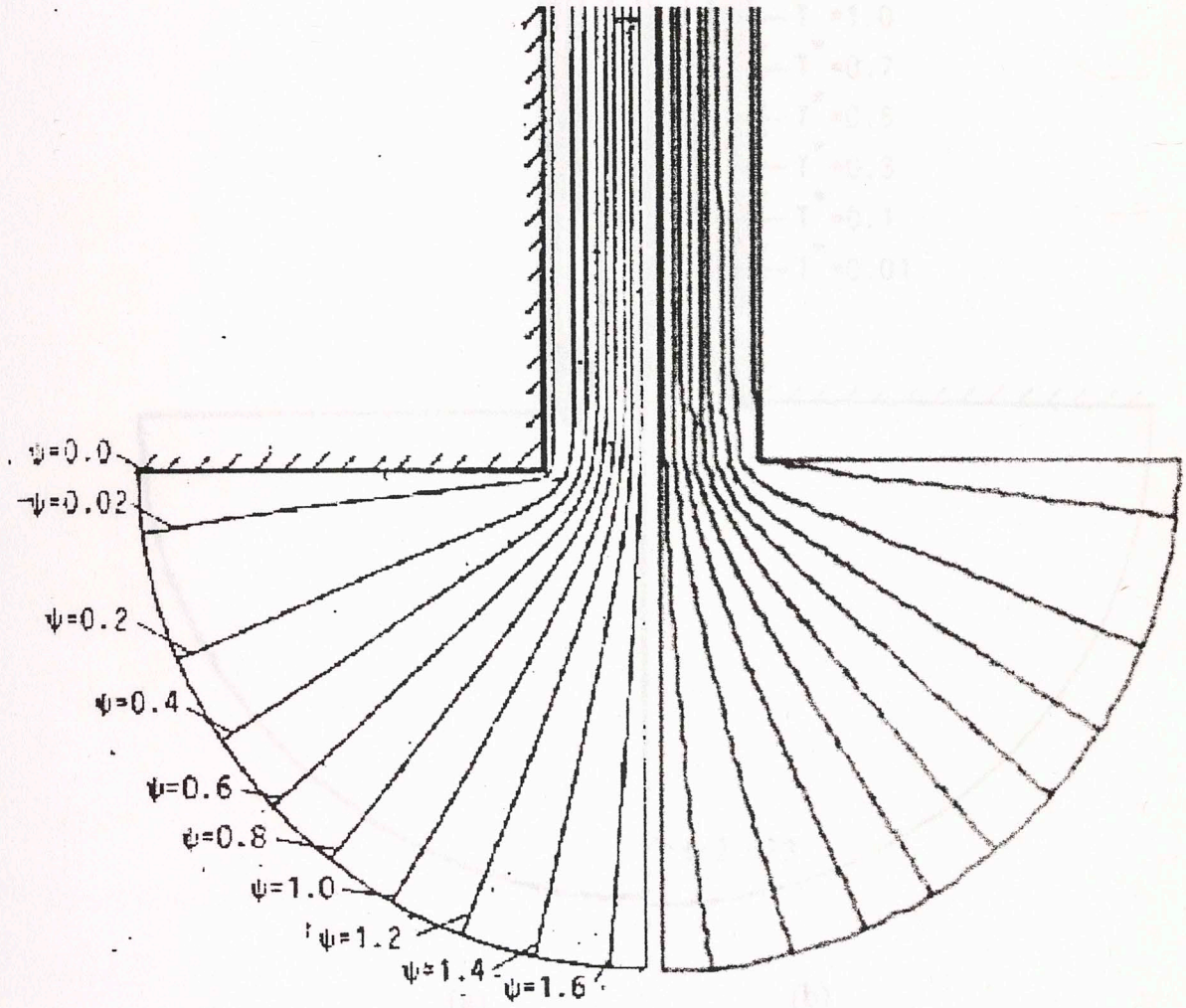

(a) (b)

Figure 2.8 Streamline Contours ($\Delta\Psi = 0.2$):
(a) Naylor [27] (b) present study (Gr = 50, Steady State)

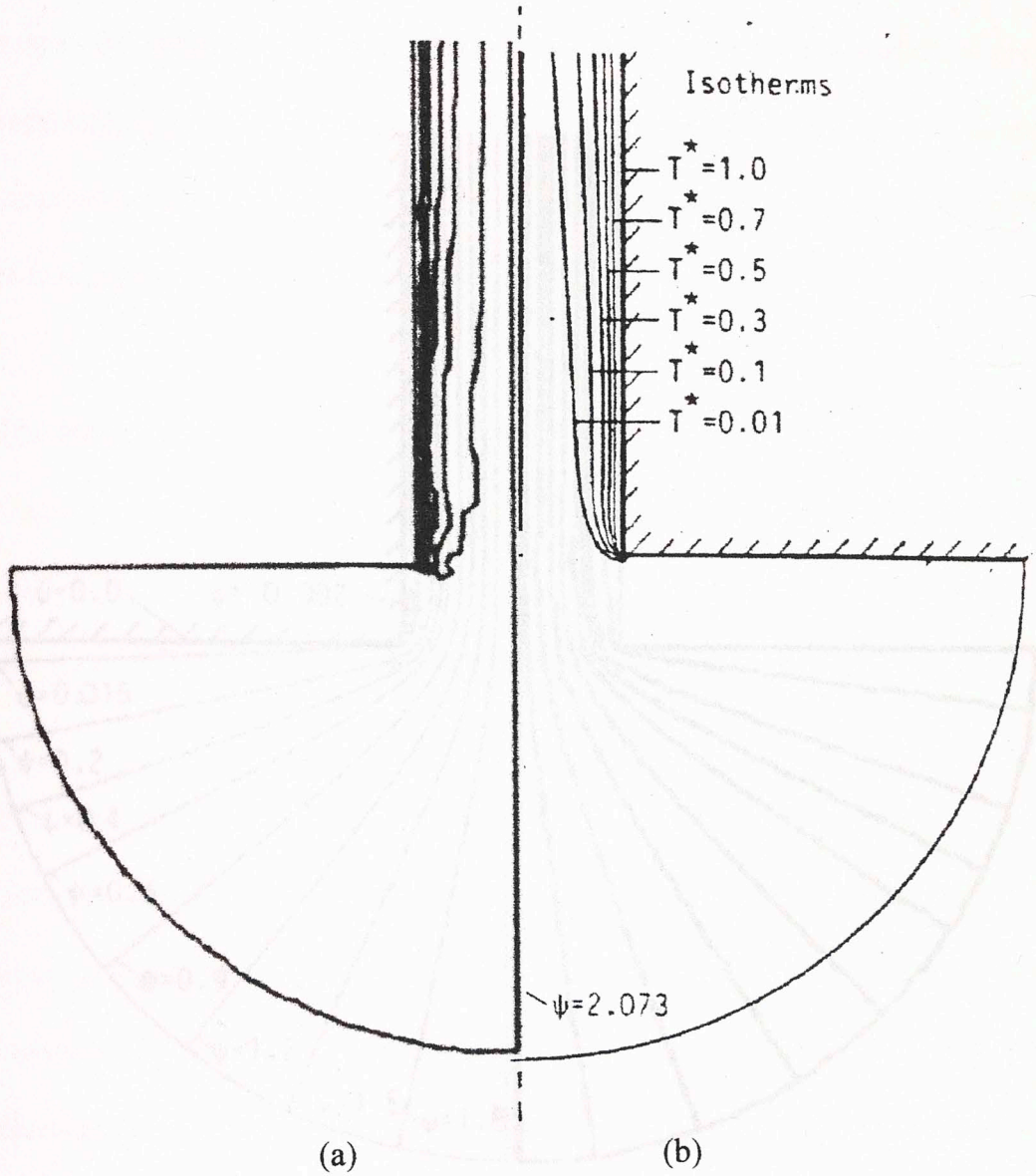

Figure 2.9 Isotherm Contours: (a) present study (b) Naylor [27] ($Gr = 10^4$, Steady State)

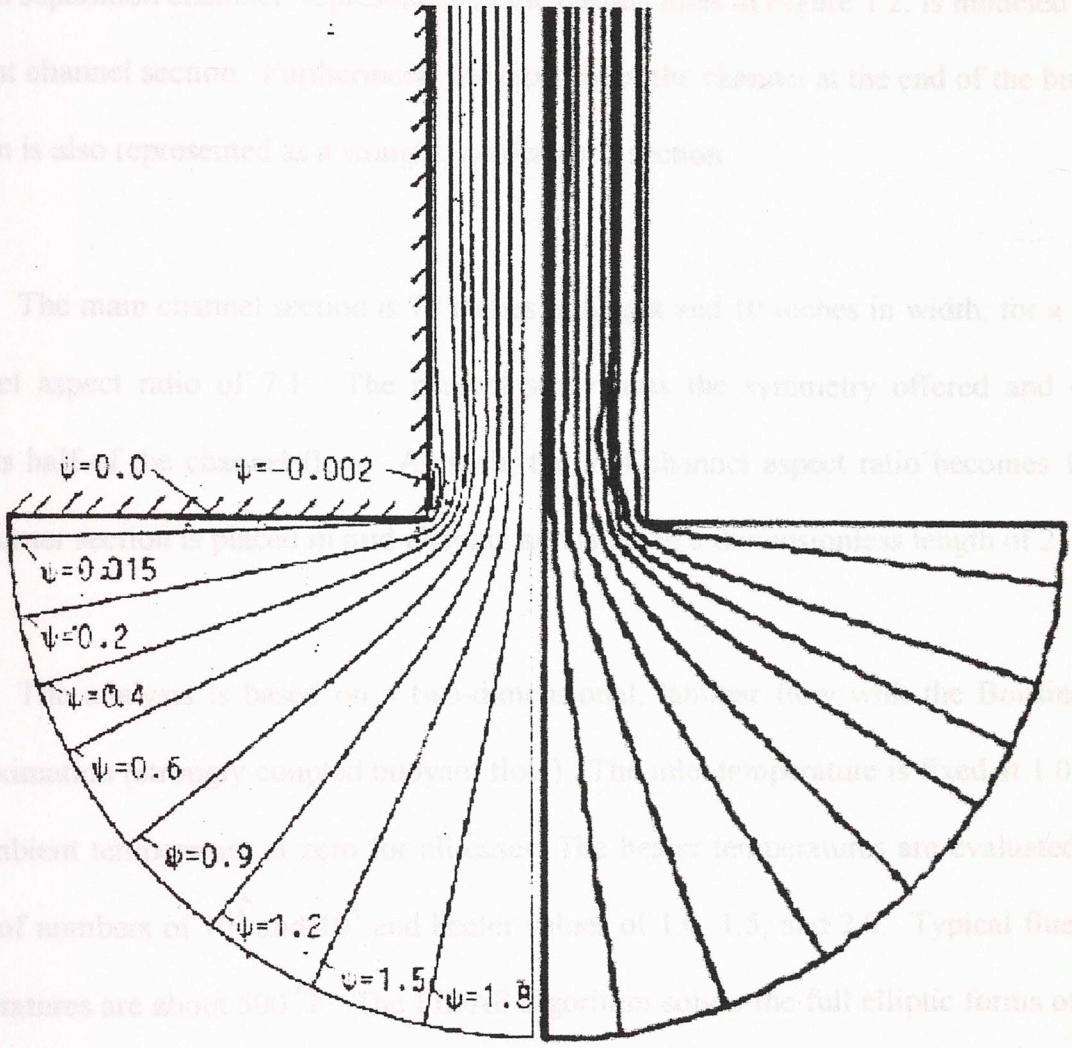

Figure 2.10 Streamline contours: (a) Naylor [27]
(b) present study ($Gr = 10^4$, Steady State)

2.6 Model for the Present Study

The model for the present study (Figure 2.11) is derived from the Naylor model [27] and adapted to meet the specifications of the prototype model (Figure 1.2). The present study models the 70 inches chimney from the inlet into the ash separation chamber up to the outlet of the burner section. In order to simplify the numerical process, the ash separation chamber, represented by the dashed lines in Figure 1.2, is modeled as a straight channel section. Furthermore, the tapering of the channel at the end of the burner section is also represented as a straight, non-tapered section.

The main channel section is 70 inches in height and 10 inches in width, for a full-channel aspect ratio of 7:1. The present study uses the symmetry offered and only models half of the channel flow. As such, the half-channel aspect ratio becomes 14:1. The burner section is placed in mid-channel and is given a dimensionless length of 2.

The analysis is based on a two-dimensional, laminar flow with the Bousinessq approximation (strongly coupled buoyant flow). The inlet temperature is fixed at 1.0 and the ambient temperature at zero for all cases. The heater temperatures are evaluated for Grashof numbers of 10^4 and 10^5 and heater values of 1.0, 1.5, and 2.0. Typical flue gas temperatures are about 500 ^{0}F. The FIDAP algorithm solves the full elliptic forms of the Navier-Stokes and energy equations. The Newton-Rhapson method is utilized with streamline upwinding to ensure proper solution convergence. The Restart method is also used, as in the model verification, to speed the solution convergence.

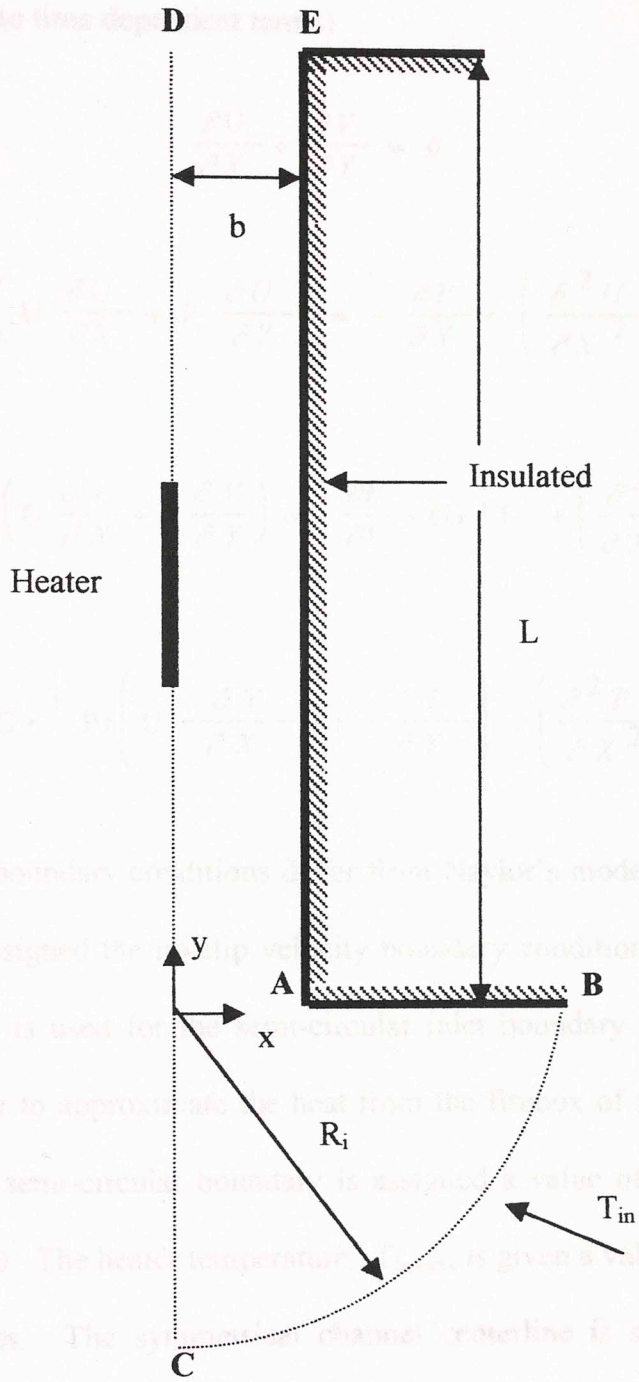

Figure 2.11 Model for the present study

The dimensionless parameters listed in equations (2.14a)-(2.14h) are used and the governing transient equations become (which are identical to equations (2.15)-(2.18) with the introduction of the time dependent terms)

$$\frac{\partial U}{\partial X} + \frac{\partial V}{\partial Y} = 0 \tag{2.23}$$

$$\frac{\partial U}{\partial \tau} + Gr^{\frac{1}{2}}\left(U\frac{\partial U}{\partial X} + V\frac{\partial U}{\partial Y}\right) = -\frac{\partial P}{\partial X} + \left(\frac{\partial^2 U}{\partial X^2} + \frac{\partial^2 U}{\partial Y^2}\right) \tag{2.24}$$

$$\frac{\partial V}{\partial \tau} + Gr^{\frac{1}{2}}\left(U\frac{\partial V}{\partial X} + V\frac{\partial V}{\partial Y}\right) = -\frac{\partial P}{\partial Y} + Gr^{\frac{1}{2}}T + \left(\frac{\partial^2 V}{\partial X^2} + \frac{\partial^2 V}{\partial Y^2}\right) \tag{2.25}$$

$$\frac{\partial T}{\partial \tau} + Gr^{\frac{1}{2}}\,\mathrm{Pr}\left(U\frac{\partial T}{\partial X} + V\frac{\partial T}{\partial Y}\right) = \left(\frac{\partial^2 T}{\partial X^2} + \frac{\partial^2 T}{\partial Y^2}\right) \tag{2.26}$$

The dimensionless boundary conditions differ from Naylor's model [27]. The walls are adiabatic and are assigned the no-slip velocity boundary condition. The Jeffrey-Hamel flow approximation is used for the semi-circular inlet boundary region as in Naylor's study [27]. In order to approximate the heat from the firebox of the fireplace, the inlet temperature on the semi-circular boundary is assigned a value of 1.0 and the ambient temperature is $T_o = 0$. The heater temperature, T_{heater}, is given a value of 1.0, 1.5, and 2.0 for specific analyses. The symmetrical channel centerline is specified with U = 0 although the y-direction velocity V is allowed to vary along the line of symmetry. As discussed previously, the OUTFLOW boundary condition is specified at the channel exit. The boundary conditions for the present study are given below

$$\frac{\partial T}{\partial Y} = U = V = 0 \qquad \text{for} \quad 1 \le X \le \frac{R_i}{b}, Y = 0 \qquad \text{(AB)}$$

$$\frac{\partial T}{\partial X} = U = V = 0 \qquad \text{for} \quad 0 \le Y \le \frac{L}{b}, X = 1.0 \qquad \text{(AE)}$$

$$\frac{\partial T}{\partial Y} = \frac{\partial U}{\partial Y} = \frac{\partial V}{\partial Y} = 0 \qquad \text{for} \quad 0 \le X \le 1.0, Y = \frac{L}{b} \qquad \text{(DE)}$$

$$\sigma_r = V_\theta = -P + \frac{2\partial V_r}{\partial R} = 0, T = 1.0 \qquad \text{for semi - circular boundary} \qquad \text{(BC)}$$

$$\frac{\partial T}{\partial X} = U = 0 \qquad \text{for symmetrical centerline} \qquad \text{(DC)}$$

$$T = T_{heater}, U = V = 0 \qquad \text{for heater}$$

Two different mesh densities were used in the present study, one for the steady state analysis and a separate mesh for the transient analysis. Each case used nine-node quadrilaterals. The steady state condition allows for a relatively coarse mesh to be used for solution convergence while reducing the required computational time. The nodal density of the inlet region did not vary appreciably between the steady state and transient cases. The steady state mesh used 20 nodes in channel width with finer grading toward the channel centerline. The transient case also used a 20-node channel; however, convergence was not possible with the steady state mesh. Therefore, the grading of the mesh in the channel was changed to allow for a fine mesh toward the channel centerline and the channel wall. FIDAP's interpolation function allowed the steady state results to be converted to the new transient mesh. The mesh becomes successively more coarse toward the middle of the half-channel when approached from either direction. Figure 2.12 shows the steady state mesh and Figure 2.13 illustrates the transient mesh.

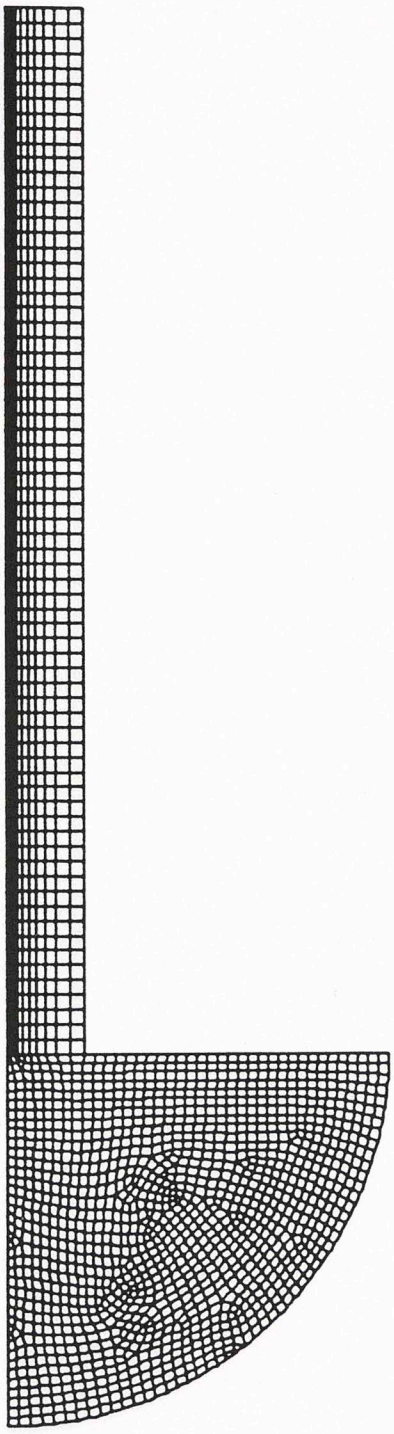

Figure 2.12 Mesh used for present study - steady state analysis

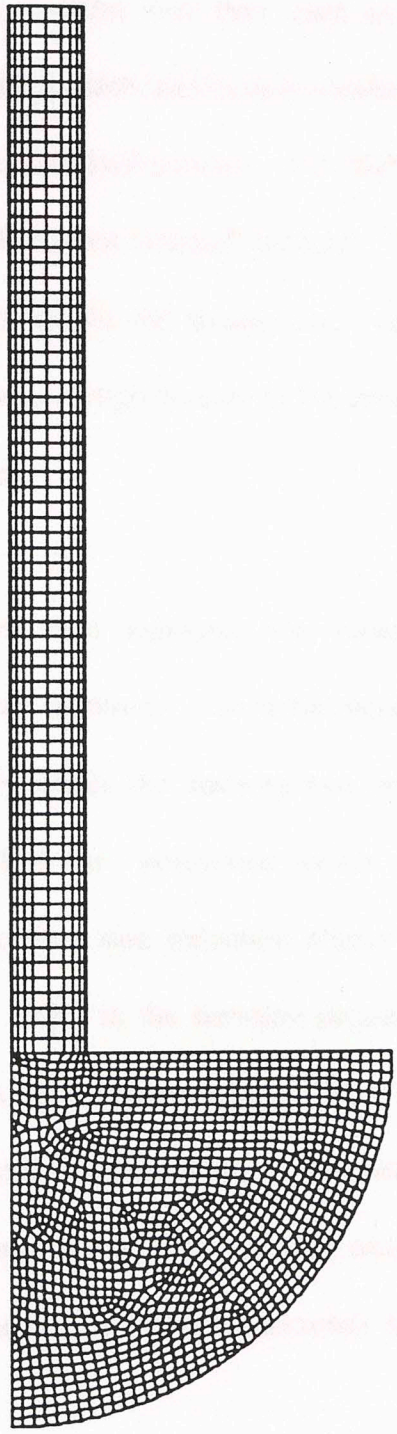

Figure 2.13 Mesh used for present study - transient analysis.

The steady state solutions were completed first. This was to verify the flow patterns, flow rates, and isotherms associated with a non-cyclic heater operation. Furthermore, the steady state solution was then used as the initial solution for the transient cases. In order to reach the desired Grashof numbers, the steady state runs were completed beginning with lower Grashof numbers, with each previous solution serving as the initial condition for the subsequent Grashof number. Grashof numbers of 50, 100, 500, 10^3, 10^4, and 10^5 were solved for the steady state conditions. However, only the solutions of $Gr = 10^4$ and 10^5 were of significance to the present study, as the other values are considered weak convection.

The transient solutions were analyzed for various combinations of heater operating conditions and Grashof numbers. The initial time step used for each iteration was 10^{-4}. However, FIDAP evaluates the convergence criterion at each iteration and reduces the time step by half if the "non-linear solver not converging" warning is displayed. FIDAP's automatic time step reduction allows for the analysis to continue without operator intervention. Early in the iteration process a larger time step may be satisfactory for proper solution convergence whereas later steps may demand a smaller time step. However, the overall number of steps required with this approach can be significantly reduced rather than if the smaller time step were used from the beginning of the iteration. This results in no loss of solution accuracy but a significant reduction in CPU time.

FIDAP allows for time-varying boundary conditions specified by the user. Polynomial functions and user-defined subroutines may be used. The present study uses a step change in the heater temperature based on a series of time-function inputs (t, f(t) pairs). The present study employs three separate heater operating time ratios, defined as follows

$$\omega = \frac{\text{heater off time}}{\text{heater on time}} \tag{2.27}$$

The heater operating time ratios used were ω = 5.0, 2.5, and 1.0. These ratios are somewhat arbitrary and are designed to capture flow variations over a range of cycle times. Experimental measurements from the prototype model were not recorded and therefore data does not exist to allow for a direct correlation. The FIDAP command TMFUNCTION required the user defined input with parameters that reflected the desired cycle ratio ω. The time data reflects a step-change in heater temperature and does not model heat-up or cool-down rates that might be associated with the heater. FIDAP does allow for more advanced time functions, and even FORTRAN code subroutines that could better model the heater operation based on inlet and plume temperature differences. However, the primary goal of this study is to verify the presence of a flow reversal phenomenon under cyclic heater operations. As such, the specific means of numerically modeling the cyclic heater are not considered critical to the analysis of flow reversal. Furthermore, the more involved programming associated with complex time functions is not warranted in this preliminary study.

2.7 CPU Time and Memory Requirement

The FIDAP processing was completed on a Sun Ultra 1 workstation. The amount of processing time, real time and CPU hours, involved in the present study was significant and warrants discussion. The FIDAP program was purchased by the University of Oklahoma, School of Aerospace and Mechanical Engineering, in September 1998, to provide a Finite Element CFD program for use in graduate research. The present study was the first to utilize this program at the University of Oklahoma. Iterations in the present study ranged from relatively short steady state runs on the order of 5 CPU minutes (25 minutes real time) to extremely long transient runs on the order of 18 CPU hours (95 hours real time). The length of time required to complete the iterations demands further discussion.

The analysis for the present study was performed in three phases: code validation, steady state runs, and transient runs. The code validation runs required multiple restart iterations to achieve the appropriate range of Grashof number. The code validation runs were completed for Gr = 50, 100, 200, 500, 10^3, and 10^4. The average run time for each iteration was 0.12 CPU hours (0.6 hours real time).

Steady state runs were completed for T_{heater} = off, 1.0, 1.5, and 2.0 at Gr = 50, 100, 500, 10^3, 10^4, and 10^5. The average run time was 0.15 CPU hours (0.75 hours real time). Additionally, two runs for T_{heater} = 1.5 and 2.0 at Gr = 10^6 were performed.

Transient runs were performed for T_{heater} = 1.5 and 2.0 at ω = 1.0, 2.5, and 5.0 for Gr = 10^4. The average run time for each of these runs was 11 CPU hours (55 hours real time). The three runs for Gr = 10^5, T_{heater} = 2.0, ω = 5.0 averaged 19.11 CPU hours (95 hours real time).

The total run time to complete the range of iterations performed in this study was approximately 136 CPU hours (690 hours real time or nearly 29 continuous days). This time does not include early runs that were aborted due to poor solution convergence, which required mesh refinement or the addition of streamline upwinding to ensure solution convergence. The time required to complete these preliminary iterations significantly added to the overall processing time.

Furthermore, the memory resources required to complete the present study were significant. The total memory required to save each of the runs totaled over 8 Gigabytes. The longer transient runs, specifically the $Gr = 10^5$ runs, required a large amount of dedicated memory to perform the data processing. This information is critical for those who may use similar workstations to employ FIDAP for CFD analyses.

CHAPTER 3

RESULTS AND DISCUSSION

3.1 Steady State Analysis

The steady state case was solved prior to the transient case. This was done in order to determine base-line steady state channel flow rates, isotherms, and streamlines for comparison with the transient solutions. Furthermore, the steady state solutions are used as the initial conditions for the transient solutions.

The steady state analyses were performed with constant temperature heater conditions of T_{heater} = off, 1.0, 1.5, and 2.0. These iterations were performed for Grashof numbers of 50, 100, 500, 10^3, 10^4, and 10^5. The incremental increase of Grashof number was required to achieve proper convergence using the FIDAP restart option. The T_{heater} = off and T_{heater} = 1.0 conditions produced identical results and therefore these results will only be reported by the T_{heater} = 1.0 case. The absence of a temperature differential between the inlet temperature and the heater temperature for the steady state case of T_{heater} = 1.0 ($T_{heater} - T_{inlet} = 0$) prevents any energy transfer and the steady state results for this condition are identical with the T_{heater} = off condition. Table 3.1 lists the dimensionless (half-channel) steady state flow rates for various heater conditions.

Table 3.1 Comparison of steady state dimensionless flow rates for natural convection in a vertical channel with an internal heater.

	Heater Temperatures		
Gr	1.0	1.5	2.0
50	2.375	2.566	2.741
100	2.864	3.026	3.176
500	3.791	3.871	3.944
10^3	4.088	4.141	4.190
10^4	4.679	4.699	4.717
10^5	4.908	4.915	4.921

The flow rates shown in Table 3.1 are also illustrated in Figure 3.1. These results clearly indicate that the flow rate increases with heater temperature. The results also show the dependence of the channel flow rate on the Grashof number. At smaller Grashof numbers of 50, 100, and 500, the channel flow rate shows a larger rate of change for the higher heater temperatures. Therefore, it can be concluded that for the weakest convection flows the heater temperature contributes more significantly to the channel flow rates. As the Grashof number increases, the channel flow rates tend to approach each other regardless of the heater temperature. This indicates that at the higher values of $Gr = 10^4$ and 10^5 the energy input from the heater does not significantly contribute to the channel flow rate. The flow plot shown in Figure 3.1 clearly displays the convergence of flow rates as the Grashof number increases. Another factor contributed to the decreasing channel flow rate for an increasing Grashof number is the boundary layer separation that occurs at a higher Grashof number. The streamline plots for the steady-state cases are shown in Figures 3.2 to 3.4 and the flow separation effect is discussed below.

Each of the heater conditions indicate the onset of flow separation at the channel wall for $Gr = 10^3$. A close inspection of the streamline plots for the $Gr = 10^3$ shows an increase in size of the flow separation region with increasing heater temperatures; i.e. the flow separation is more pronounced at the condition of $T_{heater} = 2.0$ compared to those at $T_{heater} = 1.5$ and 1.0. Furthermore, for each of the heater temperatures, the flow separation increases with the Grashof number. This result is supported by Naylor [27] who found the onset of flow separation in the undivided isothermal channel at $Gr = 10^4$. The onset of flow separation at lower Grashof numbers in this study, compared to the Naylor's study [27], is attributed to the difference in the thermal boundary conditions. The primary buoyant force for the present case is due to heating from below with a less significant contribution from the channel heater. However, this general consistency with the Naylor's study [27] provides further independent verification of the results obtained in this study.

As the flow begins to separate from the channel wall with increasing Grashof number, the separation begins to choke the channel flow. Therefore, the Grashof number creates competing effects, where an increase in the Grashof number causes a choke in channel flow due to a widening flow separation region and also causes an increase in flow by increasing the buoyancy force on the fluid. To verify this effect, a separate steady state analysis was performed for the cases of $T_{heater} = 1.0$ and 2.0 at $Gr = 10^6$, which produced flow rates of 4.643 and 4.637, respectively. These values are below the $Gr = 10^5$ flow rates and confirms that the widening separation zone ultimately overcomes the resultant increased buoyancy and begins to reduce the channel flow rate. The flow

conditions at Grashof numbers of 10^6 and above are higher than those expected in a home fireplace and this range of Grashof number is not analyzed further in this study, either in steady state or transient conditions.

The isotherms for the steady state and transient cases are not presented in the present study. The isotherms are primarily located along the channel centerline and appear as wake lines trailing from the heater. Resolution between the isotherms is poor without significant magnification. The level of magnification required to distinguish between the isotherms prevents the full channel from being displayed, thereby diminishing the usefulness of these plots.

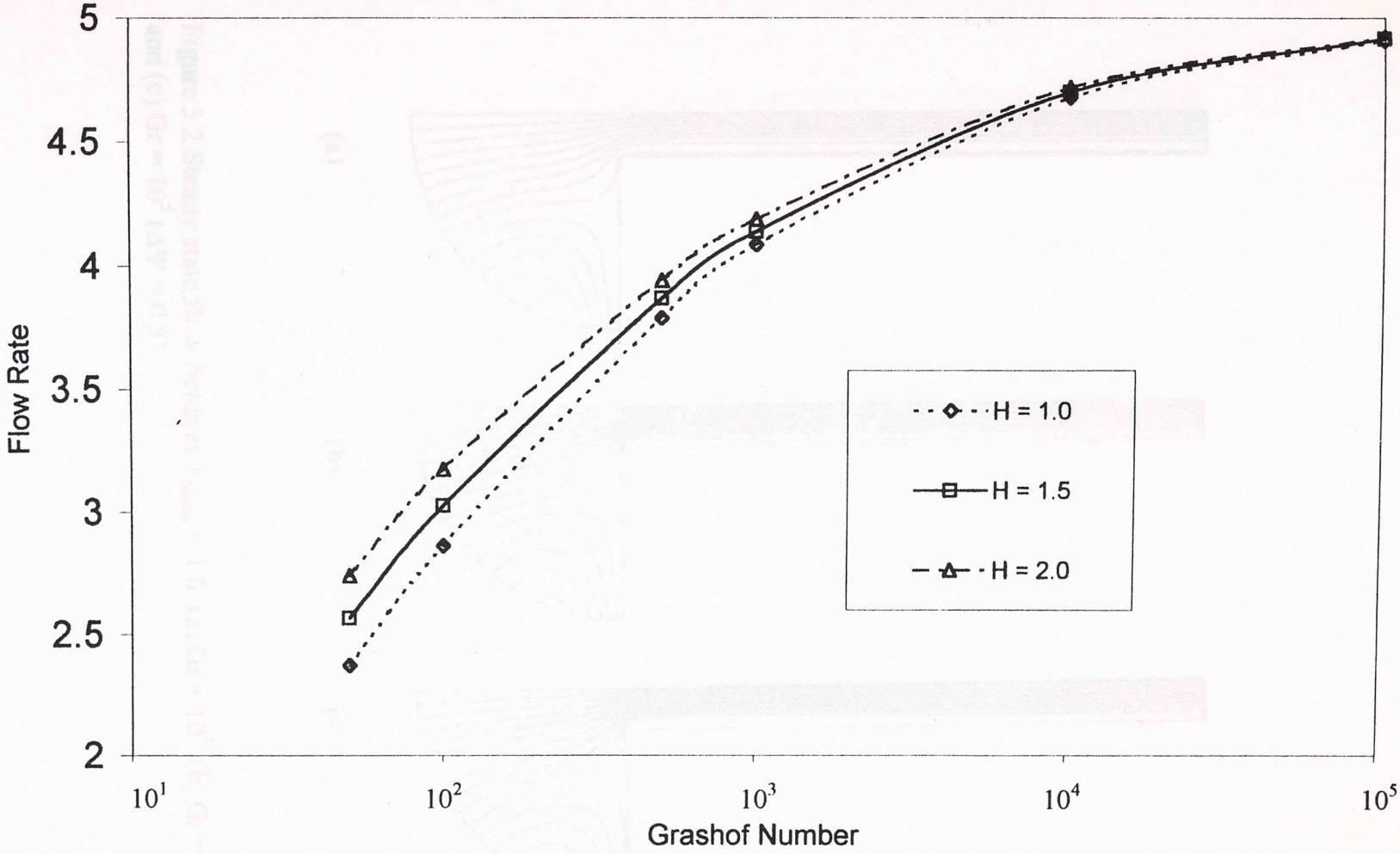

Figure 3.1 Steady state flow rates for T_{heater} = 1.0, 1.5, and 2.0.

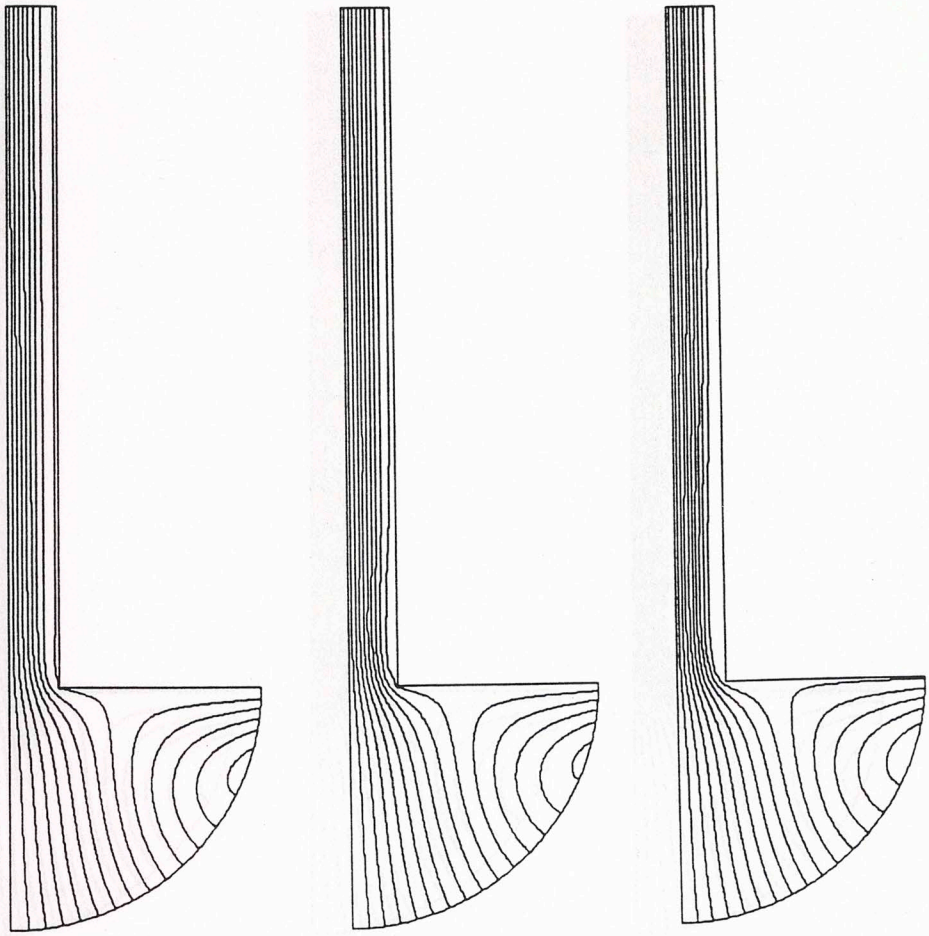

(a) (b) (c)

Figure 3.2 Steady state flow fields at $T_{heater} = 1.0$: (a) $Gr = 10^3$, (b) $Gr = 10^4$, and (c) $Gr = 10^5$ ($\Delta\Psi = 0.5$).

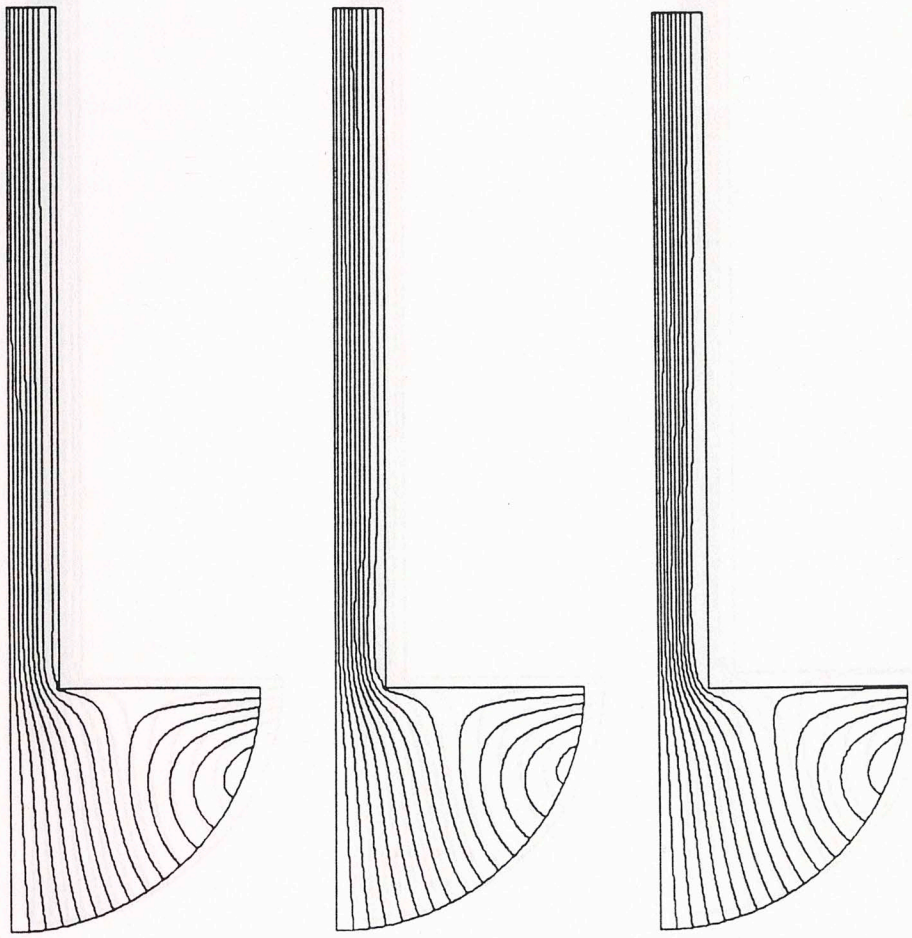

Figure 3.3 Steady state flow fields at $T_{heater} = 1.5$: (a) $Gr = 10^3$, (b) $Gr = 10^4$, and (c) $Gr = 10^5$ ($\Delta\Psi = 0.5$).

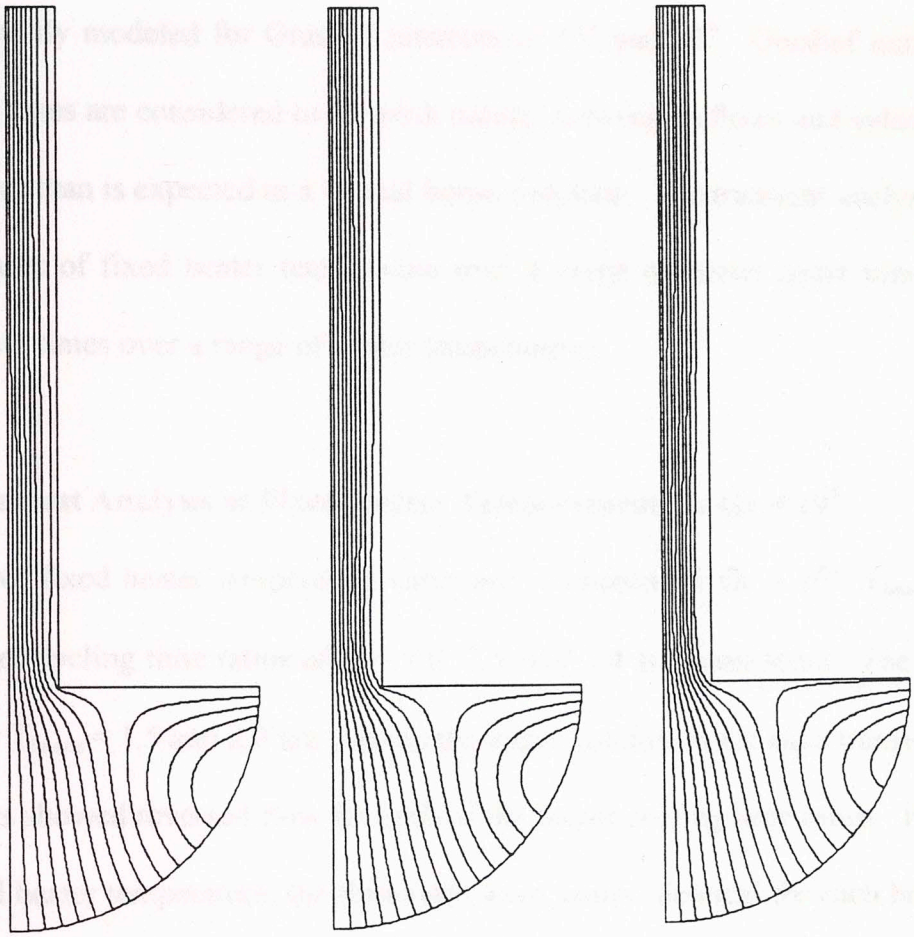

(a) (b) (c)

Figure 3.4 Steady state flow fields at $T_{heater} = 2.0$: (a) $Gr = 10^3$, (b) $Gr = 10^4$, and (c) $Gr = 10^5$ ($\Delta\Psi = 0.5$).

3.2 Transient Analysis

Several different permutations of the operation parameters were performed in order to provide detailed insight into the development of flow and flow reversal in a vertical channel when the channel heater is allowed to cycle. The transient flow cases were primarily modeled for Grashof numbers of 10^4 and 10^5. Grashof numbers below these two cases are considered to be weak natural convection flows and values above 10^5 are stronger than is expected in a typical home fireplace. The transient analysis examines several cases of fixed heater temperature over a range of heater cycle times and fixed heater cycle times over a range of heater temperatures.

3.2.1 Transient Analysis at Fixed Heater Temperatures for Gr = 10^4

Two fixed heater temperature cases are examined for Gr = 10^4: T_{heater} = 1.5 and 2.0. Heater cycling time ratios of ω = 1.0, 2.5, and 5.0 are considered. The steady state results for T_{heater} = 1.5 and 2.0 are used as the initial conditions for each transient analysis. The results showed reversed flow for each of the heater cycling time ratios. Furthermore, for a fixed heater temperature, the flow rates were nearly identical for each heater cycling time ratio. Thus, the flow rates for T_{heater} = 1.5 are almost identical for ω = 1.0, 2.5, and 5.0 and the same is true for the flow rates at T_{heater} = 2.0. The specific flow rates are shown in Table 3.2. The streamline plots for nearly identical for each heater temperature reported above. However, the streamline plots are shown for all cases in Figures 3.5-3.10 for completeness and for verification that the flow patterns are in fact nearly identical.

Table 3.2 Transient channel flow rates for $T_{heater} = 1.5$ and 2.0 for $\omega = 1, 2.5, 5.0$ at $Gr = 10^4$.

	$T_{heater} = 1.5$			$T_{heater} = 2.0$		
	ω					
τ	1.0	2.5	5.0	1.0	2.5	5.0
0.0001	4.700711	4.700711	4.700711	4.719063	4.719063	4.719063
0.0025	4.454370	4.454370	4.454370	4.445040	4.445040	4.445040
0.0050	3.822204	3.822204	3.822204	3.822298	3.822298	3.822298
0.0075	3.132384	3.132383	3.132383	3.179813	3.179813	3.179812
0.0100	2.405110	2.405107	2.405106	2.525733	2.525730	2.525728
0.0125	1.651520	1.651517	1.651516	1.865606	1.865602	1.865609
0.0150	0.879858	0.879856	0.879854	1.202074	1.202071	1.202069
0.0175	0.096750	0.096745	0.096743	0.536396	0.536391	0.536388
0.0200	-0.691227	-0.691223	-0.691226	-0.131142	-0.131150	-0.131154
0.0225	-1.478673	-1.478679	-1.478683	-0.800480	-0.800488	-0.800494
0.0228	-1.572995	-1.573001	-1.573005	-0.880895	-0.880890	-0.880909

As is evident from Table 3.2, the channel flow ultimately reverses for each heater value and cycle frequency. The flow at $T_{heater} = 1.5$ reverses at a faster rate compared to that of the $T_{heater} = 2.0$ case. This is an expected result due to the increased buoyancy added to the system from the heater at a higher temperature.

As discussed previously, the steady state solution is used as the initial condition for each run. The heater cycling pattern initially starts with an off-cycle period, followed by the appropriate on-off cycle ratio for each of the ω analyzed. The results indicate that the cycle frequency, or at least the frequencies used in this study, does not affect the flow rates or streamlines. An examination of the flow rates in Table 3.2 shows variations for differing cycle timing ratios beginning at the fourth and fifth digits. This indicates that the perturbations caused by the different cycle timing ratios cause relatively insignificant changes in the flow rates. Therefore, the data supports the conclusion that the flow field

established during the initial heater off-cycle period is sufficient to initiate the formation of negative temperature gradients that lead to reversed flow. The variation in heater cycles appears to be unable to modify the established reversed flow phenomenon.

As illustrated in Figures 3.5-3.10, the initial streamlines at $\tau = 0.0001$ show strong upward flow out of the channel. The onset of flow separation is present, as discussed in section 3.1 and by Naylor [27], as well as the inlet flow entrainment. This entrainment is represented by the recirculating cell in the right-hand-side of the inlet region that enters and reverses out of the inlet of the channel. This flow entrainment is expected for the model being studied. Naylor's model [27] did not show flow entrainment; however, Naylor's model [27] also did not have the heating-from-below condition (Naylor's $T_{inlet} = 0$) and had the entire channel wall heated to isothermal condition, as opposed to the small buoyancy added to the channel by the heater in the present study. The fact that the upward flow in Naylor's model [27] was induced by buoyancy from the fully heated channel wall accounts for the absence of flow entrainment in Naylor's model [27].

As the flow is convected into the channel, the flow velocity increases (as seen by the larger streamline gradients at the entrance of the channel). This increase in velocity at the channel entrance creates a flow barrier to the flow entering from the side of the channel, which is unable to penetrate the high-velocity airflow moving up the channel. With no upward path to follow, this flow then recirculates back out of the channel entrance and is considered entrained flow.

Comparing the streamline plots for $\tau = 0.0150$ (Figures 3.5.b – 3.7.b and 3.8.c-3.10.c), the existence of a small recirculation zone adjacent to the channel wall is noted. The recirculation zone is larger for the $T_{heater} = 1.5$ case compared to that of the $T_{heater} = 2.0$ case. This trend continues, where the cases of $T_{heater} = 2.0$ at $\tau = 0.0200$ (Figures 3.8.d. – 3.10.d) and $T_{heater} = 1.5$ at $\tau = 0.0180$ (Figures 3.5.c. – 3.7.c) show a full-channel recirculation zone.

At time $\tau = 0.0200$, the $T_{heater} = 2.0$ case shows a full recirculation zone that has blocked the entire channel. At the same time, $\tau = 0.0200$, the flow field of $T_{heater} = 1.5$ shows a recirculation zone with reversed flow from the channel outlet moving into the channel along the channel wall and exiting the inlet. The $T_{heater} = 2.0$ case at $\tau = 0.0228$ is nearly identical to the $T_{heater} = 1.5$ case at $\tau = 0.0200$. This is further evidence that a lower heater temperature results in reversed flow at a faster rate than at higher heater temperatures, as illustrated in Figure 3.12. Finally, the $T_{heater} = 1.5$ case at $\tau = 0.0228$ show several streamlines that have reversed from the outlet to the channel inlet.

Figure 3.11 illustrates the flow fields during the final heater-on cycle for $T_{heater} = 2.0$ and $Gr = 10^4$. At $\tau = 0.0170$ the heater is turned on and remains on through $\tau = 0.0179$. At $\tau = 0.0180$ the heater is turned off. The streamlines closest to the centerline show a small increase in channel velocity through the heater-on cycle. This increase in velocity demonstrates the positive buoyancy added to the channel while the heater is energized.

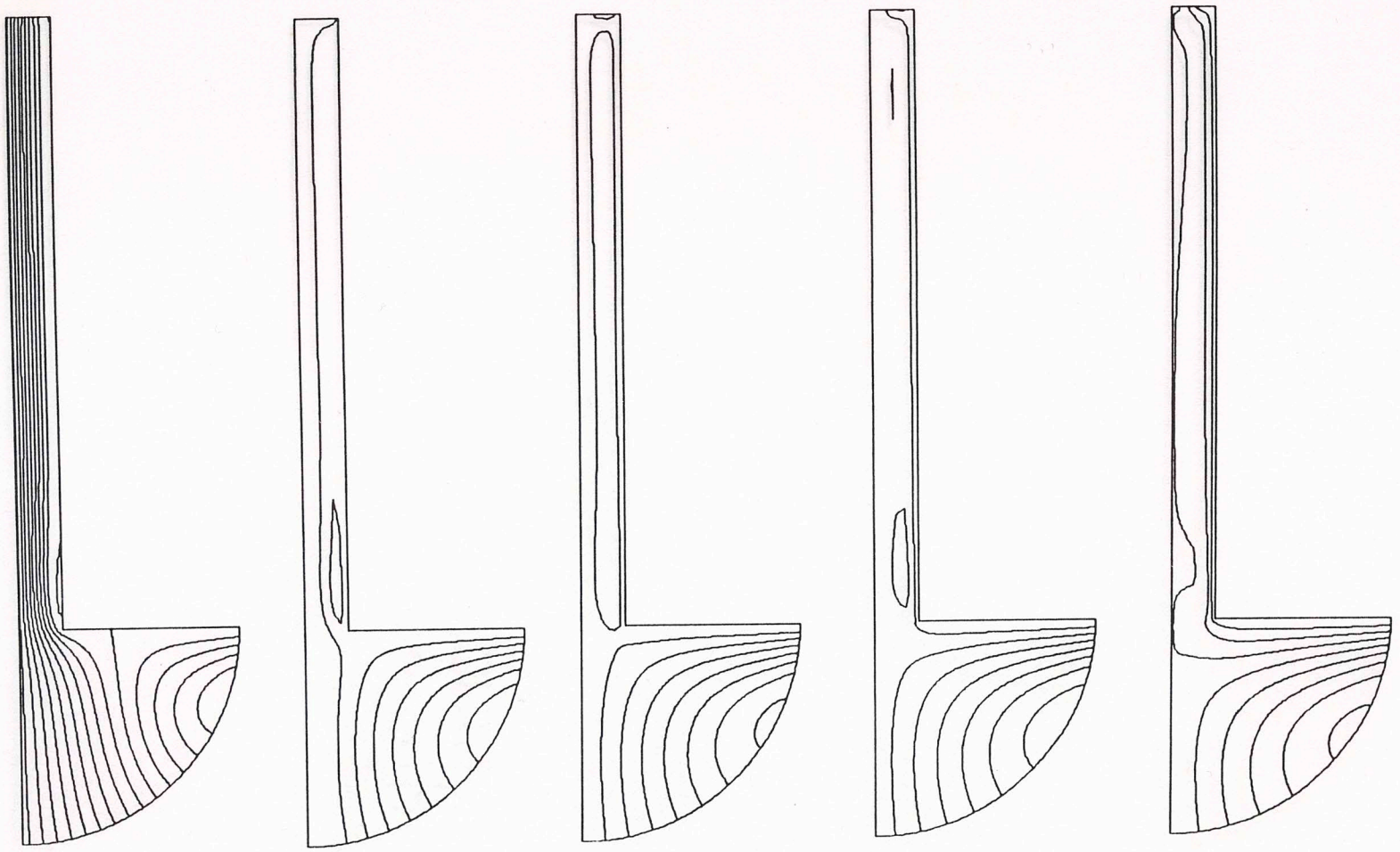

(a) $\tau = .0001$ (b) $\tau = .0150$ (c) $\tau = .0180$ (d) $\tau = .0200$ (e) $\tau = .0228$

Figure 3.5 Transient streamline contour plots for $Gr = 10^4$, $\omega = 1.0$, and $T_{heater} = 1.5$ $(\Delta\Psi = 0.5)$

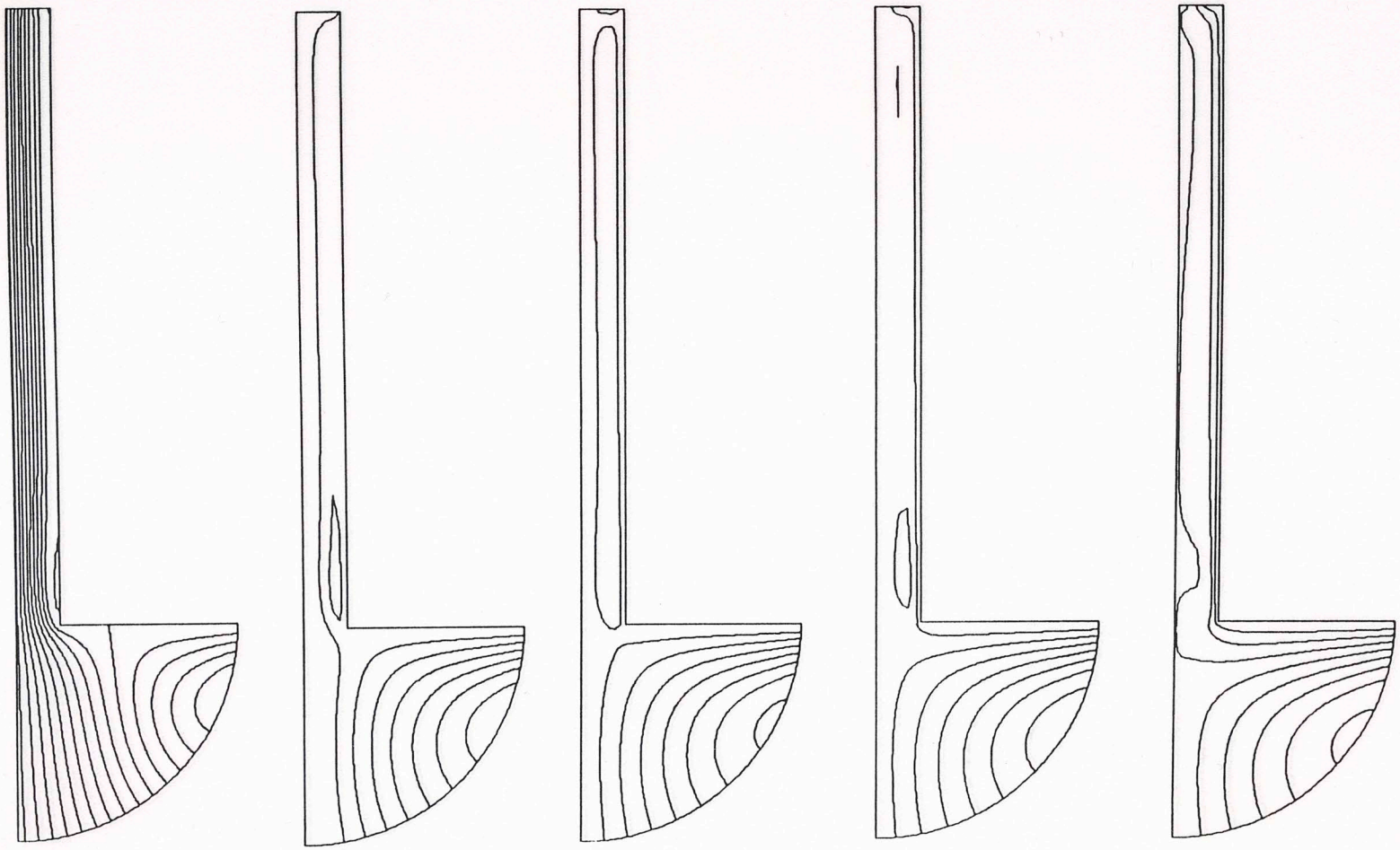

(a) $\tau = .0001$ (b) $\tau = .0150$ (c) $\tau = .0180$ (d) $\tau = .0200$ (e) $\tau = .0228$

Figure 3.6 Transient streamline contour plots for $Gr = 10^4$, $\omega = 2.5$, and $T_{heater} = 1.5$ $(\Delta\Psi = 0.5)$

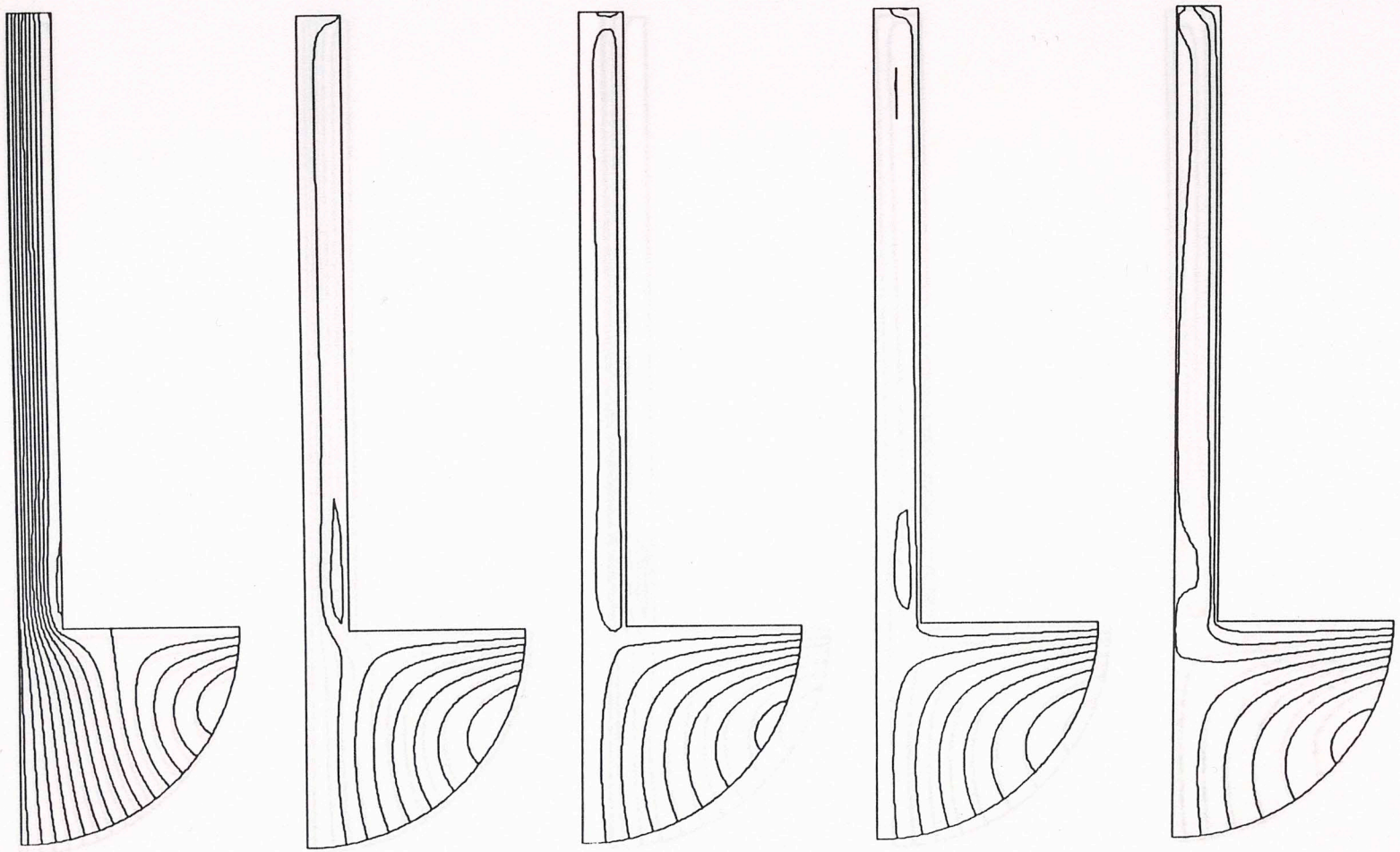

(a) $\tau = .0001$ (b) $\tau = .0150$ (c) $\tau = .0180$ (d) $\tau = .0200$ (e) $\tau = .0228$

Figure 3.7 Transient streamline contour plots for $Gr = 10^4$, $\omega = 5.0$, and $T_{heater} = 1.5$ $(\Delta\Psi = 0.5)$

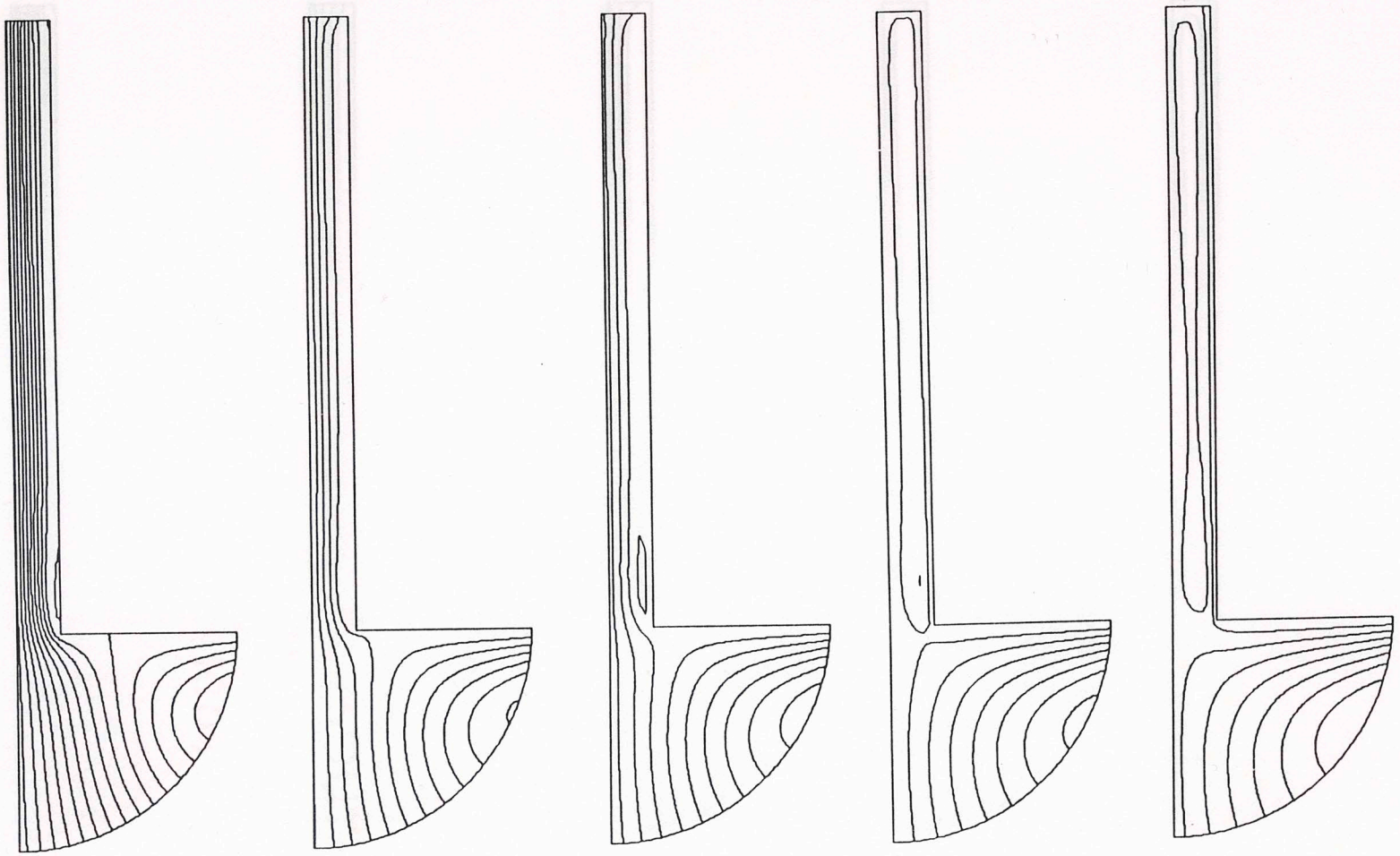

(a) $\tau = .0001$ (b) $\tau = .0120$ (c) $\tau = .0150$ (d) $\tau = .0200$ (e) $\tau = .0228$

Figure 3.8 Transient streamline contour plots for $Gr = 10^4$, $\omega = 1.0$, and $T_{heater} = 2.0$ $(\Delta\Psi = 0.5)$

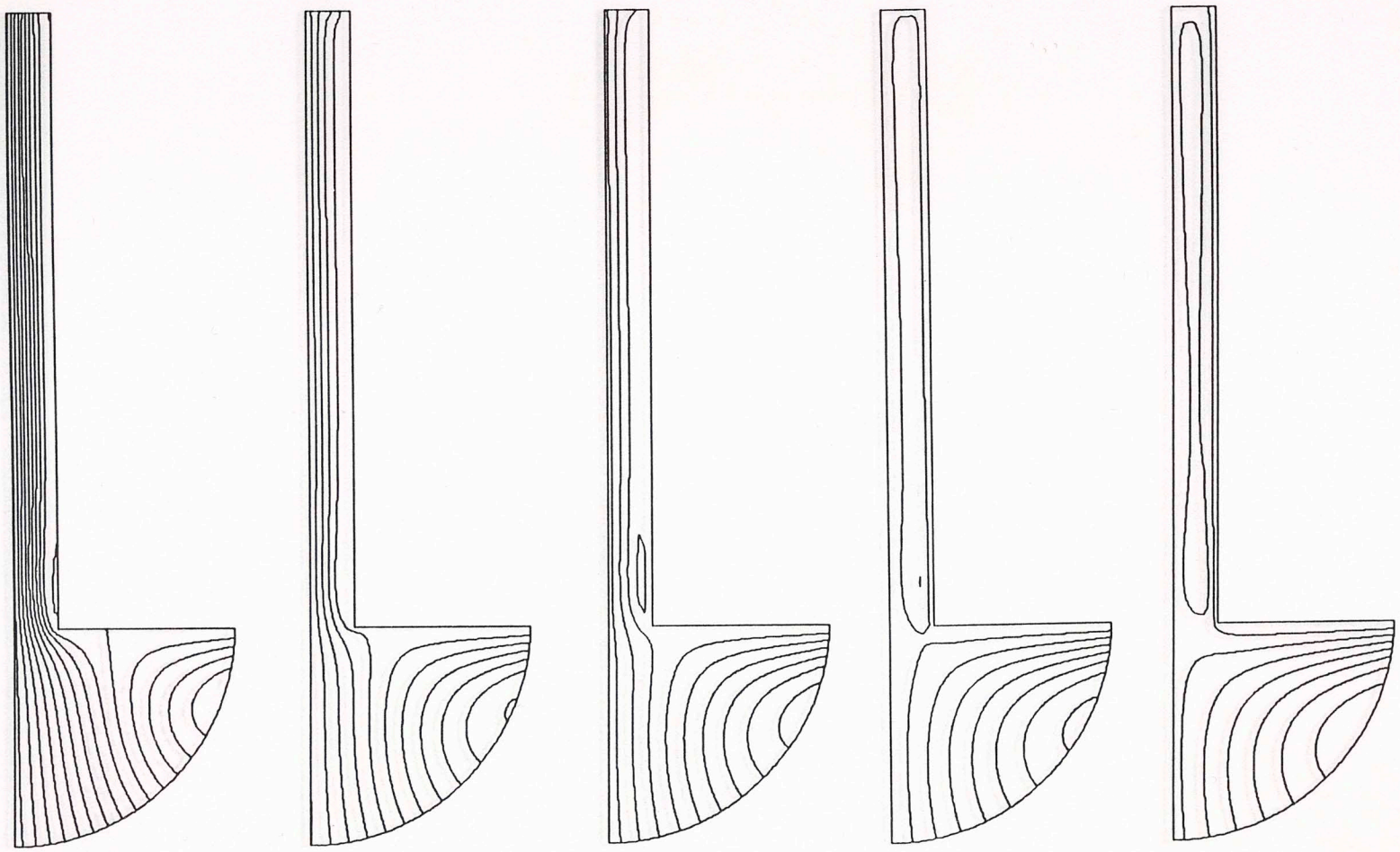

(a) $\tau = .0001$ (b) $\tau = .0120$ (c) $\tau = .0150$ (d) $\tau = .0200$ (e) $\tau = .0228$

Figure 3.9 Transient streamline contour plots for $Gr = 10^4$, $\omega = 2.5$, and $T_{heater} = 2.0$ $(\Delta\Psi = 0.5)$

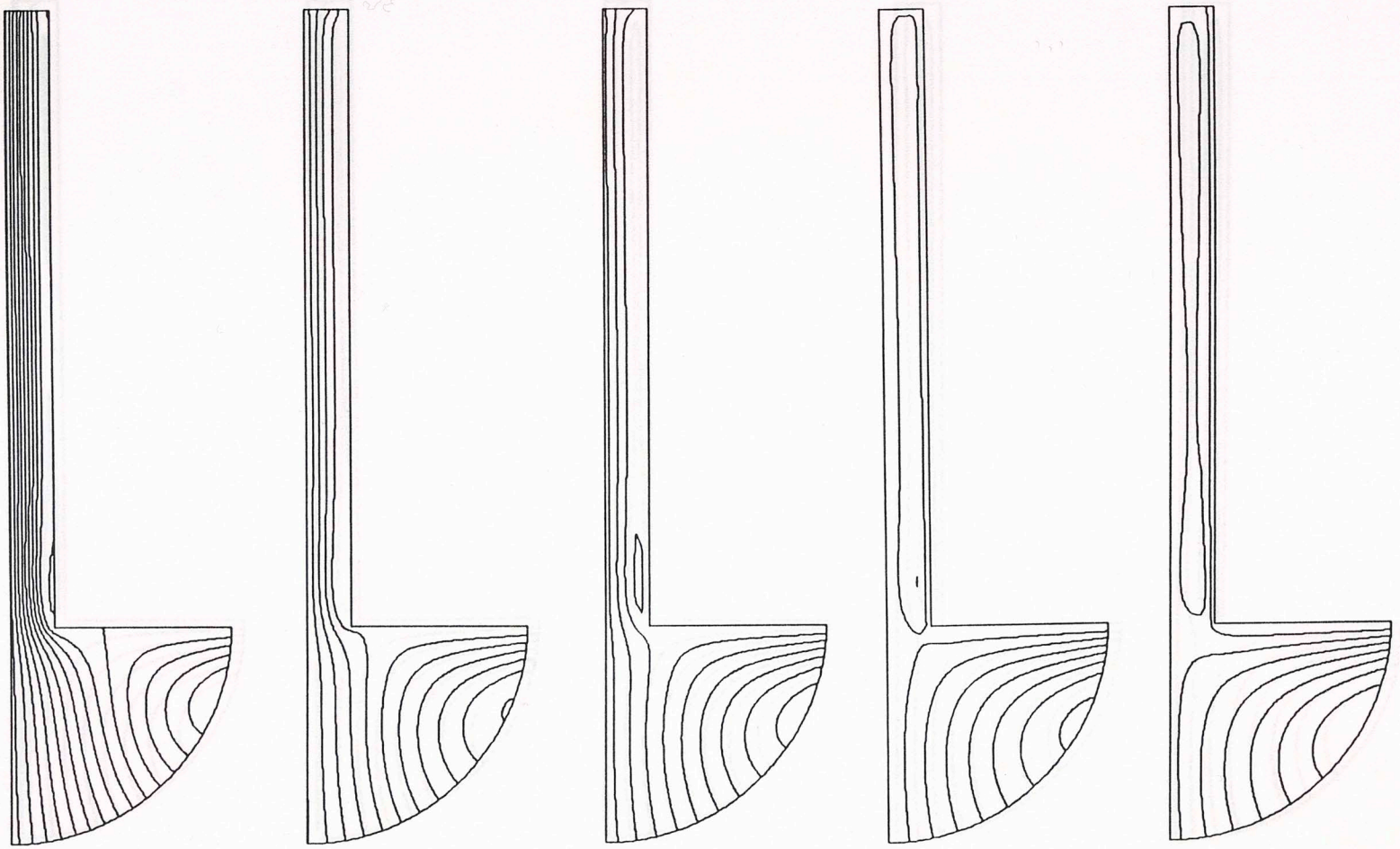

(a) $\tau = .0001$ (b) $\tau = .0120$ (c) $\tau = .0150$ (d) $\tau = .0200$ (e) $\tau = .0228$

Figure 3.10 Transient streamline contour plots for $Gr = 10^4$, $\omega = 5.0$, and $T_{heater} = 2.0$ $(\Delta\Psi = 0.5)$

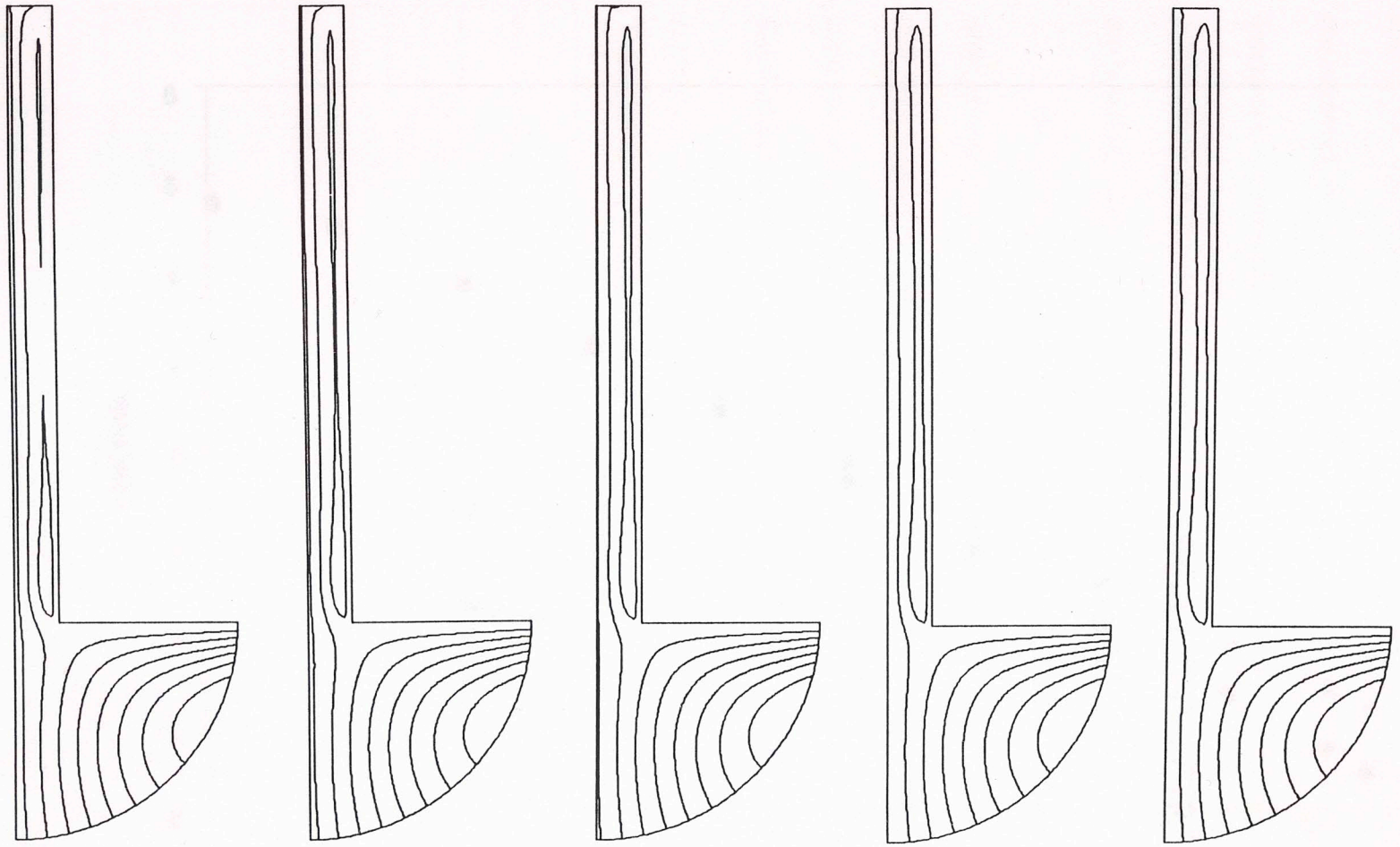

(a) $\tau = .0170$ (b) $\tau = .0173$ (c) $\tau = .0176$ (d) $\tau = .0179$ (e) $\tau = .0182$

Figure 3.11 Transient streamline contour plots for one heater operation cycle at $Gr = 10^4$, $\omega = 5.0$, and $T_{heater} = 2.0$ ($\Delta\Psi = 0.5$)

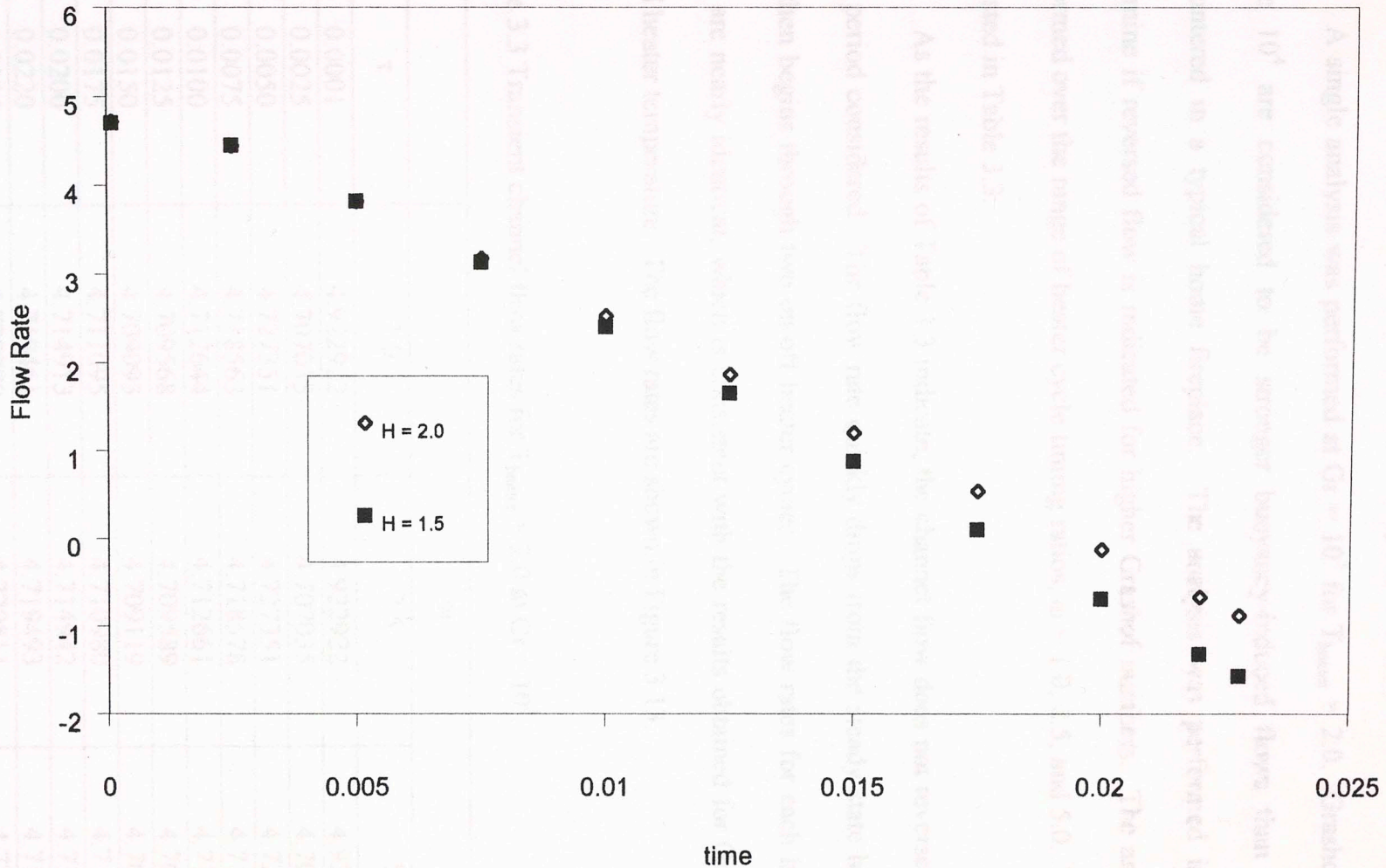

Figure 3.12 Transient flow rates for $\omega = 5.0$ and $Gr = 10^4$ for $T_{heater} = 1.5$ and 2.0.

3.2.2 Transient Analysis at a Fixed Heater Temperature for Gr = 10^5

A single analysis was performed at Gr = 10^5 for T_{heater} = 2.0. Grashof numbers above 10^4 are considered to be stronger buoyancy-induced flows than would be encountered in a typical home fireplace. The analysis was performed in order to determine if reversed flow is indicated for higher Grashof numbers. The analysis was performed over the range of heater cycle timing ratios, ω = 1.0, 2.5, and 5.0. The results are listed in Table 3.3.

As the results of Table 3.3 indicate, the channel flow does not reverse within the time period considered. The flow rate quickly drops from the steady state heater value and then begins through two on-off heater cycles. The flow rates for each heater cycle ratio are nearly identical, which is consistent with the results obtained for Gr = 10^4 at a fixed heater temperature. The flow rates are shown in Figure 3.13.

Table 3.3 Transient channel flow rates for T_{heater} = 2.0 at Gr = 10^5.

	ω		
τ	1.0	2.5	5.0
0.0001	4.922922	4.922922	4.922922
0.0025	4.707035	4.707035	4.707035
0.0050	4.727351	4.727351	4.727351
0.0075	4.718563	4.718578	4.718577
0.0100	4.712644	4.712661	4.712660
0.0125	4.709568	4.709589	4.709589
0.0150	4.709093	4.709119	4.709116
0.0175	4.711095	4.710980	4.711978
0.0200	4.714913	4.714942	4.714939
0.0220	4.719461	4.719493	4.719489
0.0225	4.720780	4.720811	4.720808
0.0240	4.725150	4.725186	4.725181
0.0244	4.726418	4.726455	4.726450

The flow rate for Gr = 10^5 drops to a minimum value at time $\tau = 0.0025$ and then rises slightly at $\tau = 0.0050$. The flow then slowly decreases until a local minimum is reached at $\tau = 0.0150$. Once the minimum is reached, the flow then begins to increase until the solution iteration ends at time $\tau = 0.0244$. This cycle indicates that the flow is essentially perturbed by the cyclic heater at Gr = 10^5 and may be periodic in nature. However, the most important result is the absence of flow reversal. This result is due to the stronger buoyant forces created by the higher Grashof number flow. The absence of flow reversal is also clearly indicated by the streamline plots, shown in Figures 3.14-3.16. These nearly identical plots show the strong upward flow in the channel and the absence of any indication of reversed flow. The flow separation at the channel inlet does not vary appreciably during the iteration or from the steady state condition. Again, another critical result is the fact that the flow rates do not vary significantly for varying cyclic heater operating time ratios at a fixed temperature. This result is identical to the results of Gr = 10^4 and further supports the validity of those results.

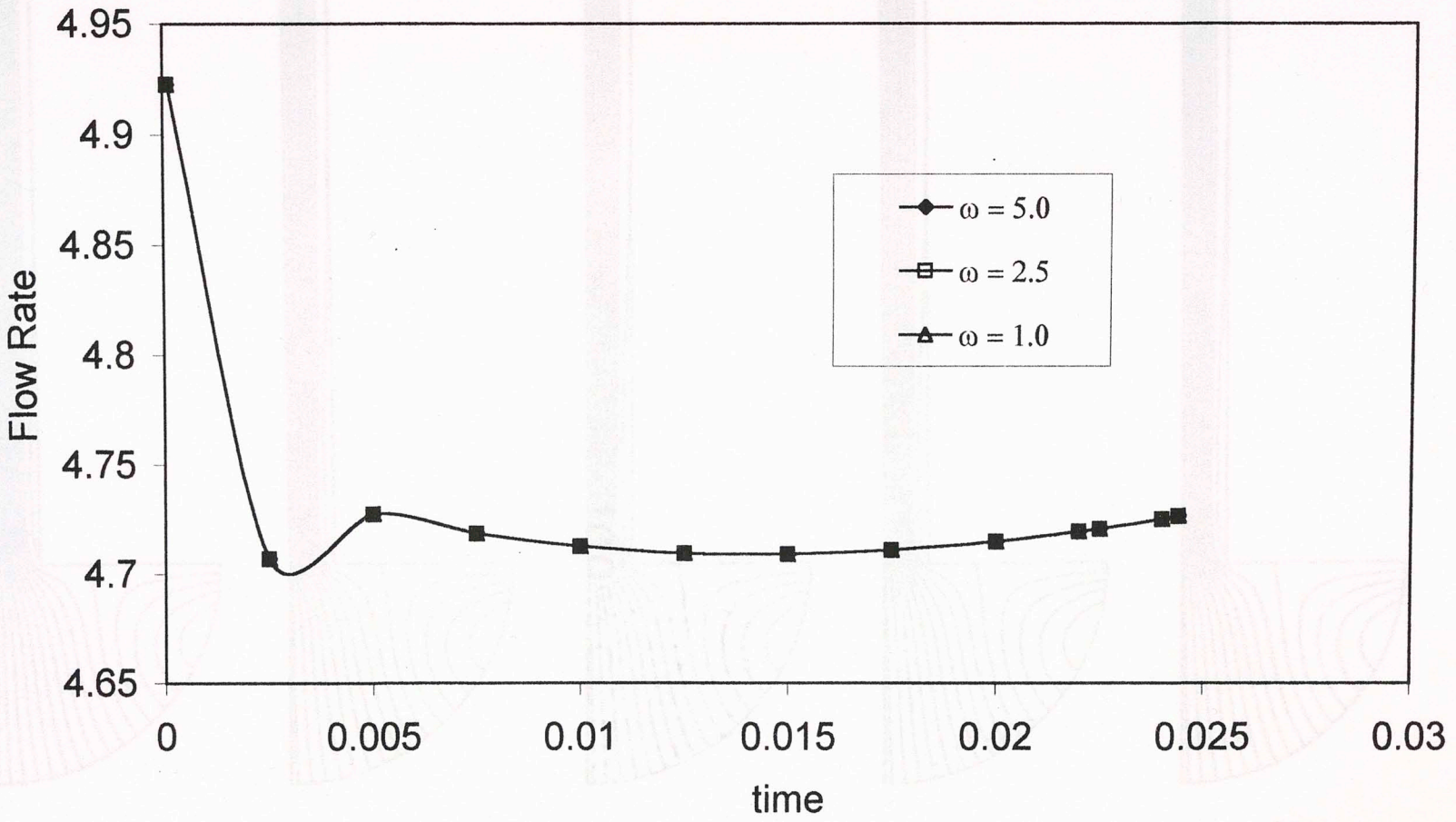

Figure 3.13 Transient flow rates for $\omega = 1.0$, 2.5, and 5.0 for $Gr = 10^5$ and $T_{heater} = 2.0$.

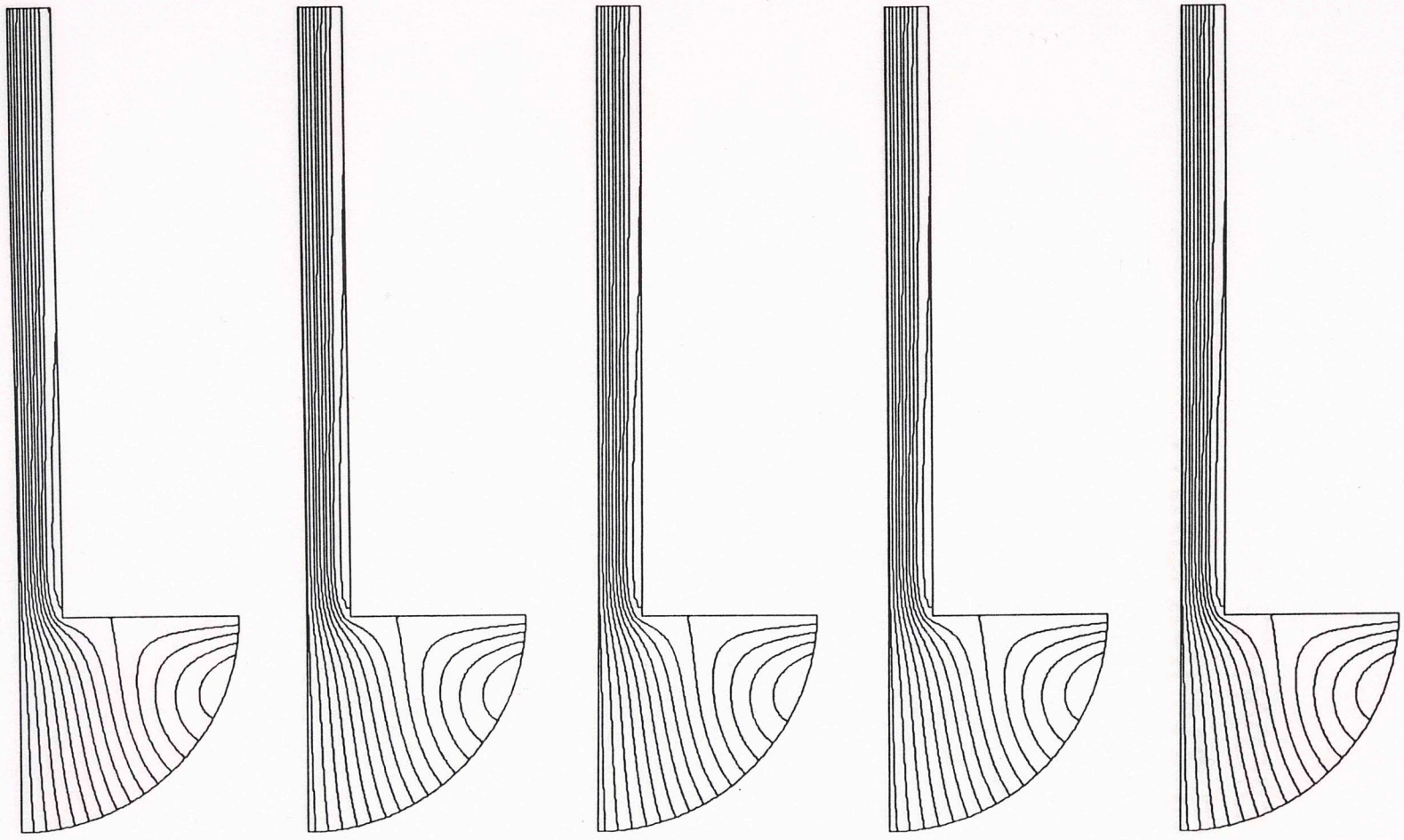

(a) $\tau = .0001$ (b) $\tau = .0150$ (c) $\tau = .0200$ (d) $\tau = .0225$ (e) $\tau = .0244$

Figure 3.14 Transient streamline contour plots for $Gr = 10^5$, $\omega = 1.0$, and $T_{heater} = 2.0$ $(\Delta\Psi = 0.5)$

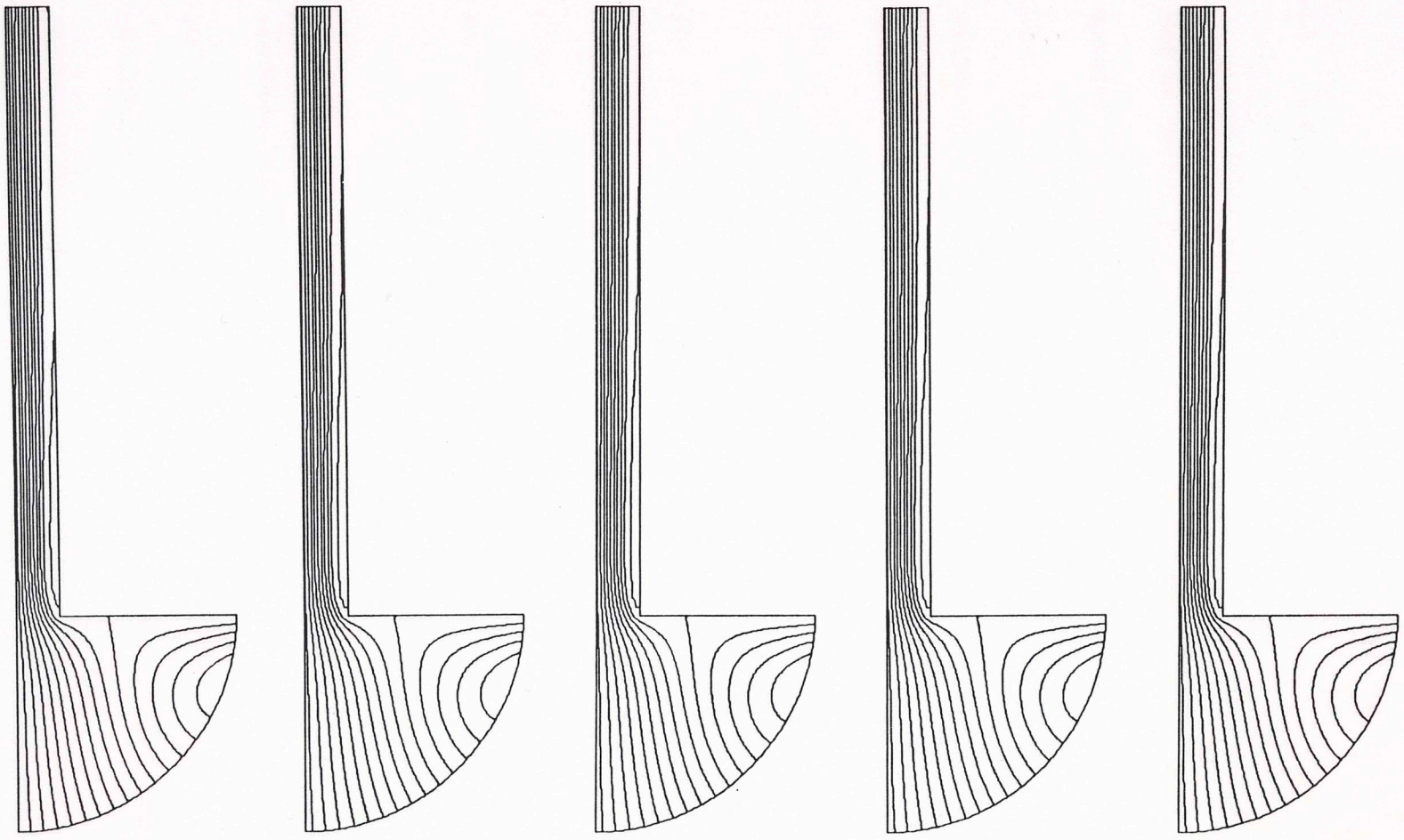

(a) $\tau = .0001$ (b) $\tau = .0150$ (c) $\tau = .0200$ (d) $\tau = .0225$ (e) $\tau = .0244$

Figure 3.15 Transient streamline contour plots for $Gr = 10^5$, $\omega = 2.5$, and $T_{heater} = 2.0$ $(\Delta\Psi = 0.5)$

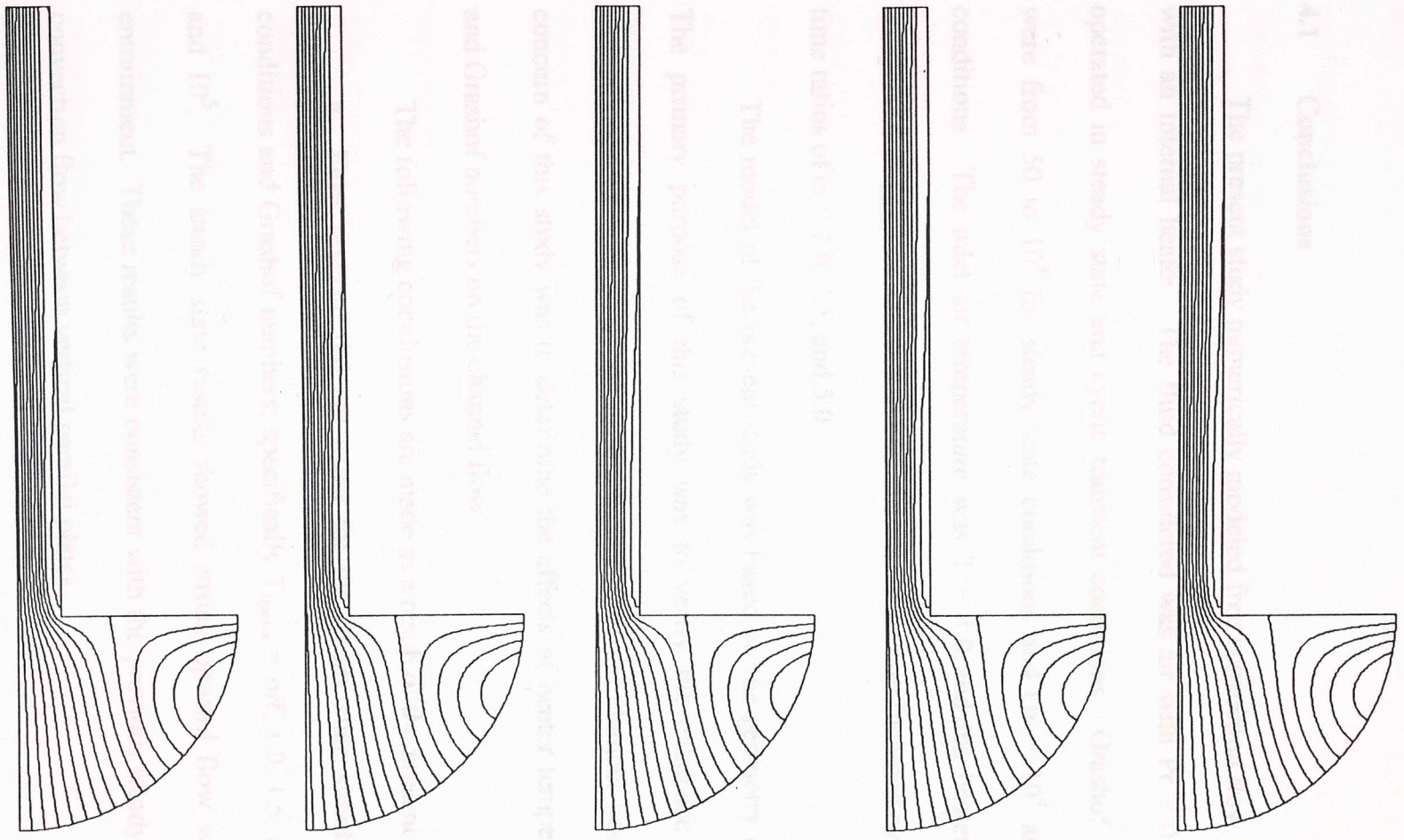

(a) $\tau = .0001$ (b) $\tau = .0150$ (c) $\tau = .0200$ (d) $\tau = .0225$ (e) $\tau = .0244$

Figure 3.16 Transient streamline contour plots for $Gr = 10^5$, $\omega = 5.0$, and $T_{heater} = 2.0$ $(\Delta\Psi = 0.5)$

CHAPTER 4

CONCLUSIONS

4.1 Conclusions

The present study numerically modeled free convection flow in a vertical channel with an internal heater. The fluid considered was air with Pr = 0.7. The heater was operated in steady state and cyclic transient conditions. Grashof numbers considered were from 50 to 10^5 for steady state conditions and Gr = 10^4 and 10^5 for transient conditions. The inlet air temperature was T = 1.0 and the heater temperatures were analyzed for T_{heater} = 1.0, 1.5, and 2.0. The transient runs included cyclic heater operating time ratios of ω = 1.0, 2.5, and 5.0.

The model of the present study was based on the geometry of a home fireplace. The primary purpose of this study was to verify the existence of a flow reversal phenomenon as a result of the cyclic operation of the channel heater. The secondary concern of this study was to determine the effects of heater temperatures, cycle ratios, and Grashof numbers on the channel flow.

The following conclusions are made as a result of the present study:

a. Flow reversal did not occur for the steady state simulations for all heater conditions and Grashof numbers; specifically T_{heater} = off, 1.0, 1.5, and 2.0 for Gr = 10^4 and 10^5. The steady state results showed strong upward flow with some inlet flow entrainment. These results were consistent with the previous steady state studies of free convection flow between vertical parallel plates.

b. Reversed flow was present for all cyclic operating conditions and heater temperatures for $Gr = 10^4$. This result is the most important conclusion of the present study. The prototype model that was tested by UL failed due to the reversed flow of combustion by-products out of the firebox into the living space. The major significant deviation of the prototype model from existing conventional fireplaces was the installation of a cyclic heater. The present study confirmed that the cyclic nature of the channel heater resulted in flow reversal. Therefore, the primary objective of the present study is satisfied in demonstrating flow reversal due to a cyclic heater.

c. The flows at $Gr = 10^5$ did not result in flow reversal for the range of cyclic heater operating time ratios $\omega = 1.0$, 2.5, and 5.0 for $T_{heater} = 2.0$. The flow underwent a small perturbation over the dimensionless time period analyzed, decreasing to a local minimum and slowly increasing until the final iteration time was reached. However, the flow did not reverse. This was also expected, as the higher Grashof number flows should provide enough buoyancy to prevent the negative temperature gradient of the cyclic heater from providing sufficient channel flow resistance and reversed flow.

d. The heater operating time ratios used in the present study provided nearly identical results for a given heater temperature and Grashof number. The common factor between each heater ratio is the initial heater off pattern, which is equivalent to 50 dimensionless time periods. After this initial period, the heater then cycles through its on-off pattern in accordance with its ratio. This leads to the conclusion that the initial off period is sufficient to initiate a strong negative temperature gradient that effectively suppresses the channel flow.

e. The heater temperatures did provide different rates of reversed flow at Gr = 10^4. The higher heater temperature values were slower to reverse flow compared to the lower heater temperature values. This indicates that the higher the heater temperature, the more buoyancy that is added to the channel flow and therefore the slower the flow will be to reverse. However, although the rates of reversed flow varied, the flow did reverse for each heater condition at Gr = 10^4.

4.2 Final Discussion

The present study successfully verified the flow reversal phenomenon, thereby satisfying the major objective of this research. However, several aspects of this study warrant further discussion and possibly further research.

The cyclic heater operating time ratios used in this study were chosen arbitrarily to represent a reasonable range of heater operating conditions for analysis. Actual data on the rate of heater cycling from the prototype model tested by UL was not recorded. The fact that the range of heater operating time ratios used in this study all resulted in reversed flow (for Gr = 10^4) does not imply that all ranges of heater cycle time ratios will result in reversed flow. Further modeling with additional time ratios may be required to determine if a range of heater operating time ratios does exist whereby reversed flow is not always the end result. Additionally, the prototype model used a microprocessor and temperature monitoring system to cycle the heater between the prescribed air inlet and channel temperatures. The actual data of these temperatures and their respective times was also unavailable. However, Fortran subroutines could be generated for use in the FIDAP program that could attempt to simulate the cycling that actually occurred, by

design, in the prototype model due to temperature differences. The present study did not employ such subroutines due to the complexity of the programming involved and the fact that the goal was to verify and report on the mere existence of flow reversal due to the cyclic operation of the channel heater.

Along with the varying heater operating time ratios, the full possible range of heater temperatures was not studied. Future numerical modeling may attempt to determine if a range of heater temperature exists that does not result in reversed flow for $Gr = 10^4$.

Another less significant, but potentially important aspect of the model is the location of the heater and the geometry of the heater. The heater in the present study was placed in the channel centerline in mid-channel. Other locations within the channel were not investigated. The heater was placed mid-channel for the present study in order to remain consistent with the goal of the heater; specifically, to limit pollution and combustion by-products. If the channel heater is placed too close to the firebox, the heater may not be effective in reducing pollution emissions. A channel heater placed at the upper portion of the chimney may result in a disruption of the flow at the outlet of the channel. However, varying the heater location within the channel is a reasonable approach from a fluid dynamics aspect and the effect of heater location on pollution control is a subject left for another study.

The heater in the present study was modeled as a thin foil heater with zero thickness. The heater in the prototype model covered a larger dimension of the channel might more accurately be modeled as a porous medium through which the heated air must travel. Since the results of the present study predicted the flow reversal

phenomenon that was observed in the UL testing, the modeling of the heater in the present study was considered sufficient. However, future studies may need to more accurately model the heater element to ensure that the results obtained account for the mass and thermal capacity of the heater.

The designs of a typical home fireplace do not vary appreciably from the prototype model or the present numerical model. Nevertheless, only a single aspect ratio was examined in the present study. Although it is not anticipated that a chimney with a slightly different aspect ratio will produce significantly different results, future studies might need to be performed to verify the effect of chimney aspect ratios on channel flow.

The boundary conditions of the present study stipulated that the fireplace walls were insulated. The prevention of heat transfer across the fireplace boundaries provided for an ideal model and was a necessary condition to simplify the computer analysis. However, this condition, although reasonable for an initial numerical study, is not entirely realistic. All fireplaces will suffer some heat loss to the ambient surroundings. This loss of heat may affect the channel flow and cause variations in the flow reversal patterns. The fireplace boundaries could be specified with the necessary specific material properties, such as thermal conductivity and film coefficient (effectively the Biot number), to account for heat loss across the boundary. Accounting for this heat transfer could require significant resources due to the relatively large range of materials and thicknesses that may be modeled.

Finally, as illustrated in Figure 1.2, the prototype model also has a set of interior channels used for ash separation. These channels are represented by the dashed lines in Figure 1.2. Initially, it was thought that these channels may create a tortuous flow path

that would disrupt the natural buoyancy of the incoming heated air. Obviously, such a disruption of the upward momentum of the flow could also lead to reversed flow. The present study did not incorporate these ash-collecting channels into the model. This was intentional in order to ensure that the primary factor that could result in reversed flow was the heater. If the interior channels were included along with the cyclic heater, then any resultant reversed flow could not clearly be attributed to any single aspect of the fireplace. Furthermore, modeling the interior channels would add to the complexity of the mesh and the boundary conditions that would in turn increase the solution times, memory required, and the difficulty in achieving solution convergence. However, future studies should include the interior channels to ensure that the actual operating conditions do not ultimately lead to reversed flow.

4.3 Additional Engineering Implications

The results of the present study have engineering implications beyond the specific application to home fireplaces and the prototype model previously discussed. There exist a variety of other natural convection problems that are potentially affected by this study.

The application of natural convection to electronic cooling has long since been researched and studied. Much of the focus has been on the elimination of forced convection systems used for cooling electronic components, specifically Printed Circuit Boards (PCBs), in order to save on the cost of operating and maintaining such systems. Most of the work in this area has focused on models with isothermal or isoflux boundary conditions within the PCB. However, some electronic systems are likely to be cyclic in nature, whereby the system may cycle through periodic on-off phases. As shown in the

present study, under certain conditions such a cyclic load can lead to reversed flow. Obviously, if a system were to rely on natural vice forced convection, and if the system underwent cyclic loading, then a disruption of the anticipated free convection flow could result. Such a disruption of cooling flow could prevent necessary waste heat removal and ultimately lead to equipment damage. Clearly the nature of any electronic systems that rely on natural convection cooling should be examined to ensure that they do not create cyclic conditions that could result in reversed flow.

The HVAC industry also has potential uses for the phenomenon of the present study. Many structures, specifically taller buildings, experience an internal "chimney effect" that causes drafts of air to rise through the building due to the natural buoyancy of warmer air on the ground level. This "chimney effect" is sometimes an undesirable consequence that is difficult to solve. One possible solution to the disruption of this effect may include the placement of hot air ducts or waste heat at pre-determined locations within the structure. This could produce a similar effect of flow reversal to that observed in the present study. This would conceivably be a passive and cost-effective means of reducing the internal chimney effect within susceptible structures.

However, some structures actively utilize the chimney effect for ventilation. One such example would be structures that house animals that require a constant flow of ventilation to remove the build-up of gases and supply fresh air. The addition of heated air pipes or electric heaters can enhance free convection flow and result in increased ventilation performance. Conversely, any heated elements that may be cyclic in nature should be identified in order to avoid possible disruption of a desired chimney effect.

REFERENCES

1. Chimney Safety Institute of America, www.csia.org/home/fireplace.htm, 1996.

2. Hayden, A. C. S., Should Fireplaces Be Illegal?, *Home Energy Magazine*, www.hearth.com, 1997

3. Turns, S. R., *An Introduction to Combustion*, McGraw-Hill, 1996.

4. Lai, F. C., Thermal Analysis in Fireplace Emission Control, proposal submitted to Environmental Computing Applications Systems, University of Oklahoma, 1996.

5. Cheesewright, R., Natural Convection from a Plane, Vertical Surface in Non-Isothermal Surroundings, *International Journal of Heat and Mass Transfer*, vol. 10, pp. 1847-1859, 1967.

6. Eckert, E. R. G. and Carlson, O., Natural Convection in an Air Layer Enclosed Between Two Vertical Plates with Different Temperatures, *International Journal of Heat and Mass Transfer*, vol. 2, pp. 106-120, 1961.

7. Chu, H. H. –S., Churchill, S. W. and Patterson, C. V. S., The Effect of Heater Size, Location, Aspect Ratio, and Boundary Conditions on Two-Dimensional, Natural Convection in Rectangular Channels, *Journal of Heat Transfer*, vol. 98, pp. 194-201, 1976.

8. Yin, S. H., Wung, T. Y. and Chen, K., Natural Convection in an Air Layer Enclosed with Rectangular Cavities, *International Journal of Heat and Mass Transfer*, vol. 21, pp. 307-315, 1977.

9. Batchelor, G. K., Heat Transfer by Free Convection Across a Closed Cavity Between Vertical Boundaries at Different Temperatures, *Applied Math*, vol. 12, pp. 209-233, 1954

10. Schmidt, F. W. and Newell, M. E., Heat Transfer Laminar Free Convection within Rectangular Enclosures, *ASME*, 1969.

11. De Vahl Davis, G. and Jones, I. P., Natural Convection in a Square Cavity: A Comparison Exercise, *International Journal for Numerical Methods in Fluids*, vol. 3, pp. 227-248, 1983.

12. De Vahl Davis, G. and Jones, I. P., Natural Convection of Air in a Square Cavity: Bench Mark Numerical Solution, *International Journal for Numerical Methods in Fluids*, vol. 3, pp. 249-264, 1983.

13. Cless, C. M. and Prescott, P. J., Effect of Time-Varying Thermal Boundary Layer Conditions on Oscillatory Natural Convection of a Low Prandtl Number Fluid, *Numerical Heat Transfer*, Part A, vol. 29, pp. 645-669, 1996.

14. Ju, Y. and Chen, Z., Numerical Simulation of Natural Convection in an Enclosure with Discrete Protruding Heaters, *Numerical Heat Transfer*, Part A, vol. 30, pp. 207-218, 1996.

15. Aung, W., Fletcher, L. S. and Sernas, V., Developing Laminar Free convection between Vertical Flat Plates with Asymmetric Heating, *International Journal of Heat and Mass Transfer*, vol. 15, pp. 2293-2308, 1972.

16. Ofi, O. and Hetherington, H. J., Application of the Finite Element Method to Natural Convection Heat Transfer from the Open Vertical Channel, *International Journal of Heat and Mass Transfer*, vol. 20, pp. 1195-1204, 1977.

17. Bodoia, J. R. and Osterle, J. F., The Development of Free Convection between Heated Vertical Plates, *Journal of Heat Transfer*, vol. 84C, pp. 40-44, 1962.

18. Ramanathan, S. and Kumar, R., Correlations for Natural Convection between Heated Vertical Plates, *Journal of Heat Transfer*, vol. 113, pp. 97-107, 1991.

19. Hung, Y. and Chang, K., Transient Free Convection Heat Transfer in a Vertical Finite Length Channel, *National Heat Transfer Conference ASME*, vol. 10, pp. 17-24, 1997.

20. Hung, Y. H. and Perng, S. W., An Experimental Technique for Measuring Transient Natural/Forced Convective Heat Fluxes in a Vertical Channel, *Experimental Thermal and Fluid Science*, vol. 1, no. 4, pp. 305-313, 1988.

21. Hung, Y. and Chang, K., Transient Natural Convection Between Vertical Finite Length Heated Plates, *Journal of Thermophysics and Heat Transfer*, vol. 11, pp. 203-211, 1997.

22. Aung, W. and Worku, G., Developing Flow and Flow Reversal in a Vertical Channel with Asymmetric Wall Temperatures, *Journal of Heat Transfer*, vol. 108, pp. 299-304, 1986.

18. Lin, T., Chang, T. and Chen, Y., Development of Oscillatory Asymmetric Recirculating Flow in a Transient Laminar Opposing Mixed convection in a Symmetrically Heated Vertical Channel, *Journal of Heat Transfer*, vol. 115, pp. 342-352, 1993.

24. Kettleborough, C. F., Transient Laminar Convection between Vertical Heated Plates Including Entrance Effects, *International Journal of Heat and Mass Transfer*, vol. 15, pp. 883-896, 1971.

25. Sefcik, D. M., Webb, B. W. and Heaton, H. S., Analysis of Natural Convection in Vertically Vented Enclosures, *International Journal of Heat and Mass Transfer*, vol. 34, pp. 3037-3046, 1991.

26. Straatman, A. G., Tarasuk, J. D. and Floryan, J. M., Heat Transfer Enhancement from a Vertical, Isothermal Channel Generated by the Chimney Effect, *Journal of Heat Transfer*, vol. 115, pp. 395-402, 1993.

27. Naylor, D., A Numerical and Interferometric Study of Natural Convective Heat Transfer from Divided and Undivided Vertical Channels, Ph.D. Thesis, The University of Western Ontario, London, Ontario, Canada, 1991.

28. Santra, A. K., Misra, D. and Ray, S., Analysis of Laminar Natural Convection from a Discrete Isothermal Flush Heater Mounted on the Sidewall of a Partially Open Rectangular Cavity, *Numerical Heat Transfer*, Part A, vol. 29, pp. 211-225, 1996.

29. Mao, C. P., Fernandez-Pello, A. C. and Humphrey, J. A. C., An Investigation of Steady Wall-Ceiling and Partial Enclosure Fires, *Journal of Heat Transfer*, vol. 106, pp. 221-228, 1984.

30. Zhang, Z., Bejan, A. and Lage, J.L., Natural Convection in a Vertical Enclosure with Internal Permeable Screen, *Journal of Heat Transfer*, vol. 113, pp. 377-383, 1991.

31. Naylor, D. and Tarasuk, J. D., Natural Convective Heat Transfer in a Divided Vertical Channel: Part I Numerical, *Journal of Heat Transfer*, vol. 115, pp. 377-387 1993.

32. Naylor, D. and Tarasuk, J. D., Natural Convective Heat Transfer in a Divided Vertical Channel: Part II Experimental, *Journal of Heat Transfer*, vol. 115, pp. 388-394, 1993.

33. Aihara, T., Ohara, T., Sasago, A., Ukaku, M. and Gori, F., Improvement of Free Convection Heat Transfer between Vertical Parallel Plates by Inserting an Auxiliary Plate, *Report of the Institute of Fluid Science*, vol. 8, pp. 61-74, 1996.

34. White, F. M., *Viscous Fluid Flow*, McGraw-Hill, 1991.

35. Fluent Systems, Inc., *FIDAP Theory Manual*, 1998.

36. Reddy, J. N. and Rasmussen, M. L., *Advanced Engineering Analysis*, Krieger Publishing Company, 1990.

37. Chapra, S. C. and Canale, R. P., *Numerical Methods for Engineers*, McGraw-Hill, 1988

38. Bang, H. and Kwon, Y. W., *The Finite Element Method using MATLAB*, CRC Press, 1997.

39. Fluent Systems, Inc., *FIDAP Tutorial Manual*, 1998.

40. Fluent Systems, Inc., *FIDAP Examples Manual*, 1998.